Advances in *in Vivo* Neurochemical Monitoring Using Microdialysis with Liquid Chromatography-Mass Spectrometry

by

Alec C. Valenta

A dissertation submitted in partial fulfillment
of the requirements for the degree of
Doctor of Philosophy
(Chemistry)
in the University of Michigan
2020

Doctoral Committee:

Professor Robert T. Kennedy, Chair
Professor Daniel Leventhal
Professor Mark E. Meyerhoff
Professor Brandon T. Ruotolo

Alec C. Valenta

alecv@umich.edu

ORCID iD: 0000-0002-9810-1912

Dedication

To my mother,

who taught me to never stop learning.

Acknowledgements

Many people have made contributions, large and small, to my success in getting my PhD. First and foremost I would like to thank my advisor, Professor Bob Kennedy, for mentoring me throughout a crucial stage in my development as a scientist. The resources available to me within his lab were unrivaled among academic labs. Perhaps most importantly, Bob has always encouraged me to explore my own ideas and actively fosters the creativity that drives science forward.

I would also like to thank the members of my thesis committee: Professors Brandon Ruotolo, Mark Meyerhoff, and Daniel Leventhal. They challenged me to be thorough in both my understanding and execution of the all of the work I have performed. I would also like to thank Brandon for allowing me to rotate in his lab during my first year. Although I did not end up joining I learned a lot from his emphasis on understanding fundamentals. I would like to thank numerous collaborators including Dr. Alex Kawa and Professor Terry Robinson for their work on the addiction study. I would like to thank Professor Herman Wolosker for giving me the opportunity to collaborate in studying the ASCT1 transporter. Professor Malcolm Low and Dr. Graham Jones were great to work with and although measuring the POMC peptides proved extremely difficult, I value our collaboration and greatly appreciate the support.

My favorite aspect of graduate school was undoubtedly all of the meaningful relationships I was able to form along the way. I would like to thank some of my mentors including Dr. Omar Mabrouk, Dr. Jenny-Marie Wong, and Professor James Grinias. From Omar I learned a lot about the neuroanatomy of the brain and how to think about and design studies. Aside from teaching me the vast majority of techniques that I would use again and again throughout graduate school, Jenny taught me how to be a rigorous analytical chemist and to hold myself and my work to an extremely high standard. Jim taught me a lot about the fundamentals of chromatography and, along with Jenny, remains a close friend and someone I never hesitate to go to for advice. I would like to thank Dr. Dan Steyer for being a collaborator, a friend, and my major sounding board for a lot of the craziest ideas I had during graduate school. Matt Sorensen, aside from being my crowning achievement in mentorship, was someone I was never hesitated to put my trust into and was always there to help when I was in a pinch. Thanks to Megan Connolly for all your help with taking pictures of my chips that made our boss very happy. Kelcie Zegalia and Emory Payne were both there when I needed advice about LC and microfluidic ideas. Thank you to Dr. Brian Shay for all of the ideas and instruments of yours I made use of from your brain and your basement, respectively. Thank you to Dr. Sugy Dixit for helping me to automate my data analysis, for showing me the other side of the world, and for teaching me how to cook the best foods. I would also like to thank all of the animals that made my graduate work possible, your sacrifice is not forgotten.

I would like to thank Professor Stephen Weber and Professor Adrian Michael for teaching me analytical chemistry and allowing me the wonderful opportunity to do research in your labs. Without you I undoubtedly would not be here today. Thanks to Dr. Amir

Faraji for sparking my interest in neuroscience. A special thanks to Dr. Andrea Jaquins-Gerstl for mentoring me and remaining a close friend through the years.

I would like to thank all of my great friends, old and new, who have helped me along the way. Thank you to Chris and Clay for being the goons that you are. Thanks to the crew at 903 who are some of my best friends and also some of the brightest people I've ever met.

A special thanks to my family. Mom, Dad, Ian, and Abby you all been so supportive over the years and helped to keep me grounded when I needed it most. Thanks to Erin and John for being such great additions to the family. Thanks to Avery, Sigourney, Levi, Gary, Oliver, and Isaac for bringing so much joy to us all.

Finally, special thanks to Cara D'Amico for being my rock through my hardest times in graduate school. The best part of my day was the walk to and from work with you. Without you I could never have even finished my own thesis work. It takes a special kind of collaborator to put their life on the line in the name of on-chip benzoyl chloride derivatization…

Table of Contents

List of Figures

List of Tables

List of Equations

List of Abbreviations

aCSF	Artificial cerebrospinal fluid
MWCO	Molecular weight cutoff
EE	Extraction efficiency
UV	Ultraviolet absorbance
LIF	Laser-induced fluorescence
ED	Electrochemical detection
MS	Mass spectrometry
CE	Capillary electrophoresis
HPLC	High performance liquid chromatography
RPLC	Reversed-phase liquid chromatography
HILIC	Hydrophilic interaction liquid chromatography
ESI	Electrospray ionization
MS/MS	Tandem mass spectrometry
BzCl	Benzoyl chloride
LoD	Limit of Detection
ACh	Acetylcholine
Ch	Choline
UHPLC	Ultra-high performance liquid chromatography
SIL	Stable-isotope-labeled
Glu	Glutamate
DA	Dopamine
cLC	Capillary liquid chromatography
ID	Inner diameter
LgA	Long-access model of self-administration
ShA	Short-access model of self-administration
IntA	Intermittent-access model of self-administration
RSD	Relative standard deviation
5-HT	Serotonin

Ado	Adenosine
NE	Norepinephrine
NM	Normetanephrine
3-MT	3-Methoxytyramine
Epi	Epinephrine
L-DOPA	3,4-Dihydroxyphenylalanine
5-HIAA	5-Hydroxyindoleacetic acid
Hist	Histamine
GABA	γ-Aminobutyric acid
5-HTP	5-Hydroxytryptophan
Asp	Aspartic acid
HVA	Homovanillic acid
Gly	Glycine
DOPAC	3,4-Dihydroxyphenylacetic acid
Phe	Phenylalanine
Ser	Serine
Tau	Taurine
GSH	Glutathione
Gln	Glutamine
Glc	Glucose
FR-1	Fixed ratio-1
LimA	Limited-access model of self-administration
ACN	Acetonitrile
SRM	Selected reaction monitoring
SEM	Standard error of the mean
RIC	Reconstructed ion chromatogram
n_c	Peak capacity
Rt	Retention time
NMDA	N-methyl-D-aspartate
KO	Knockout
ASCT1	Alanine, serine, cysteine, threonine transporter 1
ACST2	Alanine, serine, cysteine, threonine transporter 2
OPA	O-phthaldialdehyde

Boc-L-Cys	N-tert-butyloxycarbonyl-L-cysteine
Thr	Threonine
Ala	Alanine
WT	wild-type
TIC	Total ion chromatogram
C_{vial}	Concentration of analyte in sampling vial
C_{corr}	Recovery-corrected concentration
C_{meas}	Measured dialysate concentration
SD	Standard deviation
SR	Serine racemase
SHMT	Serine hydroxymethyl transferase
PDMS	Poly(dimethylsiloxane)
PFD	Perfluorodecalin
IS	Internal standard
Arc	Arcuate nucleus of the hypothalamus
POMC	Proopiomelanocortin
α-MSH	α-melanocyte-stimulating hormone
ACTH	Adronenocorticotropic hormone
MCR3	Melanocortin-3 receptor
MCR4	Melanocortin-4 receptor
BNST	Bed nucleus of the stria terminalis
PVH	Paraventricular nucleus of the hypothalamus
PVT	Paraventricular nucleus of the thalamus
DMH	Dorsomedial hypothalamic nucleus
AP	Antertior-posterior
ML	Mediolateral
DV	Dorsoventral
PEI	Polyethylenimine
RMSD	Root-mean-square deviation
PFDS	1H,1H,2H,2H-perfluorodecyltrichlorosilane

Abstract

Improving our understanding of the central nervous system necessitates developing techniques capable of making neurochemical measurements in the complex extracellular environment of the brain within living animal models. Microdialysis is a method in which a semipermeable membrane is implanted into the brain and snapshots of the chemical content surrounding the probe are collected and analyzed offline using a variety of analytical assays. Liquid chromatography-mass spectrometry is a powerful method for separation and detection of biomolecules in dialysate. The aim of this thesis is to improve microdialysis collection and analysis using liquid chromatography-mass spectrometry by improving quantification, analysis speed, and simplicity of operation. A method was developed for the analysis of 26 neurochemicals in dialysate with comparable figures of merit at 30% of the analysis time of previous reports. The methods are applied to the study of addiction and regulation of amino acid metabolism in the brain.

Determining absolute *in vivo* concentrations from analysis of dialysate is challenging because the mass transport processes in the extracellular space have unknown effects on probe recovery. Several methods for calibrating microdialysis *in vivo* have been implemented, though all require assumptions regarding calibrant mass transport or sacrifice of temporal information. Retrodialysis of stable-isotope-labeled forms of endogenous compounds can be used for accurate recovery calibration without losing temporal resolution. We applied this method to the study of dopamine in rat models of

cocaine addiction and as a result were able to differentiate between groups with different self-administration experience and correlate this to behavioral indicators of addiction. Microdialysis calibration was also utilized for accurate basal measurement of serine, glycine, threonine, alanine, glutamate, and γ-aminobutyric acid in mice. A comparative study was performed which demonstrated a 25% decrease in extracellular D-Ser levels in ASCT1-KO animals.

Benzoyl chloride derivatization of neurochemicals prior to LC-MS/MS analysis improves the assay; however, derivatizing large sample sets is labor intensive and prone to error. Moreover, collecting small fractions (≤ 1 min) presents challenges to benzoylation accuracy and precision. The development of a novel microfluidic device for automated, on-chip benzoylation is described. This method yielded similar limits of detection, repeatability, and linearity to offline derivatization. The platform was successfully implemented for quantitation of basal and potassium/bicuculline-stimulated neurochemicals in awake rats.

In vivo neuropeptide monitoring presents challenges due to low extracellular concentrations and poor microdialysis recovery. A capillary liquid chromatography-mass spectrometry assay for the quantitation of sub-pM levels of three neuropeptides believed to be released by proopiomelanocortin neurons: α-melanocyte-stimulating hormone (1-13), α-melanocyte-stimulating hormone (1-12), and [des-acetyl] α-melanocyte-stimulating hormone is described. An *in vivo* study of mice showed that extracellular levels of the three isoforms were below our limits of detection. Our methods will be adapted for future use in measuring other neuropeptides in dialysate.

Chapter 1: Introduction

Motivation

Our understanding of the complexities surrounding the function and regulation of the human central nervous system is often limited by the analytical tools available for making chemical measurements of the extracellular environment. While studying cultured cells or tissues *in vitro* significantly reduces the burden placed on assays, resulting data generates an incomplete picture of biological processes. Rather than attempting to recreate all aspects of the cellular environment, measurements can be made *in vivo*, or directly within intact model organisms. Although this approach makes fewer assumptions and produces more biologically relevant data, it requires more advanced assays capable of measuring biomolecules in complex matrices often at trace concentrations. Furthermore, in order to compare results across experimental groups and between studies, methods for making quantitative absolute extracellular measurements are necessary. The thesis work presented here is focused on applying techniques for measuring absolute *in vivo* concentrations, developing methods for making extremely sensitive measurements of trace biomolecules, and automating the collection and preparation of biological samples.

Cellular communication in the brain is achieved through the release of signaling molecules which diffuse through the extracellular space and act upon specialized receptors on adjacent neurons. These molecules are categorized by their role as neurotransmitters or neuromodulators. Neurotransmission encompasses synaptic transmission in which small

molecules are released by the presynaptic neuron, diffuse across the synaptic cleft, and act at receptors on the postsynaptic neuron. Neurotransmitters directly elicit either an excitatory (depolarization) or inhibitory (hyperpolarization) state in the postsynaptic neuron. Rather than directly producing excitatory or inhibitory events, neuromodulators can alter synaptic transmission of groups of neurons across larger distances with a longer course of action largely through a process known as volume transmission[1]. Volume transmission describes a mode of cellular communication in which diffuse extrasynaptic chemical messengers travel via diffusion and/or convection across large distances. This term encompasses both synaptic overflow and extrasynaptic release[2]. While small molecule neurotransmitters may be utilized by neurons for both neurotransmission and neuromodulation, larger signal molecules such as peptides are often confined to the latter. In certain cases, both small molecule and peptide neurotransmitters are co-released from the same neuron[3].

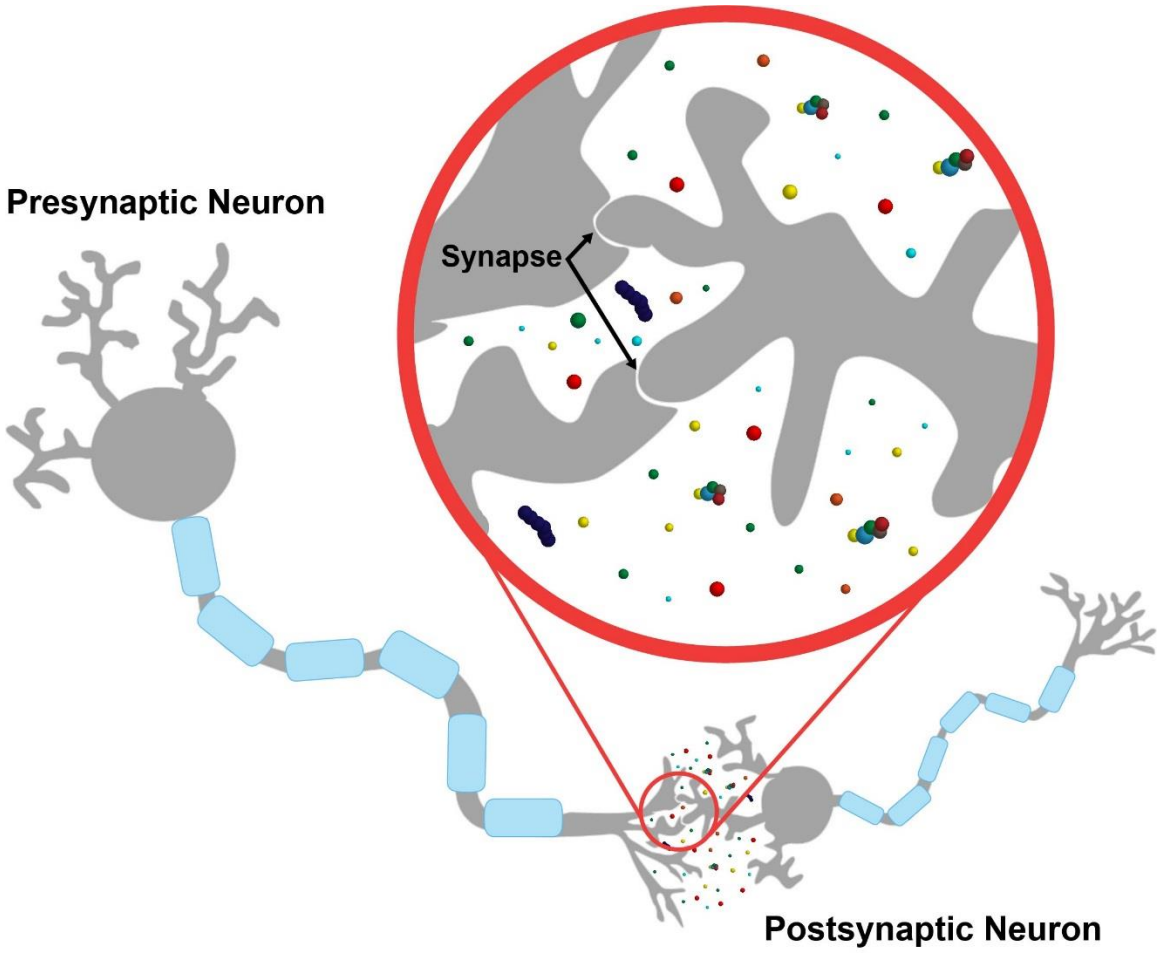

Figure 1-1: Illustration of neurotranmission. Neurons can release neurotransmitters into snapses for rapid, discrete communication or directly into the extracellular space for more dispersed signaling. A variety of signaling molecules are utilized including amino acids, gaseous molecules, monoamines, trace amines, purines, and peptides.

Dysregulation of neurotransmitter systems produces a variety of neurodegenerative diseases such as Parkinson's disease[4] and Alzheimer's disease[5] as well as psychological disorders including addiction[6]. Furthermore, pharmaceuticals can exert influence over complex biological pathways by altering neurotransmitter, precursor, and metabolite levels. Gaining insight into such mechanisms, studying neuropathology, and investigating complex brain structures and functions requires techniques capable of generating rich chemical information from within intact organisms (*in vivo*).

Microdialysis Sampling of Neurotransmitters

One such method for generating *in vivo* samples of the extracellular neurochemical environment is microdialysis. First adopted in its modern form by Ungerstedt and Pycock in 1974 for the study of dopamine circuits in the rat brain, microdialysis involves implanting a semipermeable membrane into the tissue of an intact organism[7]. The membrane is continually perfused with a buffer of similar ionic strength to that of the tissue such as artificial cerebrospinal fluid (aCSF). Molecules present in the extracellular space that fall below the membranes molecular weight cutoff (MWCO) are able to diffuse into the dialysis stream according to their respective concentration gradient across the membrane.

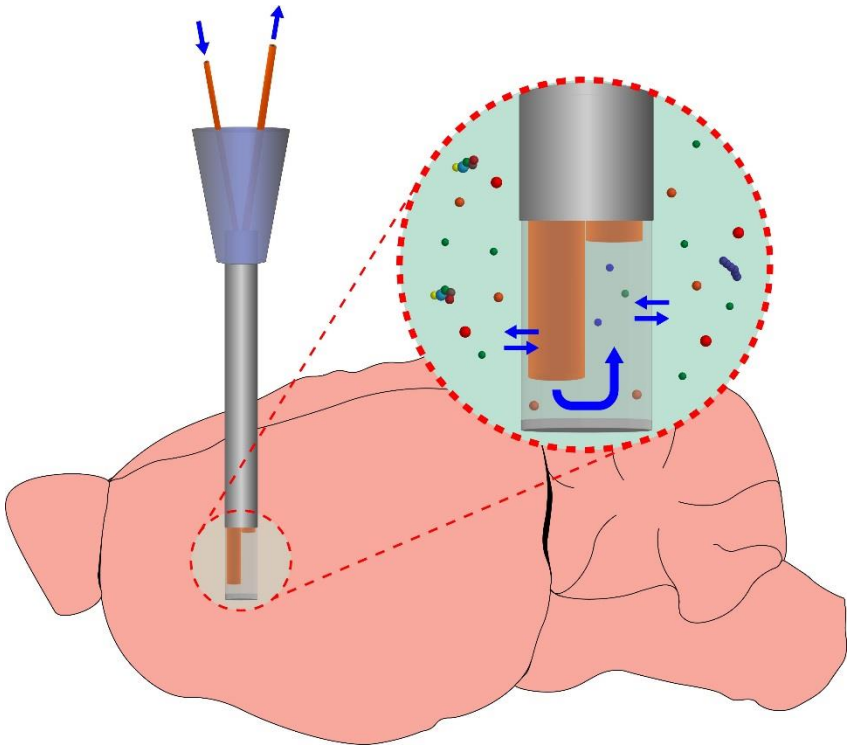

Figure 1-2: Schematic of microdialysis probe in a rodent brain. Microdialysis probes are implanted into the brain of rodents and can be sampled from while the animal is awake and behaving. Molecules below the MWCO can freely diffuse across the dialysis membrane while macromolecules are excluded. This results in a relatively clean sample that can be analyzed via a variety of analytical techniques.

Samples are collected at the outlet of the probe at time points determined by the volume of sample required for analysis as well as the desired temporal resolution. Each sample represents a discreet snapshot of the extracellular chemical environment around the probe. Because samples are collected offline as opposed to making *in situ* measurements, such as in fast-scan cyclic voltammetry, it is possible to couple to a wide variety of analytical techniques. This results in the freedom to choose a technique with appropriate analytical sensitivity, specificity, and throughput. As well as allowing for the study of a broad range of biomolecules, microdialysis also functions as a clean-up step capable of removing a significant proportion of the proteinaceous content of cerebrospinal fluid prior to collection.

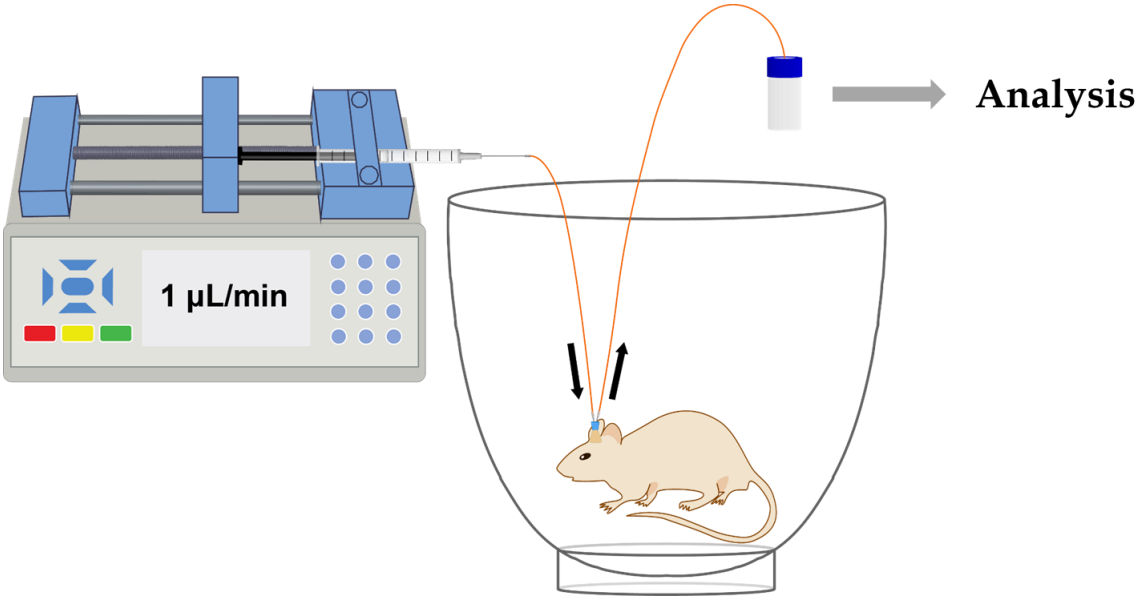

Figure 1-3: Microdialysis in awake rodents. Using a syringe pump aCSF is perfused through the microdialysis probe at a flow rate of 1 µL/min. Samples are collected offline and can be analyzed using an appropriate analytical method.

Several limitations of microdialysis sampling should be considered before its use. Although it is not possible to sample directly from a single synapse due to their small size

(~20 nm)[8], microdialysis samples represent a balance of a variety of neurotransmitter sources (synaptic and extrasynaptic release) and sinks (uptake and metabolism). Skepticism was initially present resulting from the potential for a large percentage of the neurotransmitter sampled to be from blood from damaged tissue or from non-neuronal cells. Studies that followed demonstrated a wide variety of neurotransmitters measured in dialysate arose mainly from neuronal secretion[9–12]. Tissue damage during and after probe implantation is well documented to slightly reduce the ability of microdialysis to accurately represent *in vivo* dopamine concentrations[13–16]. To address this, two major avenues have been pursued with some success, pharmacological mitigation of probe damage and probe miniaturization. Aside from improving biocompatibility of materials used for implantation, the most promising approach for reducing tissue microglial activation due to probe insertion has been use of the corticosteroid dexamethasone[17–20]. Though promising for improving dopamine terminal activity adjacent to the probe, it has yet to be tested for a variety of neurotransmitters. To date most of the success with miniaturizing sampling probes has been with microfabricated push-pull probes[21,22]. Unlike microdialysis probes, push-pull probes do not utilize membranes and the perfusate is in direct contact with the tissue. In one instance, a microfabricated microdialysis probe was used for sensitive measurement of a panel of 17 neurotransmitters[23].

Key considerations when using microdialysis sampling include spatial resolution, temporal resolution, and recovery. Spatial resolution correlates inversely with the sampling area of a probe. Temporal resolution is determined by two factors: the rate at which adequate sample volumes can be generated and the degree of sample broadening due to analyte diffusion and laminar flow in post-collection tubing. Both spatial and temporal

resolution are limited by the sensitivity of the analytical method as well as the recovery of the desired analyte. Relative recovery, or extraction efficiency (EE), is defined by the following equation:

$$\text{Extraction Efficiency} = \frac{C_{\text{measured}}}{C_{\text{endogenous}}} \quad \textbf{(1-1)}$$

where $C_{measured}$ corresponds to the analyte concentration in the dialysate and $C_{endogenous}$ is the concentration in the tissue. While delivering perfusate at higher flow rates through the probe leads to higher temporal resolution and absolute recovery (total mass of analyte at probe outlet), the relative concentration of analyte at the outlet of the probe decreases. Because only at very low flow rates (<<500 nL/min) can equilibrium be achieved across the membrane, it is often necessary to strike a balance between a flow rate high enough to preserve temporal information yet low enough to enable sufficient recovery for the available analytical method.

The most popular techniques for analyzing dialysate involve a separation such as capillary electrophoresis or liquid chromatography paired with one of several detection methods including ultraviolet absorbance (UV), laser-induced fluorescence (LIF), electrochemical detection (ED) or mass spectrometry (MS). Capillary electrophoresis (CE) enables rapid separation of charged molecules in an electric field. This separation method is advantageous in that it is rapid, sample requirements are low, and it is sensitive when paired with LIF detection. These traits make CE ideal for fast analysis of multiple amino acids in a single separation[24,25]. CE is also the most popular technique for online workflows because analysis time matches well with sample collection (~30 s – 5 min fractions). One

of the main drawbacks to CE-LIF is its limited analyte scope due to requisite derivatization protocols such as o-phthaldialdehyde/β-mercaptoethanol, which target only primary amines[26]. Although gaining popularity, hyphenating CE with MS detection has required significant advances addressing technical difficulties and robustness that have not hampered pressure-driven separations[27].

For studies investigating a broad range of target neurochemicals, high performance liquid chromatography (HPLC) offers both versatility and sensitivity. HPLC operates on the basis of analyte retention resulting from varying degrees of interaction (adsorption/partition/ion-exchange) with a stationary phase under pressure-driven flow. The two most popular modes for neurotransmitter analysis are reversed-phase liquid chromatography (RPLC) and hydrophilic interaction liquid chromatography (HILIC). In RPLC, analytes are retained based on their relative hydrophobicity, or more specifically lipophilicity, as they partition between a polar mobile phase (generally aqueous) and nonpolar stationary phase (e.g. C4 – C18). HILIC uses normal-phase stationary phases with reversed-phase mobile phases utilizing a retention mechanism which may simultaneously include partition, adsorption, and ion-exchange[28,29]. Both separation modes operate using solvents and flow rate regimes compatible with electrospray ionization (ESI), allowing for use with mass spectrometry detection in addition to optical techniques. While HILIC enables increased retention of small, polar analytes over RPLC, it has been limited by low sensitivity[30] and long analysis times[31].

RPLC is the most robust separation method commonly employed and offers separation times on the minute timescale of microdialysis fraction collection. It is well-suited for neuropeptide separations because of their high retention factor. Small molecule

neurotransmitters, on the other hand, are challenging because they tend to elute at or near the dead time along with inorganic salts and other high-concentration small biomolecules. While both LIF and ED detection are used for high sensitivity measurements, MS detection is unrivaled in specificity and versatility. MS is capable of direct detection of many neurochemicals and tandem MS (MS/MS) adds a degree of specificity. Moreover, isotopically-labeled internal standards can be used for improved precision and accuracy.

Liquid Chromatography-Mass Spectrometry Analysis of Neurochemicals

As discussed previously, one of the main challenges faced in measuring small molecule neurotransmitters and metabolites is their separation from the biological matrix components found in dialysate. One successful approach for improving reversed-phase retention for neurochemical is the use of ion-pairing agents such as tetrabutylammonium or alkyl sulfates[32]. The major drawback for using such agents is their incompatibility with MS detection because of ESI suppression and significant buildup on ion optics which can drastically reduce MS sensitivity. Volatile ion-pairing agents have been used, but still show significant reduction in sensitivity with only moderate gains in separation efficency[33]. Shi et al. demonstrated a system for online elimination of ion-pairing using two anion exchange columns which can be regenerated in an alternating fashion[34]. They were able to double the throughput of such a method but analysis time still remains at the high end of fraction collection (20 min) and requires multiple ion exchange columns.

One widely used approach is to derivatize target neurochemicals, rendering them less polar and increasing retention on traditional C18 columns. A variety of reagents have been successfully employed for improved chromatographic performance of polar compounds. The reagent(s) used are highly dependent on the functionalities of the target

compounds and offer a variety of attributes capable of aiding in analysis[35]. Among such reagents, few are capable of labeling more than a single class of neurochemicals. Both dansyl chloride[36] and benzoyl chloride (BzCl)[37] have proven useful for reacting with phenols and amines. Dansyl chloride is a sulfonyl chloride which reacts with primary amines, secondary amines, and phenol hydroxyl groups under elevated temperatures (e.g. 60˚C) for reaction times on the order of 15 min[38]. Benzoyl chloride is characterized by similar reactivity at ambient temperatures on the second timescale[37]. Additionally, BzCl is not light sensitive and is commercially available for use as isotopically labeled internal standards.

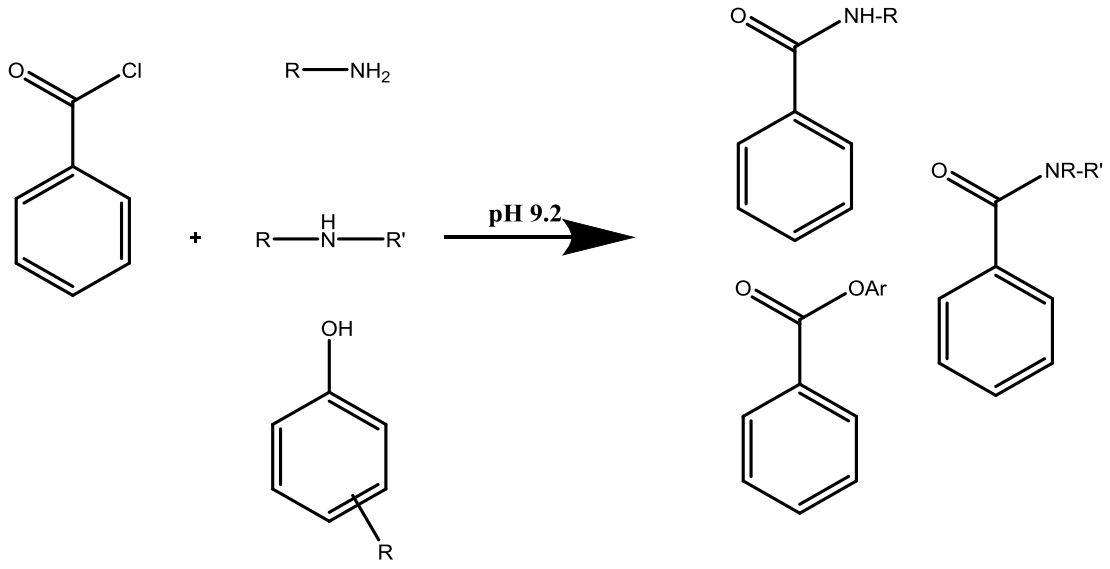

Figure 1-4: Benzoyl chloride derivatization reaction scheme. BzCl reacts with compounds possessing primary amines, secondary amines, and phenols via the Schotten-Baumann reaction[39,40]. This reaction has been applied to UV, fluorescence, and more recently, MS detection[41].

BzCl derivatization was first used in conjunction with HPLC-MS for the measurement of 17 widely studied neurochemicals in 2012 by Song et al[37]. In 2016, Wong et al. expanded the method to a 20 min, 70-compound assay with biologically relevant

limits of detection (LoD) for all analytes[42]. They were also able to successfully apply the method to detection of neurochemicals in other biofluids such as human serum and in fly tissue homogenate.

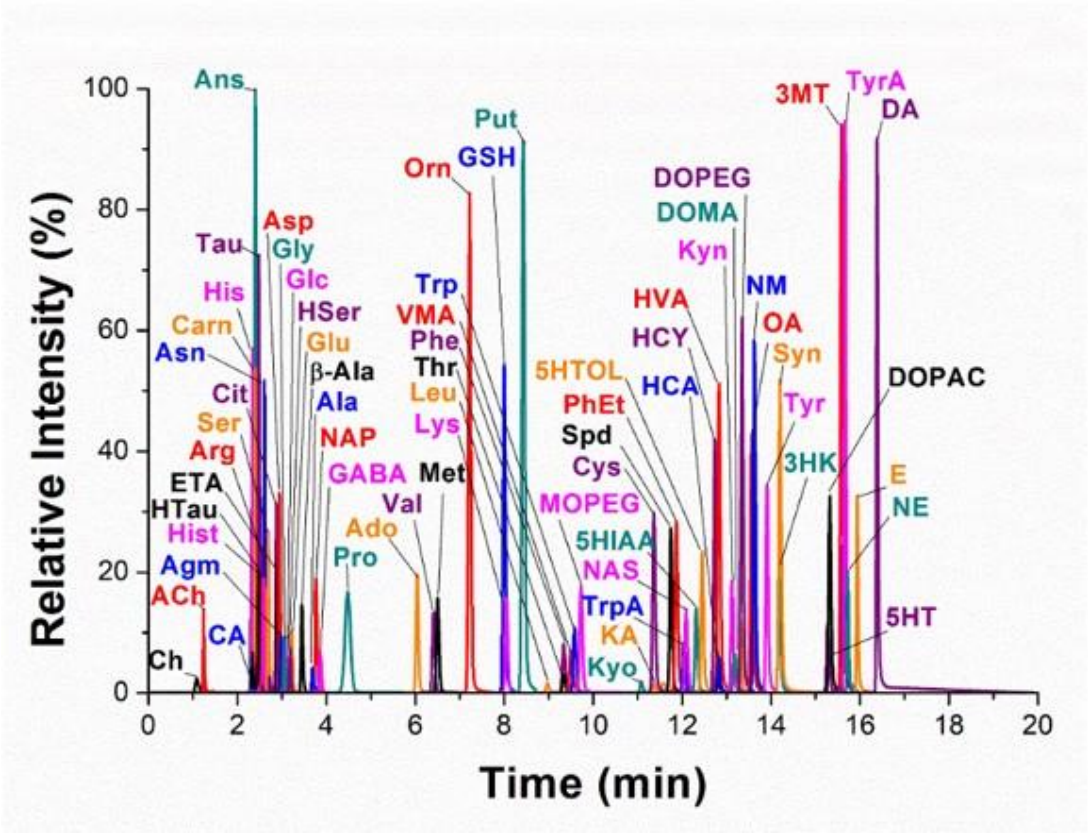

Figure 1-5: Reconstructed ion chromatogram of 70 Bz-analytes analyzed from 5 μL in a 20 min run. Most analyte LoDs were well below physiological concentrations in cerebrospinal fluid. Some analytes such as acetylcholine (ACh) and choline (Ch) were not labeled with BzCl but were still measured with high sensitivity. Reprinted with permission from Wong, J.-M. T. et al. J. Chromatogr. A 2016, 1446, 78. Copyright 2016 Elsevier.

To improve upon this derivatization scheme, one of the aims of this thesis is to automate sample preparation by generating benzoylated neurochemical products in a continuous stream on a microfluidic device. Such a device would reduce sample handling and could lead towards improving temporal resolution as well as integration into an online analysis platform coupled to UHPLC-MS.

Absolute Quantitation of Neurochemicals in Dialysate

As mentioned earlier, recovery describes the relationship between the neurochemical concentration in the extracellular space and at the outlet of the microdialysis probe. Since standard microdialysis flow rates are > 0.5 μL/min, equilibrium is never fully established between the tissue being sampled and the dialysate stream. From this we can infer that analyte concentration in dialysate ≠ analyte concentration in tissue. The result is a more complex picture of recovery that includes analyte flux through several differentially resistive media. Bungay et al. first described microdialysis recovery as process dictated by mass transport through the target tissue, the microdialysis membrane, and the dialysate using the following equation[43]:

$$\text{Recovery} = 1 - \exp\left(\frac{-1}{Q_d(R_d + R_m + R_e)}\right) \quad \textbf{(1-2)}$$

where Q_d is volume flow rate, and R is the resistance to mass transport of the dialysate ($_d$), membrane ($_m$), and the extracellular space ($_e$), respectively. Although this equation is a useful theoretical framework for considering the factors affecting recovery, it is only possible to determine recovery for a specific set of parameters using empirical methods. R_d is dictated by the concentration gradient across the probe membrane. Membrane resistance (R_m) relates to three membrane characteristics: surface area, pore size, and surface chemistry. Increasing the membrane length increases recovery by increasing probe surface area, but spatial resolution decreases as the membrane length increases. When sampling from the rodent brain, probes are 1 – 4 mm in length in order to distinguish between small, adjacent brain regions. Pore size dictates the MWCO of a membrane, or the rough mass cutoff above which analytes are not free to diffuse through the membrane in appreciable

concentrations. This can be used as a tool to exclude large biomolecules, often simplifying analysis. The final factor influencing R_m is the chemical composition of the membrane. In general, membrane polymers that cause analyte adsorption through electrostatic and hydrophobic interactions limit recovery. The resistance of the extracellular space to mass transport, or R_e, is highly variable between different tissues because it encompasses all biological and physical processes that affect analyte diffusion through the tissue. These include whether or not there is bulk flow in the tissue as well as its inherent tortuosity. Furthermore, complex biological processes such as release, reuptake, and degradation all affect an analyte's ability to reach the probe.

In light of the difficult nature of predicting recovery even between probes in the same study, several methods for calibrating probe recovery have been developed. The most straightforward and least accurate calibration procedure, termed *in vitro* recovery, is done by placing the sampling probe in a stirred vial of the target analyte and comparing the concentration in the vial to that at the outlet of the probe. Using *equation (1-1)* the extraction efficiency of the membrane and be determined. This approach is inaccurate because it isolates the effect of membrane permeability and does not account for R_e. Additionally, because the brain has no bulk fluid flow *in vitro* recovery often over approximates *in vivo* recovery. A second approach is to simply reduce the flow rate enough that equilibrium is reached across the membrane and recovery is ~100%. This requires flow rates below 500 nL/min and although it yields accurate concentrations nearly all temporal information is lost because of the length of time it takes to collect enough dialysate for analysis. This loss can be overcome through the use of CE, which is capable of analyzing extremely small volumes, or oil segmentation. Oil segmentation preserves temporal

resolution by dividing the dialysate stream into sample droplets separated by an immiscible phase, thus preventing mixing during storage and transportation. The "no-net flux" method uses retrodialysis, or diffusion of molecules in the perfusate out of the probe *in vivo*. Different analyte concentrations are perfused through the probe and the dialysate concentration at the outlet is measured. When the concentration infused matches that of the tissue there will be no-net flux of analyte into or out of the probe. By generating a curve comparing the known amount of analyte infused with the difference at the outlet of the probe an accurate measurement of the tissue concentration can be extrapolated[44].

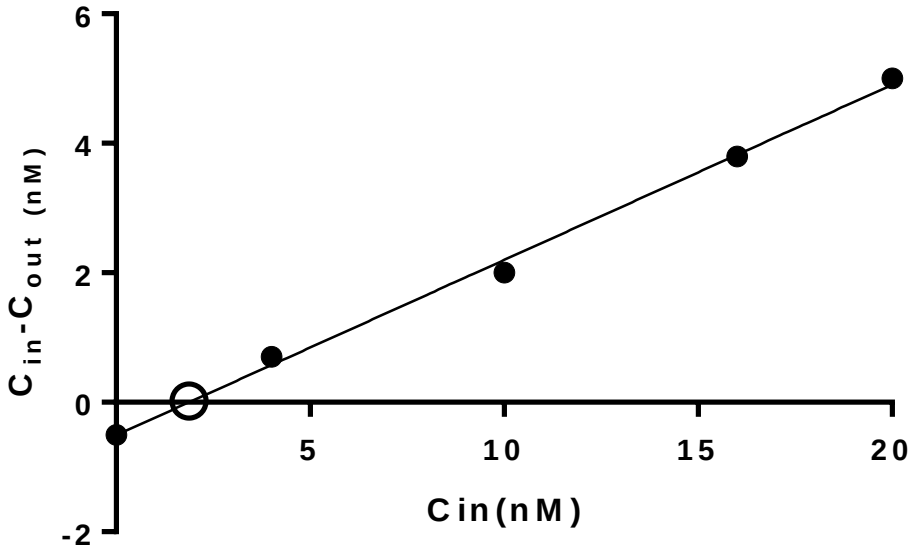

Figure 1-6: Theoretical *in vivo* no-net flux curve. The difference between the known concentration of analyte in the perfusate (C_{in}) and the concentration in the dialysate (C_{out}) is plotted against C_{in}. The slope of the curve is equal to the EE of the probe and the x-intercept, denoted by ○, is equal to the concentration of the analyte in the tissue surrounding the probe.

While accurate, no-net flux calibration does not allow for measurements of any chemical changes below the hour timescale. It is used most often when dynamic information about the system can be forfeited for a small number of accurate basal measurements. Retrodialysis of a nonendogenous chemical is used in the last calibration method. In this case, a calibrant with similar size and chemical properties not found *in vivo* is infused through the probe. The ratio of calibrant at the inlet and outlet of the probe are then considered to be the EE for the endogenous analyte. This method allows for the dynamic calibration of probe recovery on a sample-by-sample basis. Not only can recovery be controlled for, but changes in recovery can also yield interesting information about the health of the tissue and certain biological changes. This method operates on the assumption that calibrant loss accurately approximates analyte recovery. Another important consideration is that processes such as analyte metabolism and reuptake do not necessarily affect the calibrant in the same fashion as the endogenous analyte. Mass spectrometry detection enables stable-isotope-labeled (SIL) analyte to be used for calibration because of its ability to distinguish mass differences between analyte and calibrant. Furthermore, while the endogenous concentration of the labeled form is 0, it has the exact same chemical properties of the endogenous chemical. As a result, both metabolic and reuptake effects on recovery are accounted for. This has previously been used to investigate drug recovery and metabolism[45,46]. More recently, SIL calibration has been adopted for accurate dynamic measurement of glutamate (Glu) and dopamine (DA) in the rat nucleus accumbens[47]. They were able to show that the relative loss of $^{13}C_6$-DA was equivalent to the recovery of ^{12}C-DA and the calculated recovery agreed with no-net flux recovery experiments. Additionally, they showed that infusing SIL Glu and DA did not affect the endogenous

concentrations and were able to capture pharmacologically driven recovery changes for more accurate measurements of stimulated neurotransmitter release. One of the aims of this thesis is to apply SIL DA calibration to the study of drug addiction and another expands the method to include calibration of basal amino acid levels.

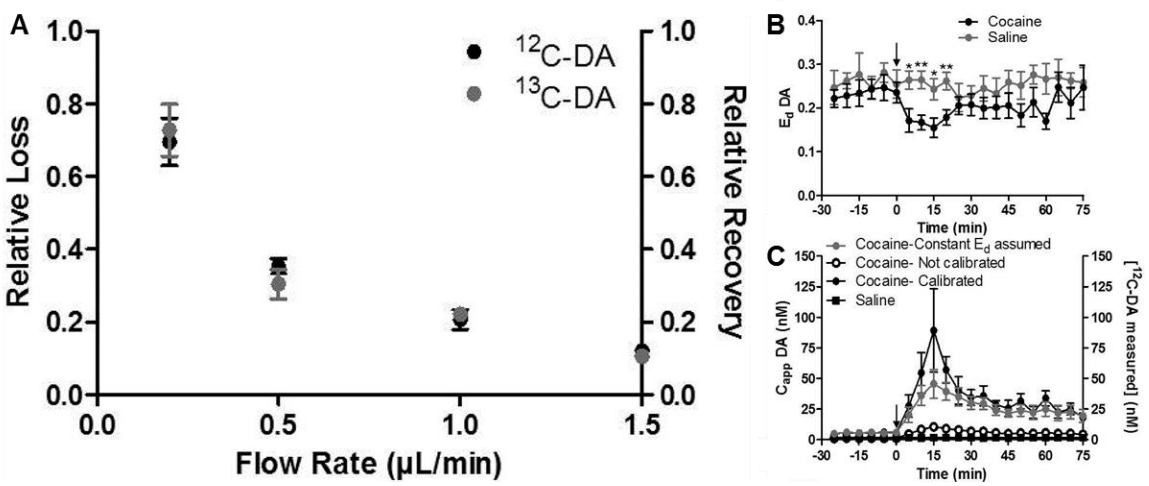

Figure 1-7: Method validation for *in vivo* SIL microdialysis calibration. A) Strong agreement between loss of SIL DA from probe and relative recovery of ^{12}C-DA from a stirred vial experiment across a range of flowrates. B) Demonstration of change in EE of ^{13}C-DA during administration of cocaine, a dopamine reuptake blocker. C) Assuming constant EE significantly underestimated absolute extracellular concentration, or C_{corr} by as much as 50%. Reprinted with permission from Hershey, N. D.; Kennedy, R. T. ACS Chem. Neurosci. 2013, 4 (5), 729. Copyright 2013 American Chemical Society.

Sensitive Neuropeptide Measurement in Dialysate

The amount of structural variability found in neuropeptides helps make them the most diverse class of signaling molecules in the central nervous system. Apart from the number of possible permutations of sequences from 3-50 amino acids, post-translational modifications also help to expand the total – yet undefined – number of signaling peptides. Aside from their diversity, neuropeptides have a few key features that help separate them from traditional neurotransmitters and make *in vivo* measurements more challenging. They are synthesized in the cell nucleus and packaged in the endoplasmic reticulum before being transported down the axon towards the nerve terminal. Modifications throughout this

process can lead to multiple subtly different peptide products from the same peptide precursor. High specificity is therefore required in order to distinguish between such neuropeptide isoforms. Whereas small molecule neurotransmitters are rapidly released in response to brief stimuli, neuropeptides generally require prolonged stimulation[48] and have longer lifetimes in the extracellular space. Small concentrations of neuropeptides are thus able to exert influence across large distances, necessitating the use of high sensitivity analytical methods to capture dynamics. Microdialysis recovery is limited by both peptide size (low diffusion coefficients) and their propensity for nonspecific adsorption to polymers (e.g. cellulose) commonly used for microdialysis membranes. Choosing an appropriate membrane material has become a key aspect of successfully sampling neuropeptides.

Radioimmunoassays and enzyme-linked immunosorbent assays have been used for neuropeptide measurements in dialysate largely due to their exceptional (often sub-pM) detection limits[49,50]. While sensitive, these methods require large volumes of dialysate (> 20 μL), which can be detrimental when studying neuropeptide concentration dynamics. Both assays also have limited specificity arising from the nature of the antibody-antigen binding on which they rely. Crosstalk among neuropeptide isoforms can constrain the use of such assays to qualitative work when multiple modified forms of a peptide sequence exist. As with small molecules, HPLC-MS/MS enhances peptide sequence specificity but is generally limited to analysis of concentrations in the high pM and greater. Capillary LC-MS (cLC-MS) utilizes column inner diameters (ID) less than 1 mm and sub-μL/min flow rates for improved sensitivity. The large gain in sensitivity arises from two factors: large volumes of well retained peptides can be effectively concentrated onto small ID capillary

columns and low flow rates improve analyte electrospray ionization efficiency[51]. Ion trap instruments can be operated in MS^n mode for added specificity and higher signal/noise. Haskins et al first used a two-pump system for rapid isocratic loading and gradient elution of leucine and methionine-enkephalin yielding a 2 pM (1.8µL injected) LoD[52].

In recent years much work has been done to improve neuropeptide recovery to enable sub-pM detection limits for a variety of neuropeptides[53–56]. One of the aims of this thesis is to measure the three endogenous isoforms of α-melanocyte-stimulating hormone in the mouse hypothalamus *in vivo* using microdialysis coupled offline to cLC-MS.

Dissertation Overview

The aim of this thesis is to improve upon previously developed analytical methods for neurotransmitter measurements in dialysate and apply them to novel biological studies. Work was also done towards automated sample preparation and its application to manually intensive workflows.

In **Chapter 2**, SIL microdialysis recovery correction was used for the study of extracellular dopamine levels in rat models of cocaine addiction. An improved UHPLC-MS/MS method for monitoring benzoylated neurochemicals was developed and validated against previous iterations. The method was then used to monitor 26 neurochemicals in 3 min dialysate fractions. By recovery correcting [DA] a hyper-responsive dopaminergic state was identified in the nucleus accumbens core of only animals with intermittent cocaine access experience. Elevated dopaminergic response to cocaine-administration was shown to positively correlate with behavior measures of addiction.

In **Chapter 3**, SIL microdialysis recovery correction was applied to serine, glycine, alanine, threonine, glutamate, and GABA for the study of the alanine-serine-cysteine-threonine transporter-1 (ASCT1). The study represents the first application of SIL recovery correction for serine, glycine, alanine, threonine, and GABA. *In vitro*, an inverse relationship was found between dialysis flow rate and calibration accuracy. A flow rate of 0.5 μL/min was chosen for the study because it more accurately corrected for recovery than 1 μL/min. A full understanding of this phenomenon will require a more in-depth study on recovery. A comparison of SIL-corrected absolute amino acid concentrations between WT and ASCT1-KO mice was used to refine a model for *in vivo* transporter function.

The aim of **Chapter 4** was to develop a microfluidic device for automated benzoyl chloride derivatization of neurochemicals and couple it to a microdialysis probe implanted in awake rats. An all-glass device was chosen because of its broad chemical compatibility and resistance to fouling in biological fluids over PDMS. To further protect against surface fouling and reagent precipitation, perfluoroalkyl surface modification was performed. Triphosphate was used to chelate divalent metal cations out of aCSF for reducing precipitation as carbonate salts. Calibration curves were generated on-chip and yielded figures of merit comparable to offline derivatization. Both *in vitro* step-change experiments and *in vivo* 75 mM K^+ stimulations in an anesthetized rat demonstrated rapid rise times for relevant neurochemicals. When returning to blank/baseline concentrations, carryover was found to increase as a function of Bz-analyte hydrophobicity. On-chip benzoylation was then applied to bicuculline retrodialysis in the striatum of awake rats. Both ACh and Ch increased with bicuculline administration, suggesting GABAergic inhibition of cholinergic interneurons found in the striatum. Future work will move toward improving surface

coverage of perfluoroalkyl modification and increasing Bz-analyte solubility with the aim of reducing carryover.

In **Chapter 5** a capillary liquid chromatography mass-spectrometry assay was developed for the measurement of sub-pM levels of POMC peptides *in vivo*. Sample injection parameters were optimized including organic content, pH, and carrier peptides. A packed emitter tip column configuration was adopted to improve peak shapes and sensitivity. High linearity and sub-pM LoDs were achieved for α-MSH, α-MSH (1-12), and [des-acetyl] α-MSH. A pilot microdialysis study of 19 mice and 2 rats was performed in which a single mouse had measurable levels of α-MSH. This system will be applied for future study of additional neuropeptides such as Met/Leu-enkephalin, oxytocin and vasopressin.

Chapter 2: *In Vivo* Microdialysis Calibration Using Stable-Isotope-Labeled Dopamine for the Study of Models of Cocaine Addiction

Reproduced in part from Kawa, A. B.; Valenta, A. C.; Kennedy, R. T.; Robinson, T. E. Eur. J. Neurosci. 2019, 50, 2663-2682. Copyright 2019 John Wiley and Sons. Specific contributions from Valenta to this work include development of LC-MS method, analysis of dialysate samples, and data analysis of samples.

Introduction

Understanding the progression from recreational drug taking behavior to addiction is critical in the development of therapeutics aimed at targeting the underlying physiological changes associated with addiction. For nearly 60 years researchers have been investigating behavioral and neurochemical changes associated with addiction-like behaviors in animal models[57]. Although such models can never fully realize the complexity of social, behavioral, and physiological factors that interact to produce addiction in humans, well designed animal models are capable of providing valuable approximations. Historically, self-administration of drugs by rodents has been considered a model of addiction. Over the past 20 years, significant doubt has been cast as to the translatability of such results to compulsive drug-taking behavior[58]. The resulting focus on better models for human addiction has driven researchers to devise new systems which are capable of discerning between compulsion and other motives for self-administration.

The most widely used model for self-administration in rodents, known as the long-access model (LgA), was introduced in 1998[59]. Evidence showed that a single hour of cocaine access per day (ShA) led to stable drug intake while 6 hour sessions lead to

escalation of drug intake. LgA has since been associated with increased motivation for drug as well as drug-seeking in the face of adverse-consequence[60]. Furthermore, studies focusing on the neurobiological consequences of LgA have shown that it causes a decrease in dopamine neurotransmission in the nucleus accumbens core[61,62]. One major assumption when using LgA is that the key factor in producing addiction-like behavior is the amount of drug exposure. Zimmer et al set out to create a model of addiction that would more closely approximate characteristic intermittency between and within bouts of drug use in humans than the LgA model[63]. Rather than 6-hour daily sessions with unlimited drug use, animals were subjected to twelve 5 min trials alternated with 25 min timeout periods. This model, known as intermittent-access (IntA), leads to rapid spikes in brain cocaine levels during the 5 min trial rather than sustained high levels as in LgA. Interestingly, IntA experience produced greater motivation for cocaine than LgA despite a significant decrease in the total drug consumption. More than just drug-seeking motivation, IntA is also more effective at producing a range of other addiction-like behaviors including drug-seeking despite negative consequences and high reinstatement of drug-seeking behavior[64–68]. It has been shown that LgA blunts DA neurotransmission while IntA increases cocaine inhibition of DA uptake as well as electrically evoked DA release in brain slices[61]. This sensitization of dopaminergic neurotransmission is believed to be a key factor in development of cocaine-seeking behavior. To date there have been no *in vivo* studies comparing the effects ShA, IntA, and LgA self-administration models of cocaine addiction on neurotransmission. There has also been no investigation of potential alterations of dopamine metabolites and other fast neurotransmitter systems. Microdialysis coupled offline to benzoyl chloride

derivatization and LC-MS, as reported previously[37,42], offers a platform capable of sensitive neurotransmitter measurements *in vivo*.

To quantify basal and stimulated DA concentrations *in vivo*, microdialysis recovery must be corrected using one of the recovery calibration methods. The method capable of generating quantitative dynamic information regarding absolute extracellular DA concentration is SIL calibration with ^{13}C-DA[47]. In these experiments EE can be calculated using the following equation:

$$\mathrm{EE} = 1 - \frac{[\mathrm{d_4{-}DA_{out}}]}{[\mathrm{d_4{-}DA_{in}}]} \qquad \textbf{(2-1)}$$

Since EE for d_4-DA is equivalent to endogenous DA, we can calculate the apparent extracellular concentration by rearranging equation **(1-1)** to give:

$$[\mathrm{DA_{endogenous}}] = \frac{[\mathrm{DA_{measured}}]}{\mathrm{EE}} \qquad \textbf{(2-2)}$$

A modified UHPLC-MS/MS method was used with work on further improving detection limits[69]. Figures of merit including LoD, linearity (R^2), peak area percent RSD, and peak capacity were compared with previously published 8 and 20 min gradient methods for BzCl-labelled neurochemicals[37,42].

Methods

Chemicals and Reagents

All chemicals were purchased from Sigma Aldrich (Saint Louis, MO) unless otherwise noted. Acetonitrile was purchased from Honeywell Research Chemicals through VWR (Radnor, PA). NaCl, KCl, $MgSO_4$, $CaCl_2$, and sulfuric acid were purchased from Fisher Scientific (Fairlawn, NJ). DOPAC, 3-MT, sodium phosphate dibasic and sodium tripolyphosphate were purchased from Acros Organics (Geel, Belgium). 5-HT was purchased from Alfa Aesar (Ward Hill, MA). d_4-DA, ACh, and Ch were purchased from CDN Isotopes. Stock solutions of 2 mM Tyr; 5 mM Ado; 10 mM 5-HT, NE, DA, NM, 3-MT, Epi, L-DOPA, 5-HIAA; 20 mM Hist, GABA, 5-HTP, Asp, HVA, Gly, Glu, DOPAC, Phe, Ser; 25 mM ACh; 40 mM Tau; 100 mM GSH, Gln, Glc; and 1 M Ch were prepared in HPLC grade water. A calibration standard mixture was prepared by diluting stocks into aCSF consisting of 145 mM NaCl, 2.68 mM KCl, 1.4 mM $CaCl_2$, 1.0 mM $MgSO_4$, 1.55 mM Na_2HPO_4, and 0.45 mM NaH_2PO_4 adjusted to pH of 7.4 with 0.1 M NaOH. Calibration curves were prepared in aCSF with 250 μM ascorbic acid for the following concentration ranges: 0.1 – 20 nM for 5-HT, NE, DA, NM, 3-MT, Epi and L-DOPA; 0.25 – 50 nM for ACh; 0.5 – 100 nM for Hist and d_4-DA; 1-200 nM for GABA, 5-HIAA, 5-HTP, GSH, and Ado; 2 – 400 nM for Asp; 2.5 – 500 nM for HVA and Tyr; 0.01 – 2 μM for Glu, Gly, Phe, Ch, and DOPAC; 0.02 – 4 μM for Tau; 0.025 – 5 for Ser, 0.05 – 10 μM for Gln, 0.25 – 50 μM for Glc.

Behavior and Self-Administration Acquisition

A total of 50 Sprague-Dawley rats weighing 250-275 g were housed on a reverse 12-hr light/12-hr dark cycle. All testing was done during the 12-hr lights off period. Rats

were acclimated for 1 week before surgery. They had access to food and water ad libitum until two days before the first day of self-administration. Food was then restricted to maintain stable bodyweight throughout the remainder of the experiment. Behavioral testing was conducted in a 22 x 18 x 13 cm test chamber within a sound-attenuating cabinet. There were two nose poke ports, one active and one inactive, on the left and right side of the chamber. A red light was at the top, center of the back wall opposite the nose ports. A syringe pump mounted on the outside of the chamber was used to deliver cocaine through a catheter port on the rat's back. Med Associates software was used for recording all measurements. An intravenous catheter was surgically implanted into the right jugular vein for cocaine infusions.

Rats were given 7 days to recovery from surgery before self-administration acquisition began. Rats were placed in the behavior chamber and after 2 min the house light was extinguished signaling the beginning of the session. Nose pokes in the active port resulted in an intravenous infusion of cocaine hydrochloride (NIDA) dissolved in 0.9% sterile saline (4 mg/kg per infusion in 50 μL delivered over 2.5 s) on a fixed ratio-1 (FR-1) schedule. Infusions were paired with a cue light. Nose pokes into the inactive port did not lead to infusions but were recorded. The length of each session was determined by the total number of infusions rather than by time to ensure that all animals received the same amount of cocaine and cue exposure. Rats experienced 9 total sessions: two 10-infusion sessions, three 20-infusion sessions, and four 40-infusion sessions. A 6 hour limit was placed on each session and sessions were terminated if the animal did not self-administer the requisite number of times. If a rat did not make twice as many active as inactive port nose pokes on

each of the last three sessions they were given three additional sessions. If they failed in the three additional sessions they were excluded.

A threshold procedure was performed in order to determine certain behavioral economic metrics. Q_0 is the amount of consumption when the price (nose pokes) is very low, P_{max} is the maximum price an animal is willing to pay to maintain the level of consumption of Q_0, and α is the slope of the demand curve or how susceptible consumption is as the price is increased (inversely proportional motivation)[70]. During 110-min sessions cocaine was self-administered on a FR-1 with the dose decreasing every 10 min on a quarter logarithmic scale. After this procedure, rats were assigned to one of the three self-administration groups with limited-access (LimA) representing ShA: LimA (n = 10), LgA (n = 12), and IntA (n = 12). Rats in the LimA group had microdialysis probes surgically implanted as described in the following section. After a 3 day recovery period LimA rats had 3 days of self-administration sessions of 40 infusions.

IntA self-administration procedure consists of 4-hour sessions. During the 5-min drug-available period any nose poke in the active port led to an infusion and a paired cue light. The only period where nose pokes had no effect were during the 2.6 s infusion. The drug-available period was followed by a 25-min period without drug and this cycle was repeated eight times. LgA sessions lasted 6 hr and rats were allowed to self-administer throughout the entire session. The self-administration procedures went on for an average of 5 days/week. The pattern of on and off days was varied to best approximate drug use in humans. After 25 self-administration sessions rats were giving the threshold procedure again. In this case the animals were tested for two days and the results were averaged. Post-threshold testing the rats underwent microdialysis probe implantation. After 3 days of

recovery each rat was given 5 more self-administration sessions. 1-3 days later rats were given the microdialysis test session. A group of LgA and IntA rats was tested for drug extinction and cue induced reinstatement. **Figure 2-1** shows the experimental timeline.

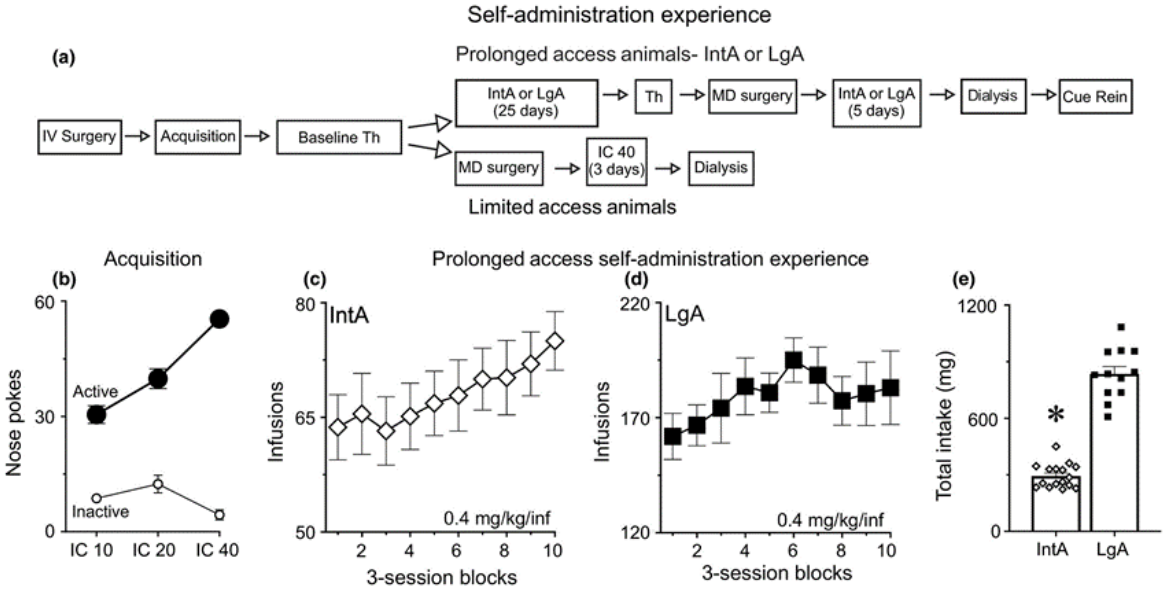

Figure 2-1: Experimental overview and preliminary data. (a) Shows the experimental timeline for each of the three self-administration groups. (b) IntA and LgA groups escalated their intake/session similarly across 30 self-administration sessions. (c,d,e) LgA rats consumed significantly more cocaine than IntA throughout sessions. Each value corresponds to the average ± SEM of three consecutive sessions.

Microdialysis Probe Construction and Implantation

Custom concentric style microdialysis probes were made in house. In brief, two 75/150 (ID/OD) fused silica capillaries were glued into 24-gauge stainless steel tubing that acted as a sheath to be inserted into the guide cannula using epoxy. The length of inlet and outlet capillary extending beyond the sheath tubing were then glued into pieces of 22-gauge stainless steel tubing to act as support. The inlet tubing beyond the other end of the sheath was covered with 18 MWCO dialysis tubing (Spectrum Laboratories, Rancho Dominguez, CA). The dialysis tubing was glued to the sheath and capped at the end using epoxy to yield

2 mm of exposed membrane. CMA 12 guide cannula were implanted directly ventral to the nucleus accumbens core. The coordinates were +1.6 mm anterior, ±1.6 mm lateral, and -6.2 mm ventral to bregma[71]. Cannula were secured using 3 skull screws and acrylic dental cement. At 12-16 hr before the experiment the stylet was removed from the guide cannula and the dialysis probe was lowered into place. Probes were perfused with aCSF at 0.5 μL/min overnight and 4 hours before collection the probe was switched to 1 μL/min of aCSF with 100 nM d_4-DA for *in vivo* probe recovery calibration.

Test Session

All microdialysis fractions collected during the test sessions were 3 min in length at a flow rate of 1 μL/min. A total of 10 baseline (30 min), 20 cocaine available (1 hr), 1 cue presentation (3 min), and 5 post-cue (15 min) fractions were collected. The cocaine available fraction collection did not begin until the animal self-administered a single 1.25 mg/kg cocaine infusion. Once the rat self-administered one infusion, cocaine was no longer available for the duration of the test. During the cocaine available portion of testing the cue light was not illuminated to isolate only the effects of cocaine. During the cue presentation, the cue light flashed 14 times for 2.6 s over a 3 min period. Both inactive and active port nose pokes were recorded throughout the entire experiment.

Neurochemical Analysis using UHPLC-MS/MS

The following reagents were prepared on the day of the experiment: 100 mM sodium carbonate in water, 2% benzoyl chloride in ACN (v/v), and internal standards were prepared in 1:1 ACN:H_2O with 1% H_2SO4 (v/v). Dialysate fractions (3 μL) were collected and 1.5 μL carbonate was added to buffer to pH ~10, 1.5 μL BzCl was added to react with

primary amines, secondary amines, phenols, and sugar hydroxyl groups, and internal standard was added enabling adjustment of pH and organic content for UHPLC injection.

All analysis was done using a Thermo Fisher Vanquish UHPLC interfaced with a Thermo Fisher TSQ Quantum Ultra triple-quadrupole mass spectrometer. Briefly, samples were injected onto a Phenomenex Kinetex C18 column (2.1 mm x 100 mm, 1.7 μm). Mobile phase A consisted of 10 mM ammonium formate and 0.15% formic acid. Mobile phase B was pure acetonitrile. The method flow rate was 600 μL/min and the gradient was as follows: initial, 5% B; 0.01 min, 19 % B; 0.68 min, 26% B; 1.055 min, 75% B; 1.805 – 2.18 min, 100% B; 2.28-3 min, 5% B. The pressure range across each gradient was 350 – 800 bar. The autosampler was at 25˚C while the column was held at 30˚C in still air mode. ESI was used in positive mode with a spray voltage of 2.5 kV. Vaporizer and transfer capillary temperatures were 400˚C. Sheath gas was set to 10 and auxiliary gas was set to 5. The skimmer offset was -1 V and tube lens values were tuned for each individual analyte. The TSQ Quantum Ultra was operated in MRM mode. **Table 2.1** includes SRMs for all compounds analyzed:

Analyte	Precursor (m/z)	Product (m/z)	Collision Energy (V)	Retention Time (min)	Tube Lens (V)
Choline	104	60	17	0.35	58
d_4-Choline	108	60	17	0.35	58
ACh	146	87	13	0.40	53
d_4-ACh	150	91	13	0.40	53
Bz-Tau	230	105	14	0.74	76
$^{13}C_6$Bz-Tau	236	111	14	0.74	76
Bz-Hist	216	95	17	0.77	62
$^{13}C_6$Bz-Hist	222	95	17	0.77	62
Bz-Ser	210	105	17	0.80	65
$^{13}C_6$Bz-Ser	216.1	111	17	0.80	65
Bz-Gln	251	105	19	0.80	63
$^{13}C_6$Bz-Gln	257	111	19	0.80	63
Bz-Asp	238	105	17	0.85	50

$^{13}C_6$Bz-Asp	244	111	17	0.85	50
Bz-Gly	180	105	13	0.88	60
$^{13}C_6$Bz-Gly	186	111	13	0.88	60
Bz-Glc	307	185	14	0.88	73
$^{13}C_6$Bz-Glc	313	185	14	0.88	73
Bz-Glu	252	105	15	0.91	69
$^{13}C_6$Bz-Glu	258	111	15	0.91	69
Bz-GABA	208	105	14	1.10	61
$^{13}C_6$Bz-GABA	214	111	14	1.10	61
Bz-Ado	372	136	27	1.40	76
$^{13}C_6$Bz-Ado	378	136	27	1.40	76
Bz-GSH	516	105	40	1.46	73
$^{13}C_6$Bz-GSH	528.1	111	40	1.46	73
Bz-Phe	270	105	17	1.54	65
$^{13}C_6$Bz-Phe	276	111	17	1.54	65
Bz-5HIAA	250	105	22	1.61	57
$^{13}C_6$Bz-HIAA	256	111	22	1.61	57
Bz-HVA	304	105	16	1.64	66
$^{13}C_6$Bz-HVA	310	111	16	1.64	66
Bz-5HTP	429	279	30	1.65	79
$^{13}C_6$Bz-5HTP	441	285	30	1.65	79
Bz-NM	374	105	35	1.66	73
$^{13}C_6$Bz-NM	386	111	35	1.66	73
Bz-Tyr	390	105	29	1.66	75
$^{13}C_6$Bz-Tyr	402	111	29	1.66	75
Bz-DOPA	510	105	31	1.72	72
$^{13}C_6$Bz-DOPA	528	111	31	1.72	72
Bz-DOPAC	394	105	20	1.73	65
$^{13}C_6$Bz-DOPAC	406	111	20	1.73	65
Bz-5HT	385	264	17	1.74	77
$^{13}C_6$Bz-5HT	397	270	17	1.74	77
Bz-NE	464	105	19	1.75	81
$^{13}C_6$Bz-NE	482	111	19	1.75	81
Bz-3MT	376	105	19	1.76	73
$^{13}C_6$Bz-3MT	388	111	19	1.76	73
Bz-E	478	105	26	1.79	93
$^{13}C_6$Bz-E	496	111	26	1.79	93
Bz-DA	466	105	22	1.86	83
Bz-d_4-DA	470	105	22	1.86	83
$^{13}C_6$Bz-DA	484	111	22	1.86	83

Table 2-1: List of SRMs for total of 26 analytes and their internal standards. Each analyte was tuned at the 600 μL/min and mobile phase composition during elution.

Perfusion with d_4-DA enabled EE to be calculated using equation **(2-1)** in which d4-DA_{out} was the concentration measured in each sample and d_4-DA_{in} was measured by derivatizing the aCSF before, during, and after the conclusion of the experiment to ensure no degradation had occurred. For a subset of the rats, aCSF without d_4-DA was perfused post-experiment. After an hour of perfusing regular aCSF, 3 samples were collected to ensure that inclusion of 100 nM d_4-DA in dialysate had not affected levels endogenous DA (**Figure 2-4**).

Probe Placement

After the microdialysis test session, rats were anesthetized using sodium pentobarbital (270 mg/kg; i.p.) and perfused intracardially with 50 ml of 0.9% saline, followed by 500 ml of 4% paraformaldehyde in 0.1 M phosphate buffer (PB). After being perfused, brains were removed, post-fixed in the same paraformaldehyde solution for 2 hr, then immersed in 20% sucrose and 0.01% sodium azide in 0.1 M PB for 48 hr at 4°C. Coronal sections (40 μm) were cut with a freezing microtome (SM 2000R; Leica), collected in PB, and mounted on to a slide immediately. Sections were imaged at 4× magnification using a Leica DM400B digital microscope to verify cannula placement.

Statistical Analysis

Linear mixed-models were used for behavioral and neurochemical repeated measures data. Because α was not normally distributed all analysis was done on log transformed values. Post hoc Bonferroni corrections were done to compare self-administration procedures between and within groups across both test sessions. Statistical significance was set at $p < 0.05$.

Results

Effect of Self-Administration Model on Behavior

To investigate behavioral differences between self-administration groups, the behavioral economic measures α, Q_0, and P_{Max} were compared. Prior to differentiation into LimA, LgA, and IntA groups, inactive port nose pokes decreased (effect of IC, *F(2,75.1) = 3.5, p = 0.04*) and active port nose pokes increased (effect of IC, *F(2,40.4) = 38.7, p < 0.001*) across self-administration acquisition sessions. There were no differences in acquisition measures after group assignments. As previously reported[64] IntA rats were quickly able to discriminate between drug and no-drug periods. There was a combined (*F(29,70.7) = 4.8, p < 0.001*) as well as separate LgA (*p = 0.02*) and IntA (*P = 0.01*) effect of increasing cocaine intake with self-administration experience. There was a significant difference in the total cocaine intake ((effect of group, *F(1,92.3) = 823, p < 0.001*) with LgA rats consuming an average of 2.8x more than IntA rats.

Threshold testing was done to measure the initial behavioral metrics α, P_{max}, and Q_0. Groups were chosen after this test and there were no group differences for baseline metrics. Interestingly, LgA and IntA experience produced different effects on α. While LgA experience did not significantly alter α (*p = 0.12*), IntA experience significantly decreased α (*p = 0.02*) signaling an increased motivation for cocaine (**Figure 2-2a**). P_{Max}, or the maximum price (in nose pokes) an individual is willing to pay for cocaine infusion, increased in the IntA group (*p = 0.001*) and remained unchanged for LgA (*p = 0.27*). Furthermore, P_{Max} was significantly higher for IntA than LgA (*p = 0.005*). Together, these metrics demonstrate a larger increase in motivation for cocaine stemming from intermittency in drug availability rather than the quantity consumed. When the cost of

cocaine consumption was negligible the preferred level of drug increased from threshold testing with LgA experience ($p = 0.01$) but did not change with IntA experience ($p = 0.25$). A comparison between groups showed a difference after prolonged self-administration experience ($p = 0.03$). This result is consistent with several previously published reports[64,66,67,72].

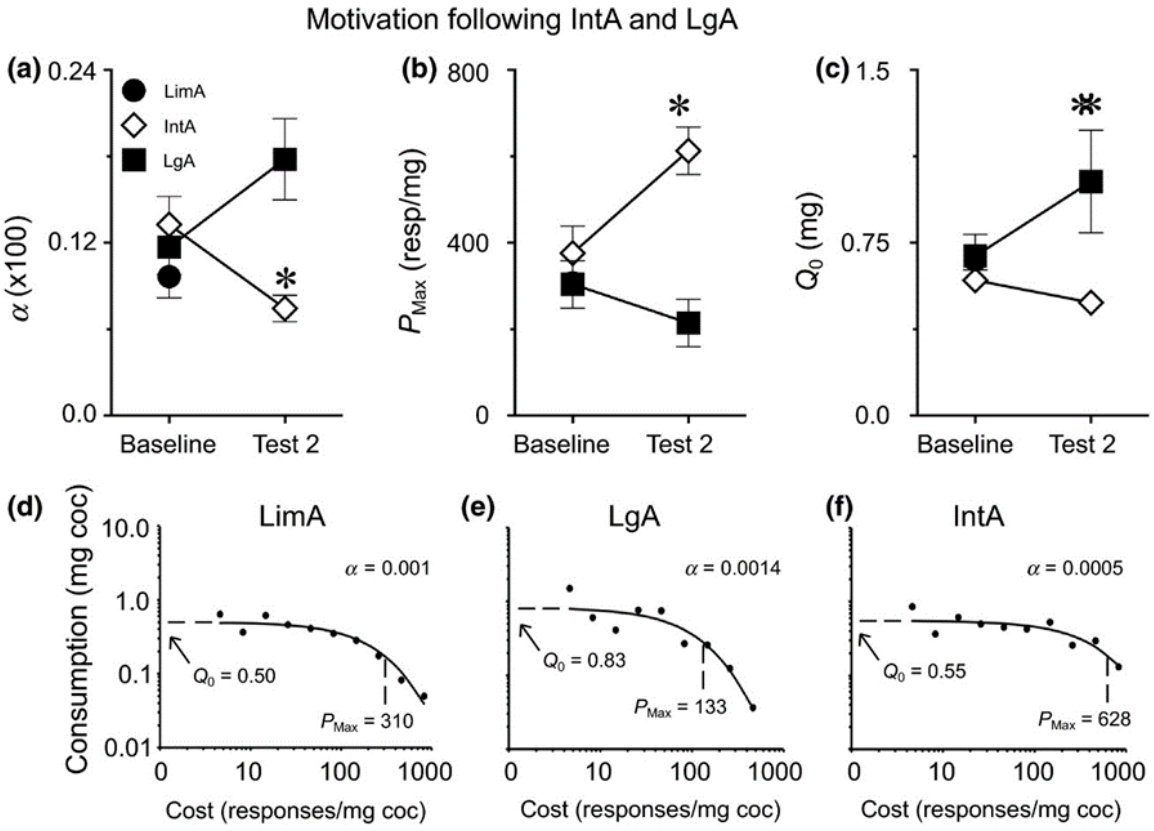

Figure 2-2: Behavioral metric assessment from threshold procedure in different self-administration groups. In (a-c), α, P_{Max}, and Q_0 are compared between LimA, IntA, and Lga baseline and IntA and LgA self-administration experience (Test 2). There were no significant baseline differences between the groups. IntA decreased α (increased demand) (a) while increasing P_{Max} (b). LgA had the opposite effect on both α and P_{Max} but increased Q_0 (c) over IntA. (d-f) show the demand curves for each group. All values are mean ± SEM, * represents significant difference ($p < 0.05$).

Ultra-high Pressure Liquid Chromatography-Mass Spectrometry Assay

To run large sample sets without sacrificing limits of detection, sensitivity, accuracy, and precision for important trace analytes such as DA, 3-MT, and ACh when

compared with previous methods[37,42,69], work was done to improve both the gradient and mass spectrometry conditions (**Table 2-1**). **Figure 2-3** shows a reconstructed ion chromatogram (RIC) summing 25 selected reaction monitoring (SRM) traces (DOPAC is excluded for scale) across the 2 min gradient. Such a method must be capable of both accuracy and precision across a variety of Bz-labeled and unlabeled analytes as well as a broad range of different analyte concentrations (pM – μM).

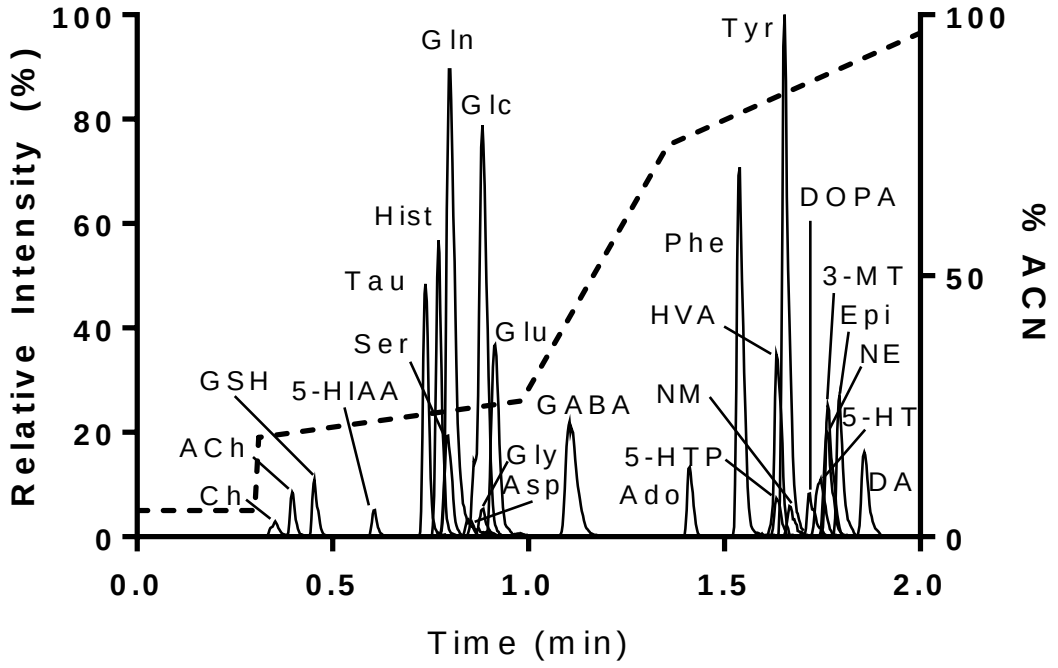

Figure 2-3: RIC of 25 analytes overlaid on gradient adjusted for system volume. Left y-axis is relative intensity normalized to the largest analyte signal, tyrosine. The right axis shows the step gradient across the separation window (dotted line). An extra min of high ACN purging and equilibration is not shown. Concentrations shown span the range between low nM (DA, ACh, 5-HT etc.) and mid μM (glucose).

For comparison with the 20 min gradient, average peak capacity (n_c) was calculated for ACh, GABA, Ado, and DA using the following equation[73]:

$$n_c = 1 + \frac{t_g}{(4\sigma)_{avg}} \quad \textbf{(2-3)}$$

where t_g is the total gradient time or the difference in retention time between the first (Ch) and last (DA) eluting analytes and 4σ corresponds to the peak width. The average n_c was taken across 4 analytes in order to represent a range of Bz-labelled and unlabeled compound classes. For the long gradient the n_c was calculated to be 168 while that of the 2 min was 64. Although there was a substantial drop in peak capacity, a variety of other metrics including LoD, linearity, and % RSD compare favorably with both the original 8 min separation[37] and the 20 min gradient (**Table 2-2**). The average retention time % RSD across all analytes was 0.68 % corresponding to a standard deviation of ± 0.4 s. Including injection equilibration, the total analysis time of each of the three methods are 4 min, 12 min, and 30 min.

	2 Min Gradient			8 Min Gradient[37]			20 Min Gradient[42]		
Analyte	LoD (nM)	RSD	R^2	LoD (nM)	RSD	R^2	LoD (nM)	RSD	R^2
Choline	14	4	0.9986	-	-	-	3	1	0.9997
ACh	4	5	0.9996	0.5	7	0.9963	1	0.7	0.9996
Bz-Tau	7	5	0.9998	250	7	0.9995	3	1	0.9998
Bz-Hist	0.3	5	0.9997	2	13	0.9961	2	3	0.9996
Bz-Ser	140	5	0.9951	250	11	0.9975	70	1	0.9976
Bz-Gln	26	5	0.9993	-	-	-	4	3	0.9998
Bz-Asp	16	8	0.9950	50	10	0.9987	8	1	0.9999
Bz-Gly	100	7	0.9835	500	5	0.9989	30	7	0.9997
Bz-Glc	90	4	0.9901	-	-	-	160	6	0.9997
Bz-Glu	14	4	0.9999	5	8	0.9995	0.3	1	1.0000
Bz-GABA	1	1	0.9997	2	5	0.9989	0.5	2	0.9997
Bz-Ado	0.5	7	0.9860	25	4	0.9974	1	0.2	0.9956
Bz-GSH	1	6	0.9986	-	-	-	10	2	0.9999
Bz-Phe	2	2	0.9996	-	-	-	3	0.8	0.9999
Bz-5HIAA	2	4	0.9942	5	7	0.9999	0.7	0.8	0.9999
Bz-HVA	4	4	0.9992	0.5	4	0.9973	0.6	0.4	1.0000
Bz-5HTP	2	8	0.9981	-	-	-	2	3	0.9996
Bz-NM	0.3	10	0.9995	0.1	2	0.9996	0.08	2	0.9988
Bz-Tyr	13	3	0.9991	-	-	-	4	3	0.9950
Bz-DOPA	0.2	9	0.9920	-	-	-	1	2	0.9999
Bz-DOPAC	1.3	4	0.9991	2	5	0.9973	0.2	2	0.9999
Bz-5HT	0.04	6	0.9922	0.1	4	0.9998	0.4	1	0.9970
Bz-NE	0.1	9	0.9924	0.2	10	0.9997	0.3	2	0.9970
Bz-3MT	0.04	3	0.9950	0.05	1	0.9999	0.2	2	0.9987
Bz-Epi	0.08	6	0.9925	-	-	-	0.3	1	0.9964
Bz-DA	0.08	5	0.9926	0.03	4	0.9981	0.3	3	0.9965

Tables 2-2: Figures of merit comparison for variations of Bz-labeled neurochemical LC-MS/MS methods. LoDs were calculated using the limit of blank equation[74] for the 20 and 2 min variations and 3s/m for the 8 min method. Because the 8 min method had only 17 of the 26 neurochemicals, cells were left blank for analytes not present. The injection volume was 5 μL for both 2 and 20 min gradients, and 9 μL for the 8 min gradient.

Stable Isotope Labeled Dopamine Infusion for Recovery Calibration

As shown in equation (**2-1**) EE can be calculated by infusing a stable-isotope labeled form of the endogenous neurotransmitter. Equation (**2-2**) can then be used to adjust probe recovery point-by-point, correcting recovery across different probes as well as any changes in recovery across the course of the experiment. This ultimately improves the accuracy of all dopamine measurements and enables basal extracellular concentrations to be calculated and compared across animals and groups. In order to demonstrate that 100

nM d_4-DA retrodialysis does not affect endogenous concentrations of DA and its metabolites, 3 dialysis fractions were collected post-dialysis session in which aCSF lacking d_4-DA was infused instead. Regular aCSF was circulated for 1 hour before collection of baseline fractions to ensure clearance of any d_4-DA. As reported previously[47] the presence of d_4-DA had no effect on DA and we further demonstrated that there is no effect on the associated metabolites: 3-MT, HVA, and DOPAC (**Figure 2-4**).

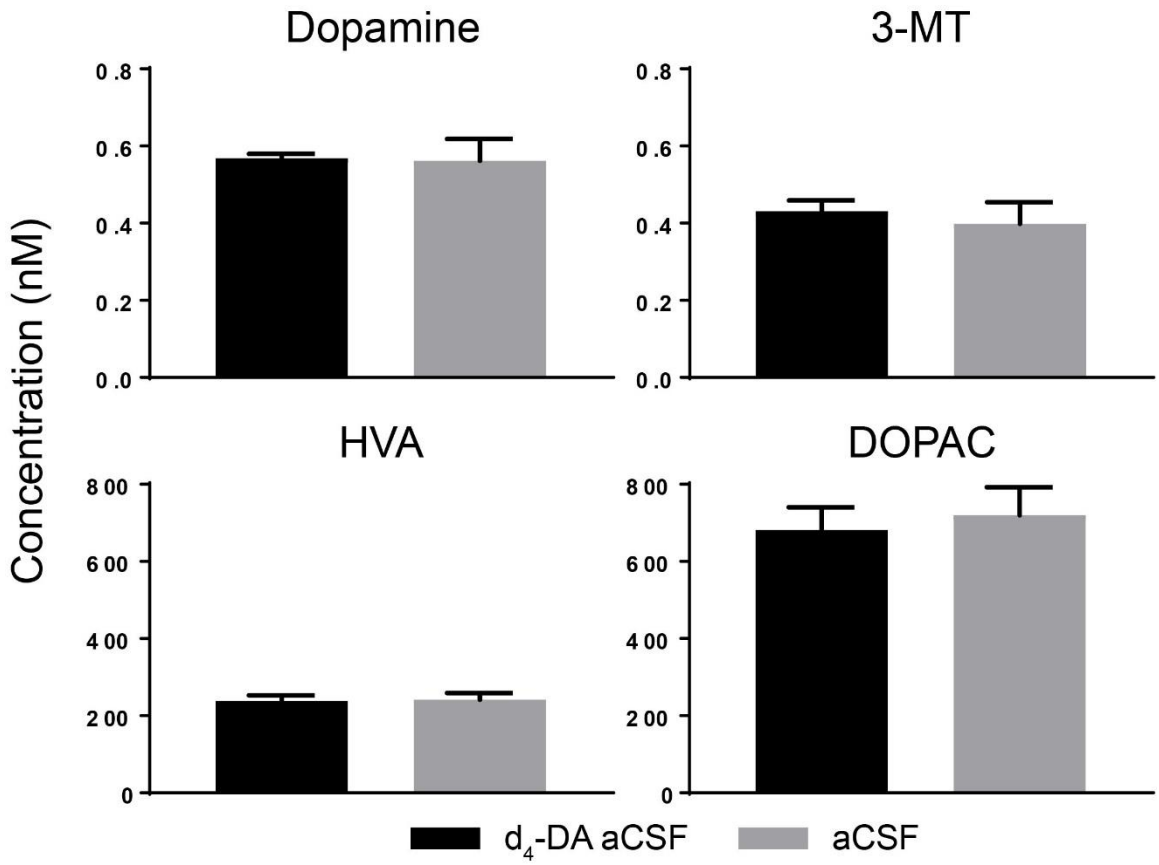

Figure 2-4: Comparison of uncorrected concentrations of DA and its metabolites when infusing aCSF with and without inclusion of 100 nM d_4-DA. Three baseline samples were taken while perfusing standard aCSF after the conclusion of the dialysis test session and with 1 hour for equilibration. Baseline values were taken from the baseline portion of the initial dialysis test. No significance was found for any analyte ($p > 0.1$). Values are mean ± SD.

Because any change in EE would produce a change in the calculated apparent concentration of DA, it was also important that any changes in recovery between groups

be noted. **Figure 2-5** shows a comparison of the sample-by-sample extraction efficiency between different groups. As no significant group differences were observed it can be concluded that any changes in extracellular concentration do not result from changes in probe recovery.

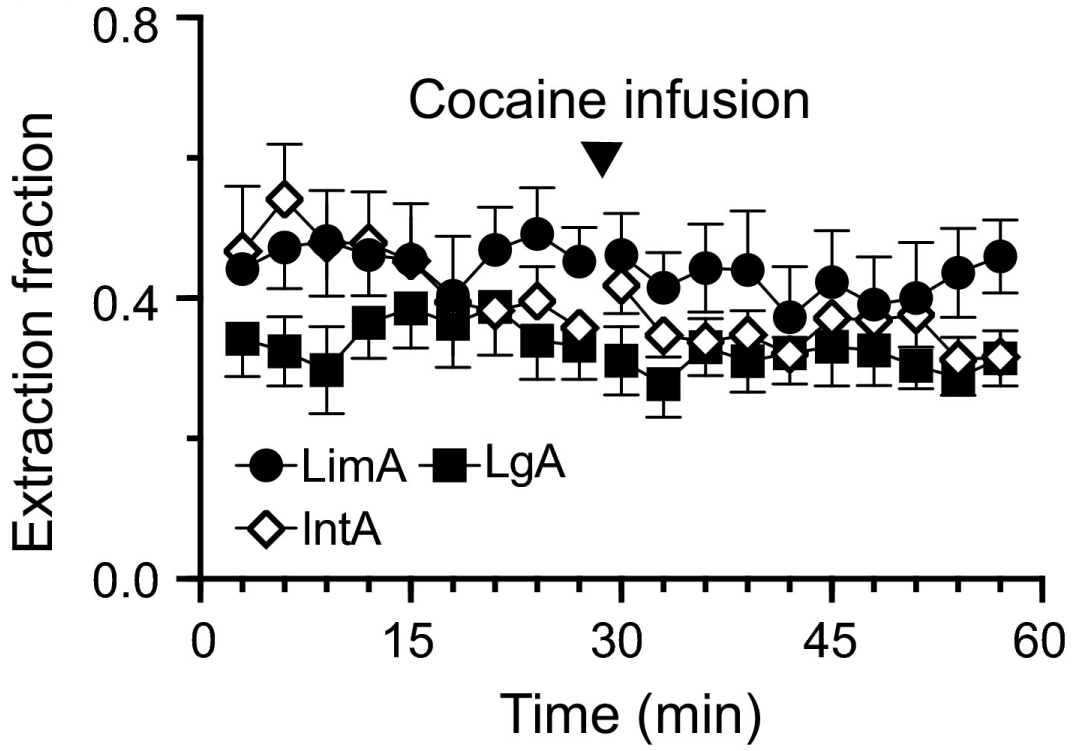

Figure 2-5: Average extraction fraction is shown for each group throughout the session. There were no significant differences within test session or across groups ($p > 0.1$). The triangle represents the point at which a single cocaine infusion was delivered.

To further demonstrate the impact of SIL recovery calibration, **Figure 2-6** shows a comparison between the DA concentration time course corrected and uncorrected for recovery. A larger increase in cocaine-evoked [DA] overflow emerges when correcting for recovery that would otherwise lose significance. Taken together, these results demonstrate the SIL method does not affect the endogenous DA or metabolite concentrations and that it more readily discerns changes in concentrations than uncalibrated methods.

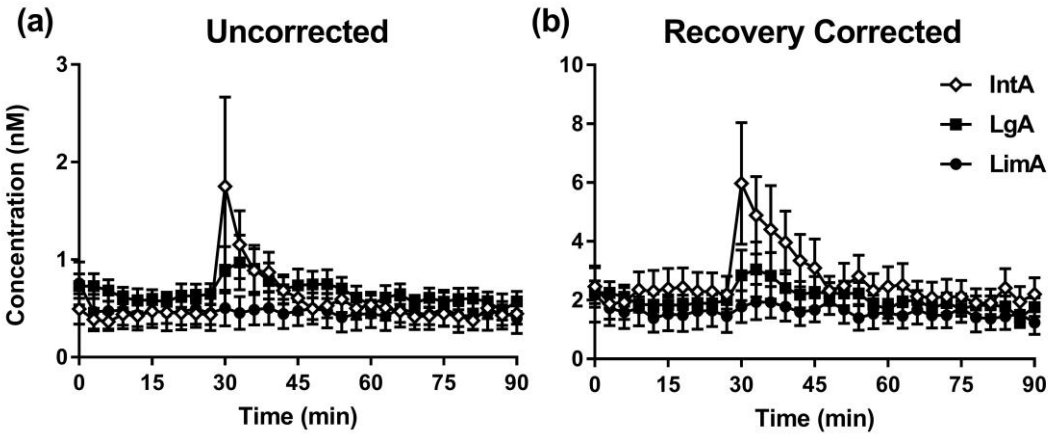

Figure 2-6: Comparison between uncorrected and recovery-corrected [DA] during the dialysis test session. There is no significant difference between IntA and LgA when uncorrected for recovery (a). Correcting for recovery causes differences in cocaine-evoked [DA] between IntA and LgA/LimA to become evident.

Prolonged IntA (but not LgA) Sensitized Cocaine-Induced Dopamine Overflow

Recovery-corrected DA concentrations were compared between groups to investigate group differences in basal and cocaine-evoked DA concentration. After collecting baseline dialysate samples for 30 min, rats were able to self-administer a single 1.25 mg/kg IV injection of cocaine followed by an additional 60 min of collection. Rats immediately nose poked once the session started demonstrating a similar latency for cocaine administration across all groups. When analyzing the 10 baseline samples and the first 10 post-cocaine samples there was a main effect of group ($F[2,326] = 10.2$, $p < 0.001$) with cocaine increasing DA concentration relative to baseline in all groups (main effect of cocaine, $F[1,331] = 8.93$, $p = 0.003$; **Figure 2-7b**). Planned post hoc analysis revealed that the main effect of group was due to a differential response to cocaine infusion. Therefore, we found no self-administration group difference in baseline DA ($p > 0.1$) but the IntA group had a greater increase in DA in response to cocaine than LgA rats ($p <$

0.001) and LimA rats ($p = 0.004$). LgA and LimA did not statistically differ ($p = 0.21$). Although the largest [DA] increase occurred within 3 fractions of infusion, the time to reach peak [DA] had individual variation. As a result, **Figure 2-7b** shows responses aligned to cocaine infusion and **Figure 2-7c** shows all groups aligned to the peak cocaine-evoked [DA] response.

All baseline values were averaged together to show the percent change from baseline in **Figure 2-7d**. There was a main effect of group ($F[2,672] = 6.04$, $p = 0.003$) and cocaine infusion increased [DA] in all groups ($F[1, 673] = 40$, $p < 0.001$). There was a difference in the cocaine-evoked increase in [DA] between the three groups (group x cocaine interaction, ($F[2,672] = 6.04$, $p = 0.003$). Planned post hoc analysis revealed that infusion increased [DA] to a similar extent in LimA and LgA ($p = 0.1$) and to a greater extent in IntA than LimA ($p = 0.016$) and LgA ($p < 0.001$). Active nose pokes in the hour following cocaine infusion were monitored (**Figure 2-7e**) and a one-way ANOVA demonstrated no group effect but a slight trend towards a higher number of responses in IntA animals (effect of group, $F[2] = 2.7$, $p = 0.08$).

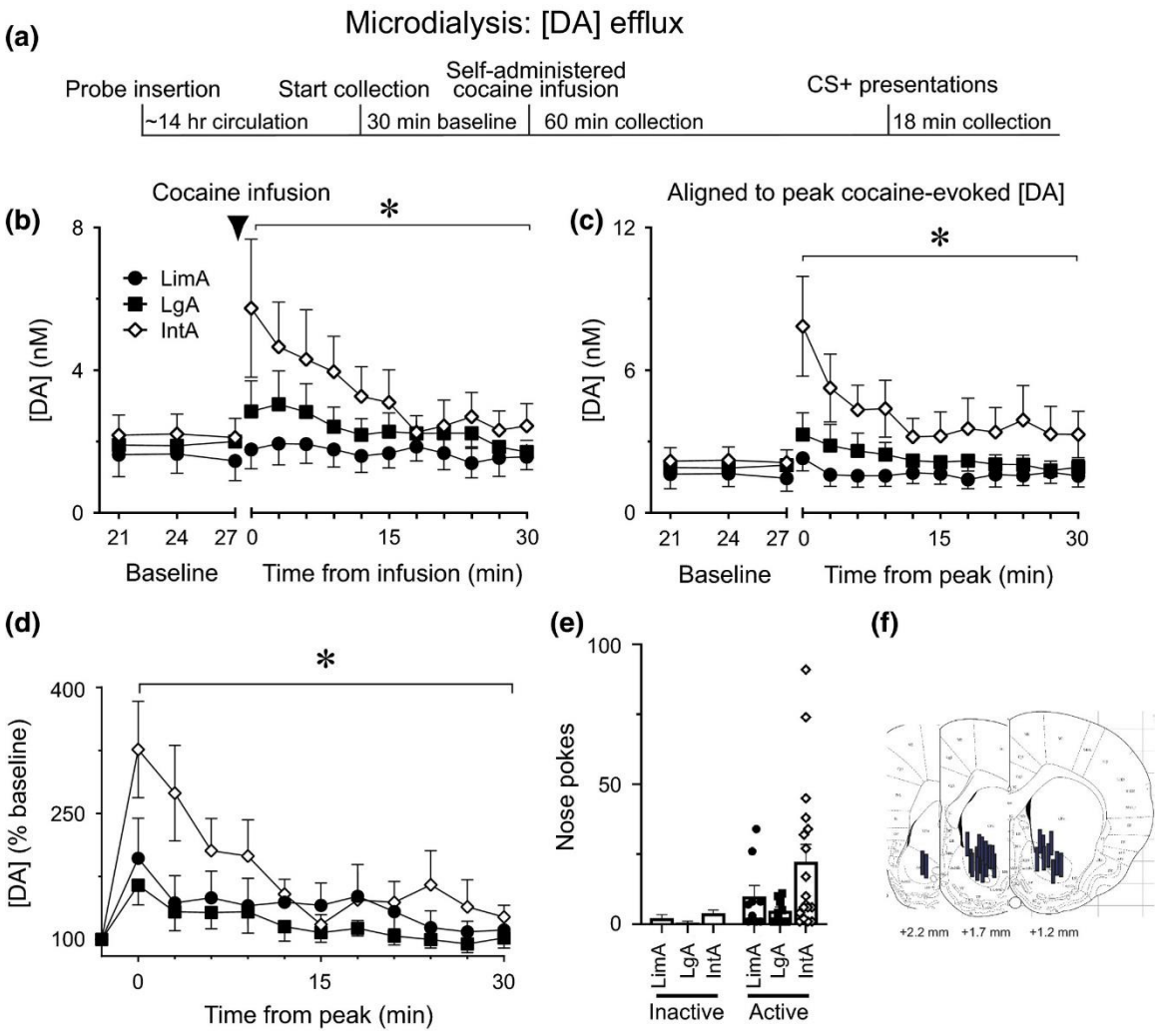

Figure 2-7: The effect of three different self-administration models on cocaine-evoked [DA]. (a) Experimental timeline in which animals were perfused overnight followed by collection of 30 min of baseline samples, 60 min of post-cocaine infusion samples, and 18 mins of conditioned stimulus samples. Conditioned stimulus is excluded because there was no effect on [DA]. (b) Cocaine-evoked [DA] response was higher in IntA than both LgA and LimA. (c) For visualization, groups are aligned to peak cocaine-evoked [DA] to remove individual variability of time to peak [DA]. (d) All baseline values were averaged together and IntA yielded the largest cocaine-evoked [DA] percent increase over baseline. (e) Active port nose pokes following a single cocaine infusion were not significantly different between groups but trended toward higher numbers for IntA. (f) Histological analysis revealed individual probe placements. All values are mean ± SEM. Significance of ($p < 0.05$) was represented with *.

Addiction-Like Behavior as a Predictor of Cocaine-Induced Dopamine Overflow

To investigate the role of DA in motivated behavior we determined the correlation between addiction-like behaviors and cocaine-induced DA overflow. **Figure 2-8** shows the

correlation between peak percent of baseline DA during the test day and three addiction-like behaviors: cocaine-induced nose pokes, P_{Max}, and Q_0 (α not shown). Post-cocaine infusion nose pokes into the active port correlated positively with increase in [DA] percent baseline ($R^2 = 0.14$, $p = 0.03$; **2-8a**). P_{Max}, or motivation for cocaine also positively correlated with [DA] increase ($R^2 = 0.32$, $p < 0.001$; **2-8b**). α also followed a similar trend ($R^2 = 0.13$, $p = 0.04$; data not shown). Preferred level of cocaine-intake at low cost, or Q_0, did not correlate with DA release ($R^2 = 0.07$, $p = 0.17$; 2-7c).

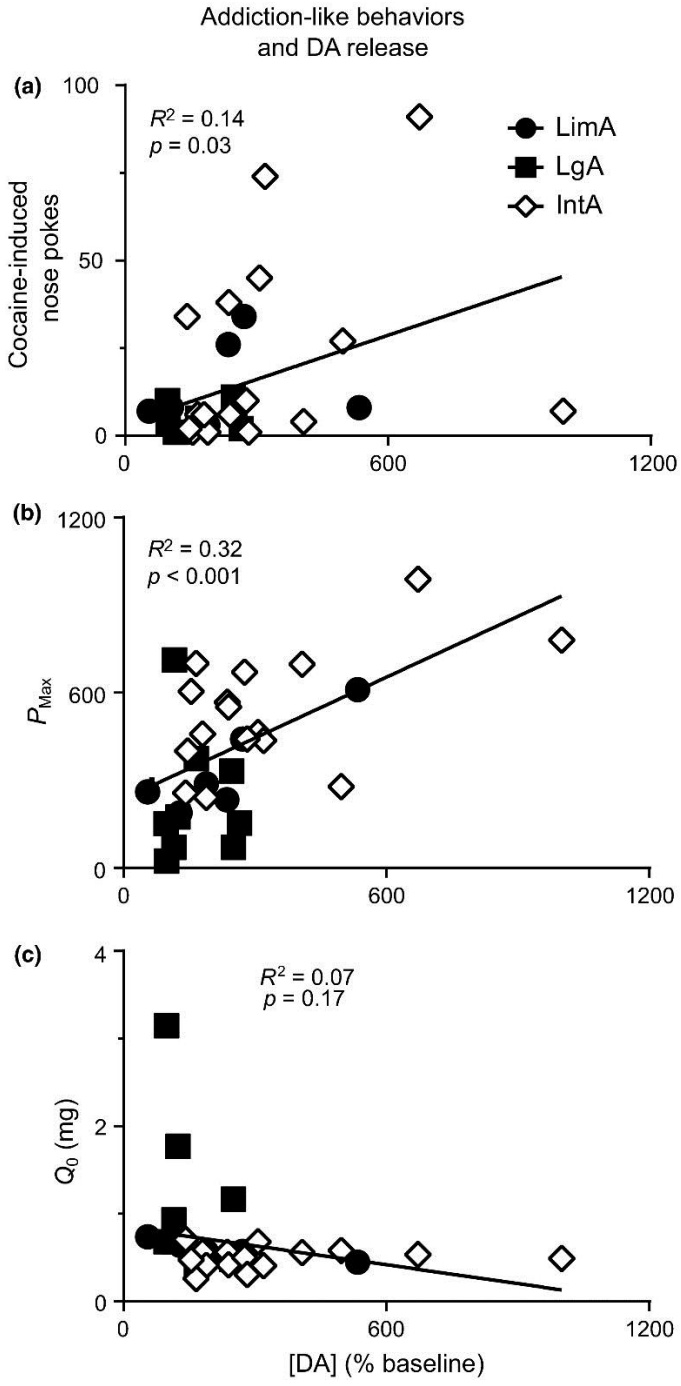

Figure 2-8: Correlation between cocaine-induced increase in [DA] (% baseline) and addiction-like behaviors. Peak [DA] response predicted cocaine-induced nose pokes (a) and P_{Max} (b), but not Q_0 (c), from the final threshold test.

Within groups subjected to prolonged IntA exposure, generally a subset of animals is particularly susceptible to multiple addiction-like behaviors[64,75]. A set of addiction

criteria termed the "IntA Addiction Score" was developed to quantify addiction behavior within the IntA group. Similar scoring metrics have been used for different sets of addiction-like behaviors[64,75,76]. Rats were separated into two groups: animals scoring 2-3 points ("high") and animals scoring 0-1 points ("low"). A point was given to animals falling within the top third of the IntA group on a given behavioral measure (α, active nose port pokes during no-drug period of self-administration session, and cocaine-induced active nose port pokes during dialysis test session). Of a total of 16 IntA animals, 9 were scored low and 7 scored high. Not shown in **Figure 2-9**, low and high groups differed on P_{Max} but not Q_0. High rats also showed a greater cocaine-evoked [DA] than low rats ($p = 0.05$; **9d**). When high rats were compared with low IntA, LimA, and LgA rats there was a larger difference in [DA] percent baseline increase (group × cocaine interaction, $F[2,484] = 19.5$, $p < 0.001$; **9e**).

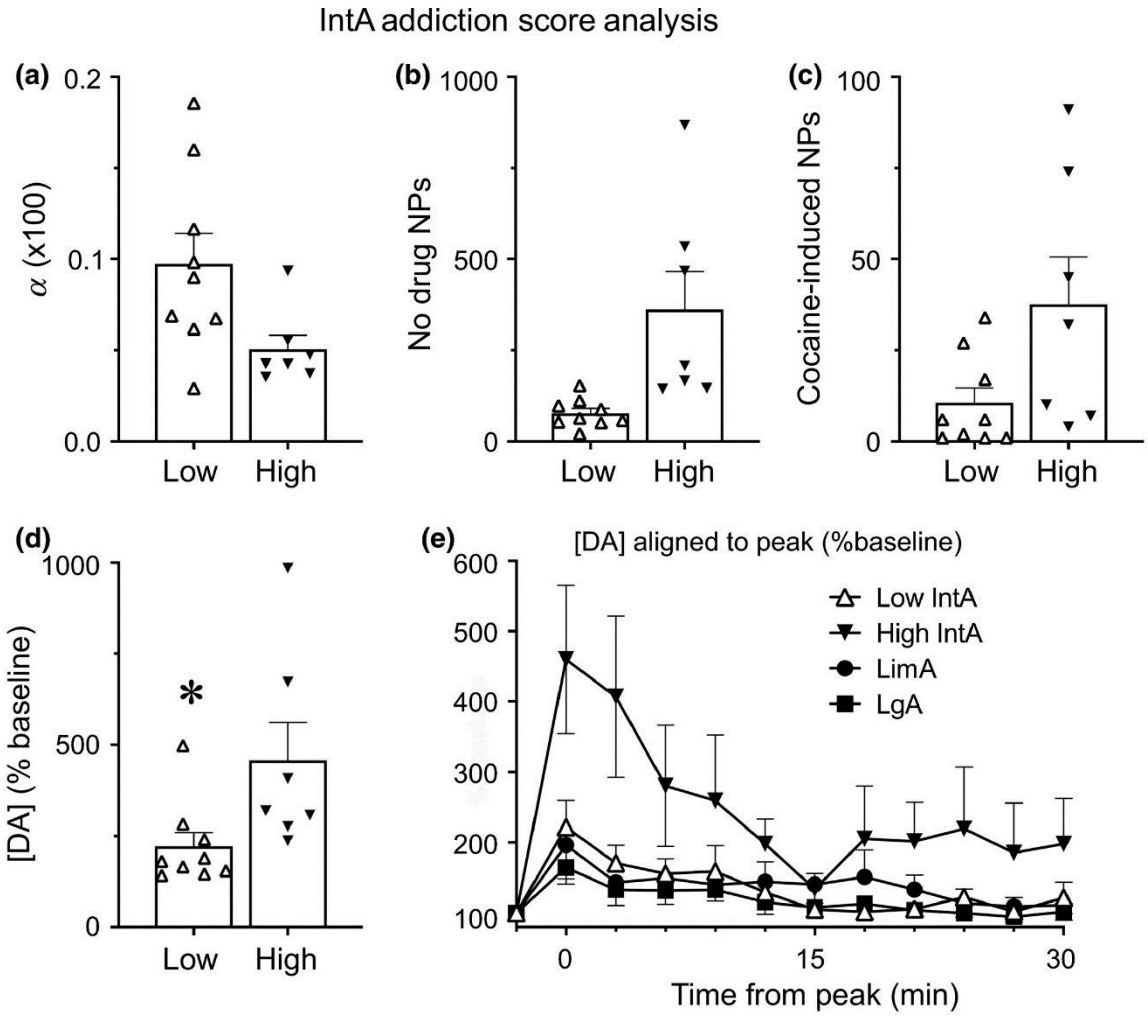

Figure 2-9: IntA addiction score analysis and comparison to cocaine-evoked [DA] release. High IntA were classified as those receiving 2-3 points low IntA rats were those receiving 0-1 point. (a) α determined during threshold testing post-prolonged IntA experience. (b) Active port nose pokes during the no-drug period of IntA sessions. (c) Cocaine-induced active port nose pokes during the cocaine portion of the dialysis test session. (d) High IntA rats had a larger increase in cocaine-evoked percent baseline [DA]. (e) High IntA showed a larger increase in cocaine-evoked [DA] release than LimA and LgA. Values are mean ± SEM. Significance of ($p < 0.05$) represented with *.

Effect of Cocaine Self-Administration on Other Neurochemical Levels

As with DA, there were no group baseline differences in levels of any of the other neurochemicals measured in the UHPLC-MS/MS assay. As a result, all values were normalized to baseline. It is important to note that EE were not calculated for any other analytes such that there is less certainty in group differences with regards to probe recovery.

Both [Glu] (effect of cocaine, $F[1,671] = 3.97$, $p = 0.04$) and [3-MT] (effect of cocaine, $F[1,581] = 10.5$, $p < 0.001$) increased significantly in response to cocaine infusion. While [Glu] showed no group differences ($p > 0.1$), [3-MT] increased to a greater extent in IntA than LimA and LgA groups (group × cocaine interaction, $F[2,580] = 4.93$, $p = 0.008$). This finding provides further confirmation of the sensitization of the dopaminergic circuitry resulting from IntA experience. Other neurochemicals which did not change were GABA, ACh, DOPAC, and HVA.

Analyte	Group Difference	Peak Change from Baseline (%)	SEM (%)
Glutamate	No	+32*	10.3
GABA	No	+1.4	4.6
ACh	No	−10	33
3-MT	Yes	+98* (IntA)	26
		+25* (LimA, LgA)	9.1
DOPAC	No	−9.9	4.1
HVA	No	+0.5	5.2

Table 2-3: List of subset of additional neurochemicals analyzed using UHPLC-MS/MS assay. There were no group differences in basal dialysate levels. As a result, all values were normalized to baseline for comparisons. Only [Glu] and [3-MT] were significantly altered following cocaine infusion. Cocaine-evoked [3-MT] was greater in IntA than LimA and LgA. Significance of ($p < 0.05$) represented with *.

Discussion

The goal of this study was to compare the ability of two prolonged models of cocaine self-administration, LgA and IntA, to produce addiction-like behavior and how each model influences basal and cocaine-evoked dopamine concentrations in the nucleus accumbens core *in vivo*. Key findings include that while both LgA and IntA produce escalation of cocaine intake with increased self-administration experience, LgA results in a much greater total cocaine consumption. LgA also results in a larger preferred level of cocaine at minimal price, Q_0. IntA produced an increase in motivation for cocaine over LimA, as reflected in both α and P_{Max}, but LgA did not. It has been suggested that the critical factor for developing addiction-like behavior is total amount of drug consumed[60,77].

In this work we demonstrate that while IntA results in less total cocaine consumption it produces stronger addiction-like behaviors as well as a sensitization of cocaine-evoked DA release than LgA (and LimA). This report of increased drug-seeking motivation is consistent with a variety of previous studies[63–65,67,78–80].

In order to study the effects of cocaine infusion on dopaminergic neurotransmission as well as 25 other neurochemicals of interest in a large number of animals (n = 42) amounting to greater than 2,500 samples, it was crucial to develop an analytical method capable of adequate throughput, sensitivity, precision, and accuracy. As reported in **table 2-2**, dramatically increasing sample throughput did not significantly impact LoDs, % RSDs (peak area and R_t), and linearity of the analytes of interest. Furthermore, all LoDs are within a range capable of measuring basal extracellular concentrations[37,42] throughout the brain. Inclusion of 100 nM d_4-DA in the perfusion buffer enabled probe recovery calibration without interfering with endogenous neurochemical levels (**Figure 2-4**). Recovery calibration allowed subtle but significant group differences in cocaine-evoked [DA] overflow to emerge (**Figure 2-6**).

There have been previous reports of decreased basal [DA] in animals after high intake (similar to LgA) self-administration experience[81,82]. In the current study neither LgA nor IntA had any significant effect on basal [DA]. In agreement with our results, other reports have found that LgA did not increase basal [DA] over LimA or drug-naïve rats[62,83]. Such reports also agree that there is no correlation between basal [DA] and measures of addiction-like behavior. With the use of SIL probe calibration we report the first accurate measurements of cocaine-evoked [DA] in rats with IntA self-administration experience and the first comparison with LgA. We have demonstrated that IntA experience produces

sensitization of the dopaminergic circuitry (increases seen in both [DA] and [3-MT]) in the nucleus accumbens core that is not seen in LgA or LimA rats (**Figures 2-7**, **2-8**). This change can be correlated with both α and P_{Max} and is thus predictive of addiction-like behavior (Figure **2-8**). Rats in the IntA group were divided based on an "addiction score" consisting of points awarded for being in the upper third of the group in drug-seeking motivation (α, nose pokes during no-drug period, and cocaine-induced nose pokes). The most motivated (high IntA) rats, scoring 2-3 points, showed a larger [DA] % increase over baseline than low IntA, LgA, or LimA animals. This suggests that even within IntA, certain individuals are particularly susceptible to both the behavioral and neurochemical effects of cocaine self-administration.

Conclusions

As a whole these results reinforce the growing body of evidence suggesting that rather than the total amount of drug consumed, the temporal pattern of drug intake is the key in developing addiction. IntA was initially used in an attempt to better model the intermittency associated with drug use in humans. It has since been shown to produce more robust addiction-like behavior than LgA and, among others[84,85], our results suggest a sensitization of the dopaminergic neurotransmission and of cocaine's ability to increase extracellular DA in the nucleus accumbens. This hyper-responsive dopaminergic state is consistent with the incentive-sensitization view of addiction[86] and may lead to a greater ability to generate preclinical models for the study of addiction in humans.

Chapter 3: *In Vivo* Microdialysis Calibration for the Study of ASCT1 Transporter Regulation of Brain Amino Acids

Reproduced in part from Kaplan, E. et al. E. PNAS 2018, 115(38), 9628-9633. Specific contributions from Valenta to this work include development of LC-MS method, *in vivo* microdialysis experiments, and data analysis.

Introduction

N-methyl-D-aspartate (NMDA) receptors have a critical role in synaptic transmission as well as in brain development, synaptic plasticity, learning, and memory[87]. They are ionotropic receptors activated by glutamate, the primary excitatory neurotransmitter in the central nervous system. Glutamate binding generates excitatory postsynaptic potentials but, unlike other neurotransmitter receptors, NMDA receptors require co-agonist binding for activation. Glycine, once viewed as the sole co-agonist of NMDA receptors[88], has more recently been shown to be one of two major co-agonists, the other being D-serine[89]. As such, both glycine and D-serine (D-Ser) have an important role in the dynamic regulation of receptor activation of one of the fundamental neurotransmitter systems in the brain[90,91]. Interestingly, D-Ser has up to a threefold higher affinity for the NMDA receptor than glycine[92]. Despite this, it was initially believed that D-serine brain concentrations were not high enough to physiologically impact NMDA receptors. This changed with the discovery that D-Ser amounts to one-third of the total brain Ser (D and L) and it exceeds levels of most essential amino acids in the rat brain[93,94].

As the importance of D-Ser in neurodevelopment and synaptic plasticity has gained attention, its dysregulation has been implicated in several diseases including schizophrenia[95] and age-related neurodegeneration[96,97]. In the brain D-Ser is synthesized

from L-Ser by serine racemase[98]. While knockout (KO) mice display a 90% decrease in brain D-Ser and exhibit impaired synaptic plasticity[99–101], little is known about the physiological regulation of D-Ser. Although serine racemase is expressed predominantly in neurons[102], L-Ser is synthesized from glucose through enzymes including 3-phosphoglycerate dehydrogenase, an enzyme exclusively expressed in astroglia[103]. This evidence has suggested the existence of a physiological crosstalk mechanism between astrocytes and neurons termed the "serine shuttle". In such a mechanism, L-serine is synthesized in astrocytes and shuttles to neurons to fuel synthesis of D-serine, which is then released and free to act upon NMDA receptors in the presence of glutamate[104]. We hypothesize that the alanine, serine, cysteine, and threonine transporters (ACST1 and ACST2), neutral amino acid exchangers, are key transporters in the serine shuttle and may ultimately regulate extracellular D-Ser and other brain amino acids.

In order to isolate the role of the ASCT1 and 2 transporters in L- and D-Ser regulation, ACST1 and 2-KO mice were studied *ex vivo* through cultured astrocytes and brain tissue homogenate and *in vivo* through quantitative microdialysis. For discrimination of L- and D-Ser an established method for separation of chiral amino acids on reversed-phase chromatographic columns with fluorescence detection was utilized[105]. This method involves derivatization of chiral amino acids with o-phthaldialdehyde (OPA) and N-tert-butyloxycarbonyl-L-cysteine (Boc-L-Cys, **Figure 3-1**).

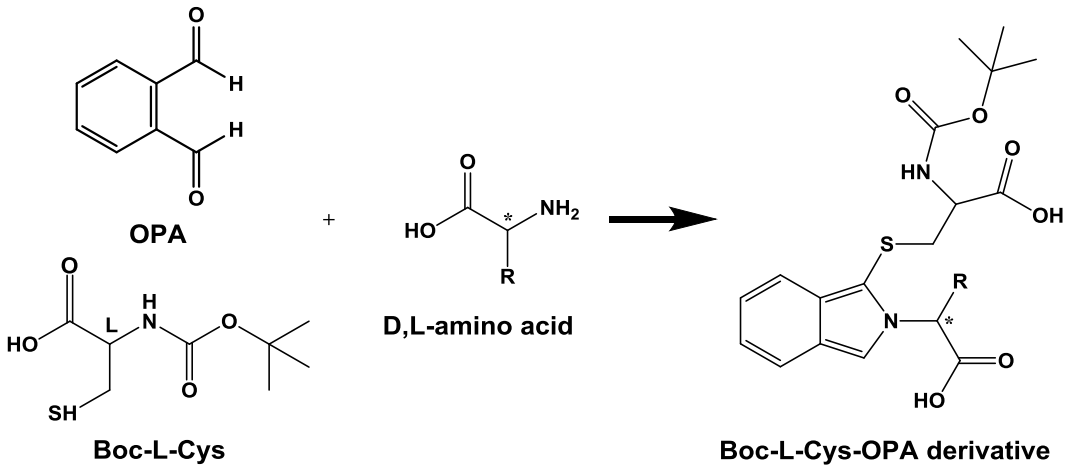

Figure 3-1: Boc-L-Cys-OPA derivatization scheme for separation of chiral amino acids by reversed-phase chromatography. Amino acid stereochemistry (*) maintained and leads to altered retention between D- and L-amino acids. Boc-L-Cys-OPA derivatives are fluorescently active.

For *in vivo* microdialysis measurements of absolute basal extracellular concentrations of serine, glycine (Gly), threonine (Thr), glutamate (Glu), alanine (Ala), and GABA a UHPLC-MS/MS method with stable-isotope-labelled (SIL) microdialysis recovery calibration was developed. Using a previously reported precolumn benzoylation procedure[42], rapid and sensitive separation of aforementioned amino acids was achieved. This method enabled accurate comparison of basal amino acid levels between 12 wild type (WT) and 12 ASCT1 KO mice to analyze the transporter's role in amino acid exchange and potential regulatory role in the serine shuttle. Whereas previous reports have used SIL microdialysis calibration for measuring absolute extracellular concentrations of dopamine, norepinephrine, and glutamate in dialysate[47,106,107], the work in this chapter represents the first demonstration of *in vivo* SIL calibration for Ser, Gly, Thr, Ala, and GABA.

Methods

Chemicals and Reagents

All chemicals were purchased from Sigma Aldrich (Saint Louis, MO) unless otherwise noted. Acetonitrile was purchased from Honeywell Research Chemicals through VWR (Radnor, PA). NaCl, KCl, $MgSO_4$, $CaCl_2$, and sulfuric acid were purchased from Fisher Scientific (Fairlawn, NJ). Sodium phosphate dibasic and sodium tripolyphosphate were purchased from Acros Organics (Geel, Belgium). Stock solutions of 20 mM Glu and GABA and 40 mM Ala, Gly, Ser, and Thr were prepared in HPLC grade water. A calibration standard mixture was prepared by diluting stocks into aCSF consisting of 145 mM NaCl, 2.68 mM KCl, 1.4 mM $CaCl_2$, 1.0 mM $MgSO_4$, 1.55 mM Na_2HPO_4, and 0.45 mM NaH_2PO_4 adjusted to pH of 7.4 with 0.1 M NaOH. Calibration curves were prepared in aCSF with 250 μM ascorbic acid for the following concentration ranges: GABA 1 – 500 nM; Glu 10 – 4,000 nM; Ala, Gly, Ser, Thr 50 – 20,000 nM.

As described previously, SIL amino acids were included into the aCSF to calibrate microdialysis recovery for all six analytes. The following amino acids were purchased from Cambridge Isotope Laboratories, Inc. (Tewksbury, MA): D_4-alanine, D_3-serine, $^{13}C,D_2$-threonine, $^{15}N,D_2$-glycine, $^{13}C_5$-glutamic acid. D_6-GABA was purchased from Sigma Aldrich (St. Louis, MO). aCSF was prepared with SIL amino acid concentrations at approximate physiological concentrations (50 nM – GABA, 500 nM – glutamate, 2.5 μM – alanine, serine, threonine and glycine) and perfused through the probe after completion of initial fraction collection. The ratio of SIL amino acid infused through the probe to that collected at the outlet measured using benzoyl chloride derivatization was used for internal calibration, yielding an amino acid-specific recovery for each probe.

Microdialysis Probe Construction and Implantation

Briefly, custom concentric microdialysis probes were constructed for bilateral implantation into the striatum of all mice. An inlet (40/110, ID/OD) and outlet (75/150) fused silica capillary were glued into a 13.5 mm (25 G) piece of stainless steel hypodermic sheath tubing (Small Parts Inc., Logansport, In) with the inlet capillary protruding from the end of the tubing and the outlet capillary several mm within. The inlet capillary was cut to a length of 2 mm extending beyond the sheath and a regenerated cellulose dialysis membrane (Spectrum Life Sciences, LLC. Rando Dominquez, CA) was placed over the inlet and inserted into the sheath. A 100 μm epoxy plug (Loctite, West Lake, OH) was placed at the tip of the membrane and epoxy was also used to seal the membrane to the sheath. Inlet (150/360) and outlet (180/360) fused silica adapting capillaries were glued onto the inlet and outlet capillaries, respectively. A small piece of pipette tip was then glued over the proximal end of the adapting capillaries to strengthen the probe. Before use the probe was rinsed with 70% ethanol, then flushed extensively with sterile aCSF.

Male WT (n = 12) and ASCT1 KO (n = 12) mice (C57B/BL6 genetic background, Sanger Institute, Cambridgeshire, UK) weighing 30-42 g were anesthetized using 1-5% isoflurane and mounted to a stereotaxic instrument (David Kopf Instruments, Tujunga, CA, USA). Microdialysis probes were implanted bilaterally into the striatum using the following coordinates with reference to bregma: +0.6 mm anterior, ±1.75 mm lateral, and -4.2 mm ventral to the surface of the brain[71]. The striatum was chosen because it is a large, relatively homogenous region in the mouse brain and little variation in amino acid concentration was expected across it. Mice were implanted with two probes to limit the number of animals required to generate adequate results. Bilateral burr holes were drilled

at the above coordinates and three stainless steel skull screws (Plastics Once Inc, Roanoke, VA) were used to mount the probe to the brain. Probes were slowly lowered into place while being continuously perfused with aCSF at a flow rate of 2 μL/min to prevent deformation of the membrane. Dental cement (A-M Systems, Sequim, WA) was used to encase the probe and skull screw to secure the probe. In order to prevent any bubbles from being trapped in the probe membrane, mice were perfused continuously with aCSF at 0.5 μL/min during the 24-hr recovery period. Blue dye was infused through the dialysis probes post-experiment for probe localization.

Microdialysis

During collection mice were freely moving with access to food and water ad libitum. While perfusing aCSF free of SIL amino acids two 40-min fractions (20 μL) were collected from each probe (hemisphere). From each fraction, 2 aliquots of 3 μL were analyzed by UHPLC-MS/MS using benzoyl chloride derivatization to quantify alanine, serine, threonine, glycine, glutamate and GABA. The remainder of each sample (16 μL) was frozen at -80˚C and later analyzed by liquid chromatography for the analysis of D- and L-Ser enantiomers[105]. Standard aCSF was then replaced with aCSF containing all six SIL amino acid calibrants at a flow rate of 1 μL/min for 10 min. The flow rate was then lowered to 0.5 μL/min for 2 hr before collection to allow for adequate flushing of the fluidic system with the SIL amino acid aCSF (~3x system volume). All fluidic switching was done with a 6-port HPLC valve (VICI, Houston, TX) for uninterrupted fluid flow and to prevent bubbles from being trapped in the probe between standard aCSF and SIL aCSF perfusion. A total of four 6 min fractions were then collected and derivatized for determination of absolute extracellular concentrations using SIL amino acid microdialysis recovery

correction. For accurate measurement of SIL amino acids, SIL aCSF was collected after passing through the HPLC valve and inlet line.

Neurochemical Analysis using UHPLC-MS/MS

The following reagents were prepared on the day of the experiment: 100 mM sodium carbonate in water, 2% benzoyl chloride in ACN (v/v), and internal standards were prepared in 1:1 ACN:H2O with 1% H_2SO_4 (v/v). Dialysate fractions (3 µL) were collected and 1.5 µL carbonate was added to buffer to pH ~10, 1.5 µL BzCl was added to react with the primary amines found in all amino acids of interest, and internal standard was added enabling adjustment of pH and organic content for UHPLC injection.

All analysis was done using a Thermo Fisher Vanquish UHPLC interfaced with a Thermo Fisher TSQ Quantum Ultra triple-quadrupole mass spectrometer. Briefly, samples were injected onto a Phenomenex Kinetex C18 column (2.1 mm x 100 mm, 1.7 µm). Mobile phase A consisted of 10 mM ammonium formate and 0.15% formic acid. Mobile phase B was pure acetonitrile. The method flow rate was 600 µL/min and the gradient was a linear gradient from 5 – 30% B over 2 min. To wash the column there was an increase to 100% B at 2.5 min, 1 min of isocratic hold, and a return to 5% B at 3.7 min. The total analysis time was 6 min/sample. The pressure range across each gradient was 350 – 800 bar. The autosampler was at 25˚C while the column was held at 30˚C in still air mode. ESI was used in positive mode with a spray voltage of 2 kV. Vaporizer and transfer capillary temperatures were 400˚C. Sheath gas was set to 10. The skimmer offset was -6 V and tube lens values were tuned for each individual analyte. The TSQ Quantum Ultra was operated in MRM mode. **Table 3-1** includes SRMs for all compounds analyzed:

Analyte	Precursor (m/z)	Product (m/z)	CE (V)	Retention Time (min)	Tube Lens (V)
Bz-Ser	210	105			
Bz-D3-Ser	213	105	17	1.27	65
$^{13}C_6$Bz-Ser	216.1	111			
Bz-Gly	180	105			
Bz-D2,15N-Gly	183	105	13	1.43	60
$^{13}C_6$Bz-Gly	186	111			
Bz-Thr	224	105			
Bz-13C,D2-Thr	227	105	17	1.63	56
13C6Bz-Thr	230	111			
Bz-Glu	252	105			
Bz-13C5-Glu	257	105	15	1.63	69
$^{13}C_6$Bz-Glu	258	111			
Bz-Ala	194	105			
Bz-D4-Ala	198	105	14	1.84	60
13C6Bz-Ala	200	111			
Bz-GABA	208	105			
Bz-D6-GABA	214.1	105	14	1.95	61
$^{13}C_6$Bz-GABA	214	111			

Table 3-1: Table of SRMs for total of 6 endogenous amino acids, 6 SIL amino acids for calibration and their internal standards. Each analyte was tuned at the 600 µL/min and mobile phase composition during elution. Both SIL and endogenous amino acids were normalized using $^{13}C_6$-Bz internal standards.

In Vitro Recovery

Validity of using SIL amino acids for recovery calibration was verified by performing *in vitro* stirred vial testing. In brief, a microdialysis probe was perfused with SIL aCSF at the experimental flow rate and submerged in a stirred vial containing the endogenous form of the amino acids kept at 37 – 38˚C. Samples were then collected at the probe outlet and derivatized. Using equations (**2-2**) and (**2-3**) the EE was calculated for the probe based on the amount of SIL amino acid lost to the solution and used to correct for probe recovery. The recovery-corrected value was compared to the concentration measured

directly from the vial to ensure accurate calibration. Both the effect of dialysis flow rate and SIL amino acid concentration were explored with regards to calibration accuracy.

Results and Discussion

UHPLC-MS/MS Method for Amino Acids

In this work a mobile phase gradient was developed targeting the early-eluting Bz-labeled amino acids Ala, Ser, Gly, Thr, Glu, and GABA for HPLC-MS/MS analysis. Because these compounds all elute within a relatively narrow retention window, a shallow gradient enabled separation from matrix components which typically hinder quantitation at low analyte levels. **Figure 3-2** shows a representative total ion chromatogram (TIC) for the method.

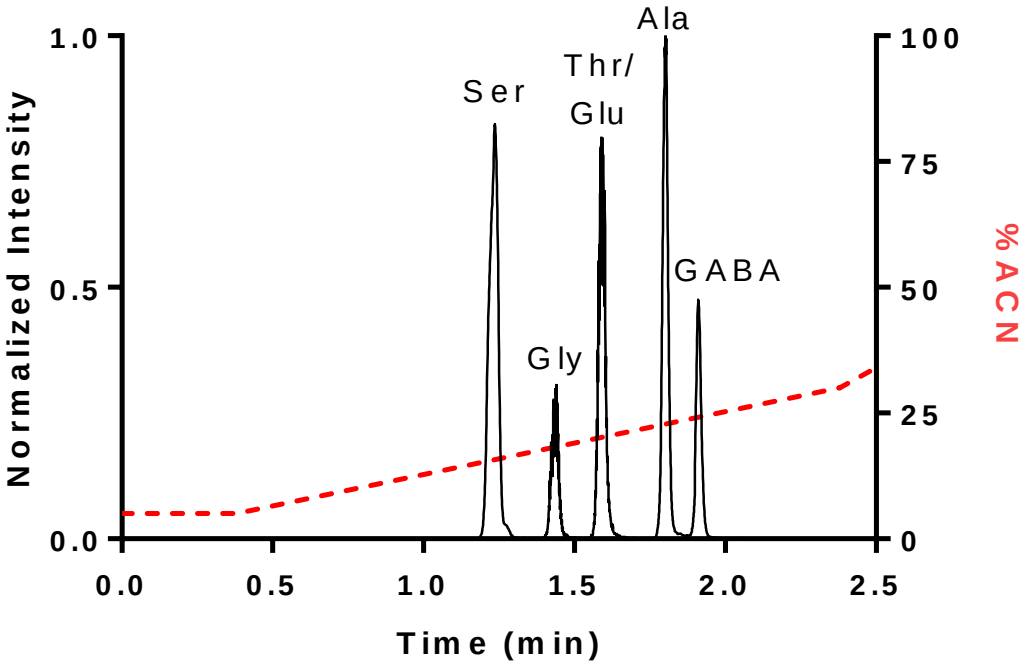

Figure 3-2: RIC for amino acid UHPLC-MS/MS method normalized to the highest intensity peak, Bz-Ala. Concentrations shown are as follows: 50 nM GABA; 500 nM Glu; 2.5 µM Ser, Gly, Thr, and Ala. Red dotted line shows dead time corrected gradient. Total analysis time was 6 min.

For a comparison of figures of merit, **Table 3-2** shows LoD, percent RSD, and R^2 from the 2 min gradient in **Chapter 2** and the amino acid-specific gradient in **Figure 3-2**. It is worth noting that LoDs are either similar or improve substantially when compared with the 26 compound method. This result is in agreement with the previously published 20 min gradient, suggesting that reducing gradient steepness markedly improves limits of detection for less retained compounds while leaving highly retained compounds less affected[42].

	Amino Acid Gradient			26 Compound Gradient[107]		
Analyte	LoD (nM)	RSD (%)	R^2	LoD (nM)	RSD	R^2
Bz-Ser	65	7	0.9998	140	5	0.9951
Bz-Gly	40	6	0.9990	100	7	0.9835
Bz-Thr	16	5	0.9997	-	-	-
Bz-Glu	8	3	0.9994	14	4	0.9999
Bz-Ala	30	2	0.9999	-	-	-
Bz-GABA	2	4	0.9996	1	1	0.9997

Table 3-2: Table of figures of merit for amino acid-specific gradient and comparison with the 26 compound gradient. Ser and Gly LoDs and linearity show significant improvement. Glu and GABA figures of merit remain unchanged.

In Vivo SIL Microdialysis Calibration of Amino Acids

In order to quantitatively compare basal concentrations of the six previously mentioned amino acids, it is essential that microdialysis probe recovery be calibrated. Variations in probe construction, implantation, and individual animals can all have significant effects on the extent to which the perfusion fluid within a microdialysis probe equilibrates with the extracellular environment. As shown in **Table 3-1**, ^{13}C-Bz internal standards could be monitored simultaneously with the endogenous and SIL amino acids. While Glu has been calibrated using *in vivo* SIL recovery calibration[47], this is the first

report of extending this to other amino acids. A pilot (N = 3) was performed to examine if the loss of SIL amino acids effectively approximated expected *in vivo* recovery for a probe length of 2 mm operated at 1 μL/min. Past experiments have revealed EE for small molecules *in vivo* for this membrane length and material to be in the range of 0.15 – 0.35[47,106,107]. As demonstrated in **Figure 3-3**, there was no difference between C_{in} and C_{out} for any of the six amino acids (*p > 0.1,* **3-3A**). Furthermore, average extraction fraction was calculated to be drastically below the projected range for amino acids (**3-3B**). C_{in} concentrations were as follows: 2.5 μM Ser, Gly, Thr, Ala; 500 nM Glu; 50 nM GABA.

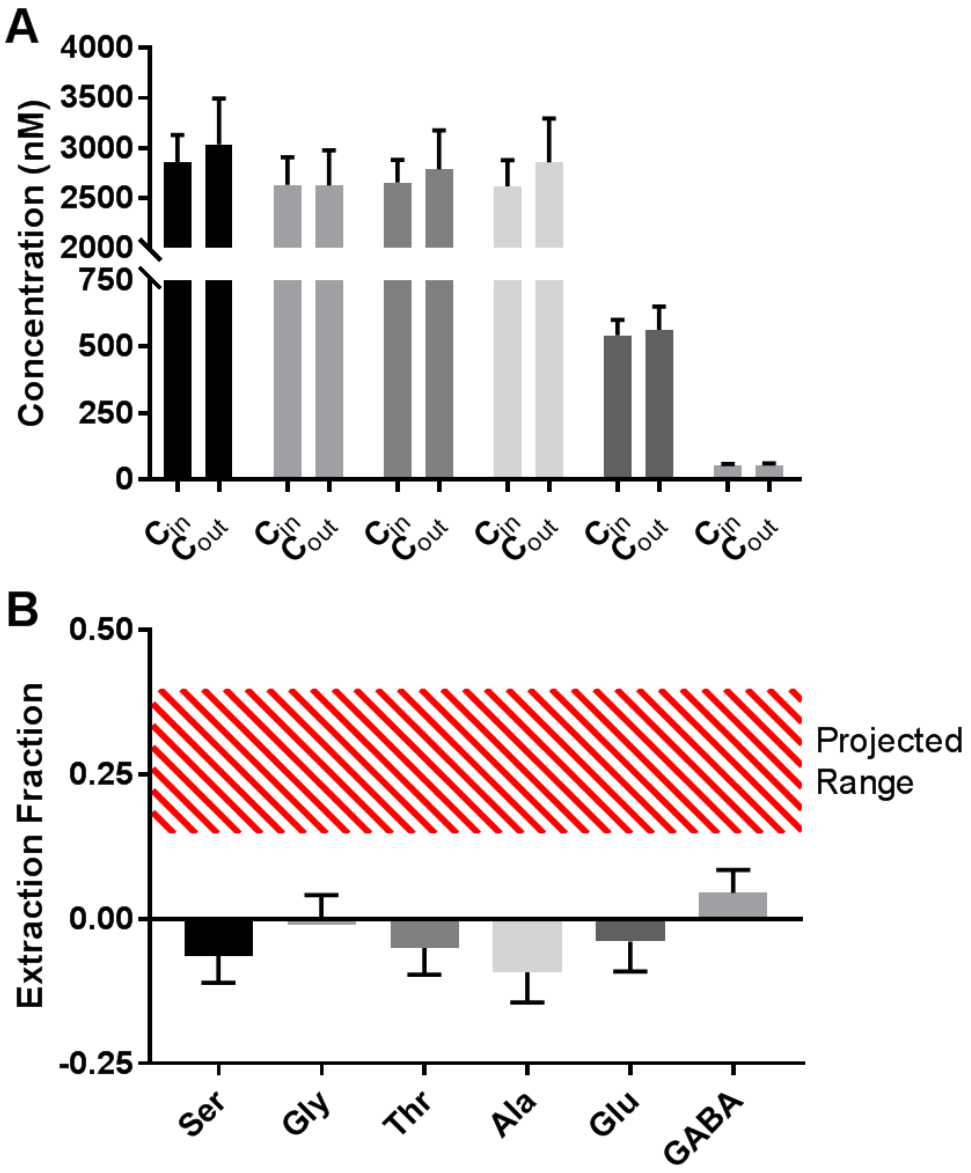

Figure 3-3: SIL amino acid concentrations at the probe inlet and outlet and corresponding extraction fractions calculated *in vivo*. No differences were found between C_{in} and C_{out}, suggesting recovery ~ 0 ($p > 0.1$, A). All calculated EE were either negative or fell significantly below the projected range (red) for small molecules (0.15 – 0.35, B). Data are average ± SD.

The discrepancy in **Figure 3-3** warranted further work to improve quantitation to validate recovery correction *in vitro*. Although *in vitro* recovery oversimplifies the factors that affect recovery *in vivo* because it ignores resistance to mass transport stemming from the extracellular space as well as biological processes regulating neurochemical levels, it is a useful tool for validating probe calibration. To determine the calibration accuracy, the

recovery-corrected concentration calculated using SIL-derived extraction fraction was compared to the concentration measured directly from the sample vial (C_{vial}). SIL amino acid concentration was examined as a contributing factor. This contribution from concentration may be two-fold: (1) SIL concentration dictates the concentration gradient with respect to the probe environment, thus potentially influencing flux across the membrane, (2) SIL calibrant purity ranged from (96-98%), thus with very high concentrations there may be artificially inflated concentrations of endogenous amino acids already present in the circulating aCSF. Neither approximate physiological (1x) nor 10-fold higher (10x) concentration of SIL calibrants accurately estimated recovery for Ser, Ala, Glu, or GABA. For Gly and Thr, 10x SIL calibrated recovery was not significantly different from true recovery ($p > 0.5$, **Figure 3-4**). In general, higher calibrant concentrations overapproximated C_{vial} while lower concentrations underapproximated C_{vial}.

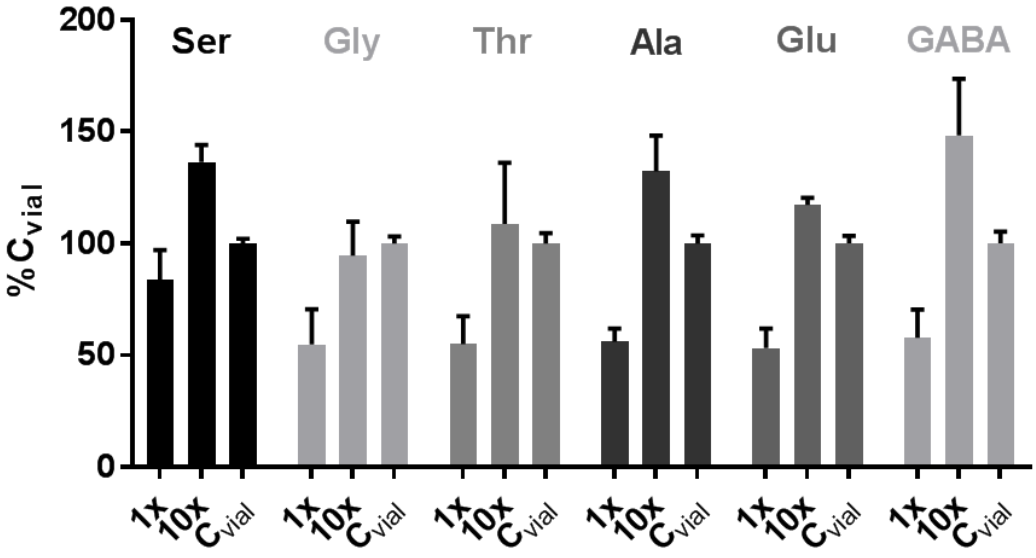

Figure 3-4: Effect of SIL calibrant concentration (1x and 10x) on C_{corr} for amino acid standards *in vitro*. Recovery corrected C_{corr} values (n = 3) are shown normalized to analyte vial concentration (C_{vial}). One-way ANOVA was used to compare recovery-corrected values to C_{vial}. All recovery-corrected values were different from C_{vial} ($p < 0.05$) except the 10x SIL concentration for Gly and Thr ($p > 0.5$) Data are average ± SD.

While increasing calibrant concentration slightly improved calibration accuracy, the majority of calculated concentrations overestimated C_{vial} and therefore further improvements were required for use *in vivo*. To elucidate the effect of flow rate on calibration accuracy, the 10x calibrant concentration (25 μM Ser, Gly, Thr, Ala; 5 μM Glu; 500 nM GABA) was used for *in vitro* calibration at three different flow rates: 1 μL/min, 0.5 μL/min, and 0.1 μL/min. **Figure 3-5** shows the measured dialysate concentration (C_{meas}), the corrected dialysate concentration (C_{corr}) and the vial concentration (C_{vial}) for each amino acid at three flow rates. Generally, calibration accuracy decreases with increasing flow rate. This suggests that at higher perfusion flow rates a fundamental difference emerges between outward SIL flux and inward analyte flux. The result is that a larger percentage of analyte diffuses into the dialysate stream than SIL calibrant diffuses outward, thus underestimating recovery and overcorrecting C_{corr}.

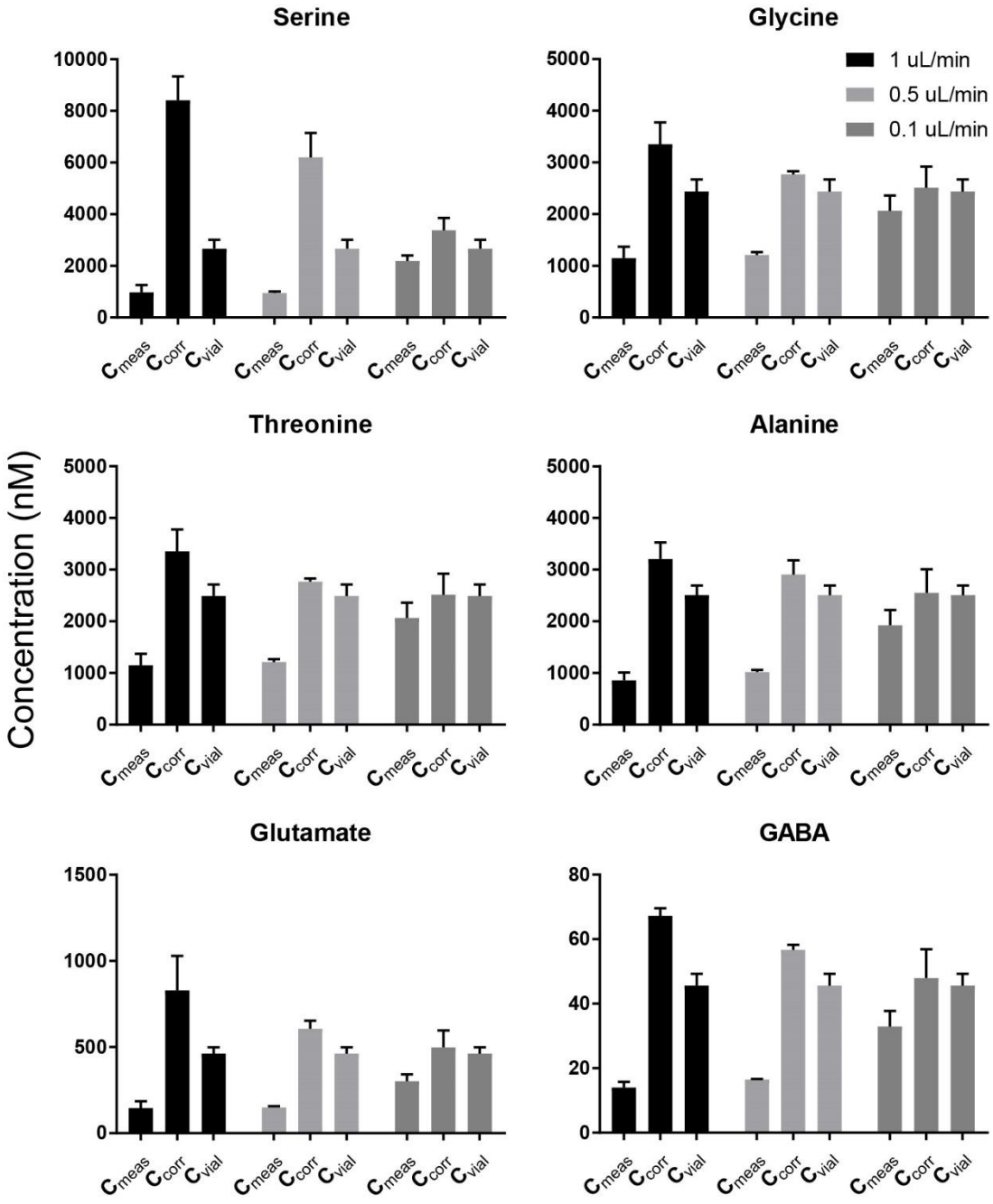

Figure 3-5: In vitro recovery experiment comparing the dialysate concentration of analyte (C_{meas}), recovery corrected dialysate concentration of analyte (C_{corr}), and the analyte concentration in the stirred vial (C_{vial}) for three dialysate flow rates. One-way ANOVA showed a significant effect of flow rate on C_{corr}. Multiple comparisons showed that all C_{corr} at 1 µL/min differed from C_{vial} ($p < 0.01$) while only for GABA did C_{corr} significantly overestimate C_{vial} at 0.5 µL/min ($p < 0.01$). No C_{corr} at 0.1 µL/min were significantly different from C_{vial} ($p > 0.1$) Data are average ± SD.

Although at flow rates below 1 µL/min recovery calibration showed agreement with C_{vial} (except for GABA) there was still a trend of overestimation present ($p > 0.05$). It was hypothesized that this trend arose from the use of high concentration SIL calibrants leading

to a substantial amount of unlabeled amino acid contaminating the aCSF as discussed previously. The *in vitro* experiment was repeated for 0.5 μL/min and 0.1 μL/min at reduced (1x, ~physiological) SIL calibrant concentrations (2.5 μM Ser, Gly, Thr, Ala; 500 nM Glu; 50 nM GABA). A one-way ANOVA showed no effect of flow rate on C_{corr} for any of the six analytes ($p > 0.1$, **Figure 3-6**). Though not statistically significant, post-hoc multiple comparisons showed that each analyte did have larger error when using a 0.5 μL/min flow rate.

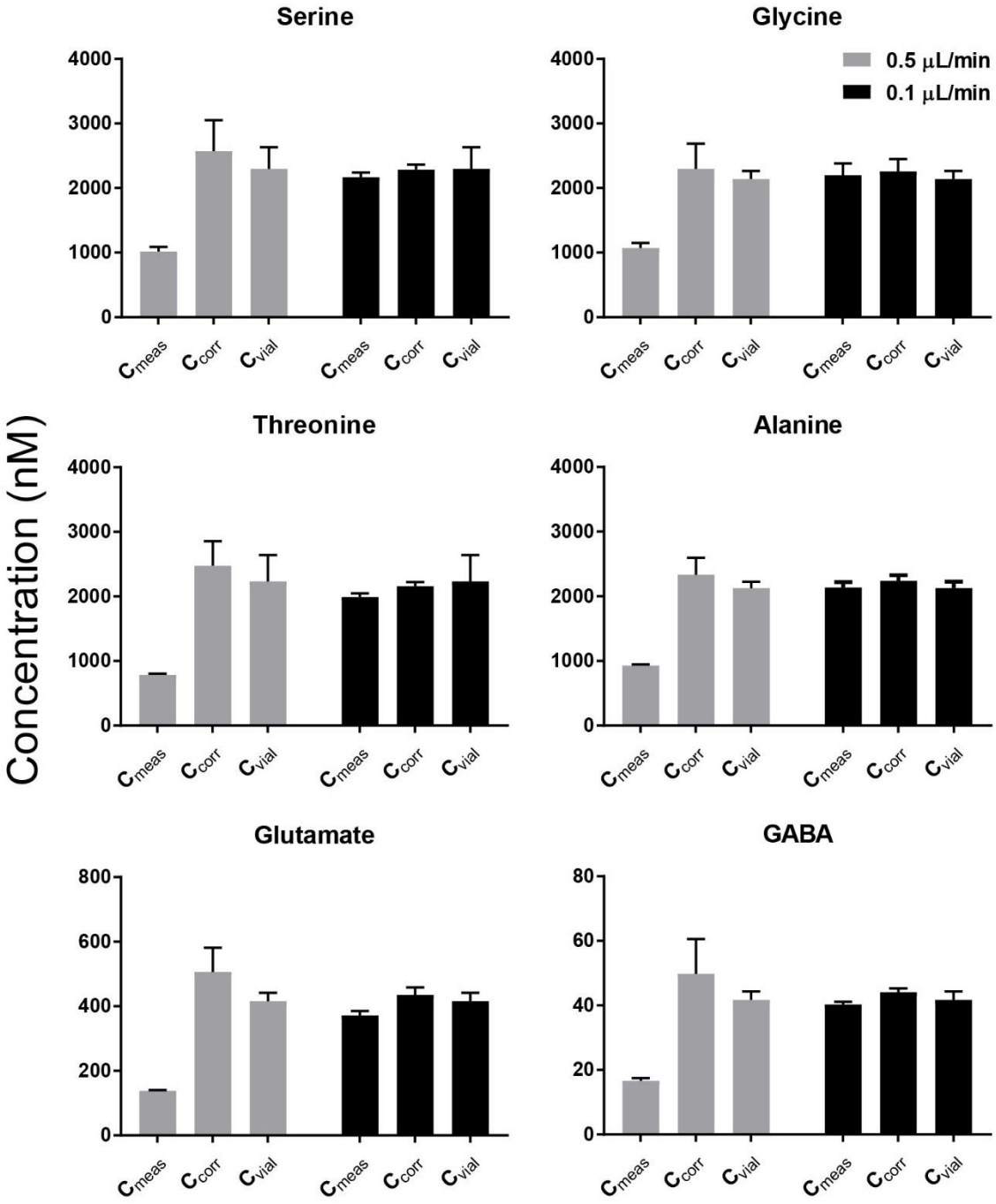

Figure 3-6: In vitro recovery experiment comparing the recovery correction for two flow rates. Dialysate concentration of analyte (C_{meas}), recovery corrected dialysate concentration of analyte (C_{corr}), and the analyte concentration were compared in the stirred vial (C_{vial}) for two different flow rates: 0.1 µL/min and 0.5 µL/min. SIL calibrant concentrations were reduced 10-fold (2.5 µM Ser, Gly, Thr, Ala; 500 nM Glu; 50 nM GABA) to decrease the amount of unlabeled analyte present in the perfusate. One-way ANOVA showed no group effect of flow rate on C_{corr} ($p > 0.1$). Multiple comparisons showed that neither flow rate differed from C_{vial} ($p > 0.05$). Data are average ± SD.

Contrary to the previous report for SIL Glu recovery calibration[47], this work demonstrates that the accuracy of the corrected concentration values for the above amino acids has a dependency on dialysis flow rate. Whether this phenomenon is related to the specific probe design or the physical properties of the membrane (surface chemistry, MWCO) will require further experimentation. Our observations suggest that at higher flow rates there is a directional difference in the rate at which analytes diffuse across the membrane. While *in vitro* this effect may be exaggerated since the vial is stirred while the perfusate flow is laminar and flux across the membrane is more likely diffusion limited, the opposite should be true with regards to sampling brain tissue lacking bulk fluid flow.

As a validation for the changes made to the SIL recovery calibration protocol, an *in vivo* pilot (N = 2) was performed and extraction fractions were calculated for each amino acid (**Figure 3-7**). All extraction fractions fell within the expected range seen in previous

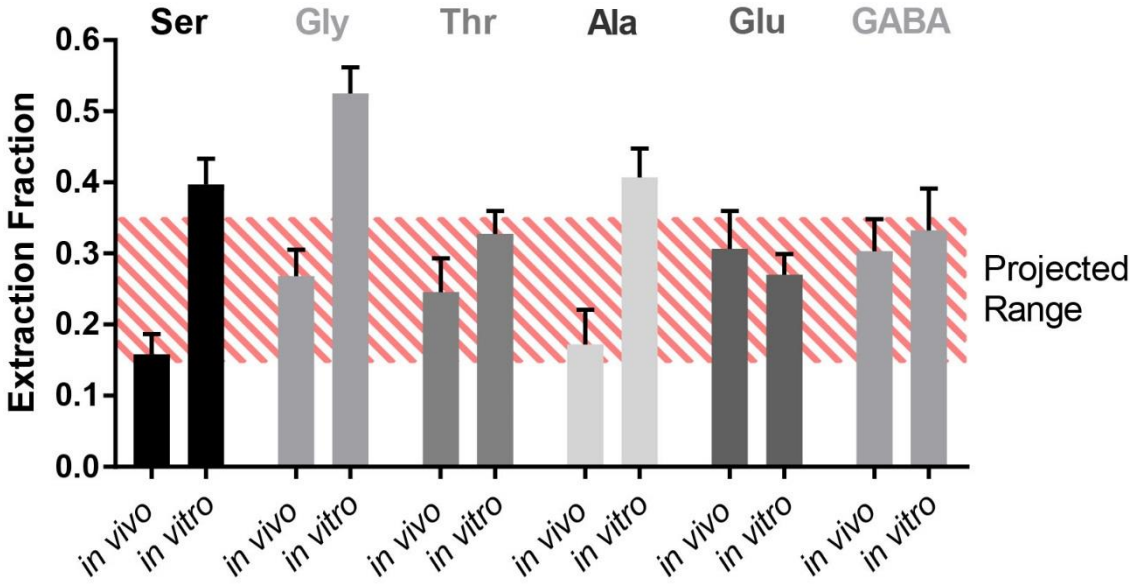

Figure 3-7: *In vivo* extraction fraction averaged across 6 samples collected from 2 separate probes perfused at 0.5 µL/min. Also included for visualization is average *in vitro* extraction fraction from the previous experiment (**Figure 3-6**). SIL calibrant concentrations were as follows: 2.5 µM for Ser, Gly, Thr, Ala; 500 nM for Glu; 50 nM for GABA. As expected the majority of *in vivo* extraction fractions were lower. Data are average ± SD.

experiments (0.15 – 0.35). This work represents the first validation of *in vivo* SIL recovery calibration for the amino acids Ser, Gly, Thr, Ala, and GABA. While more work is necessary, a similar recovery accuracy dependence on flow rate has been observed across six different amino acids.

Role of ASCT1 in Brain Amino Acid Transport, Brain Development, and Behavior

An ASCT1 and ASCT2-KO mouse colony was established for the study of the transporter's role in amino acid transport. A complete lack of ASCT1 or 2 protein in the brain was verified by Western Blot. There was an 80 – 90% decrease of D- and L- serine transport in astrocytes cultured from ASCT1-KO mice. Transport of L-Ala, L-Thr, and Gly also decreased significantly while Glu uptake was unaffected (**Figure 3-8**). There were no differences in transport between ASCT2-KO mice and WT. As a result, focus was shifted exclusively to ASCT1. In WT astrocytes, even in the presence of high concentrations of the ASCT1 substrates (L-Ala, Ser, cysteine (Cys), and Thr) D-Ser was still transported, confirming it as a high affinity ASCT1 substrate. In cortical synaptosomes ASCT1-KO preparations had a 30% reduction in uptake of D- and L-Ser. Trans-4-hydroxy-L-proline

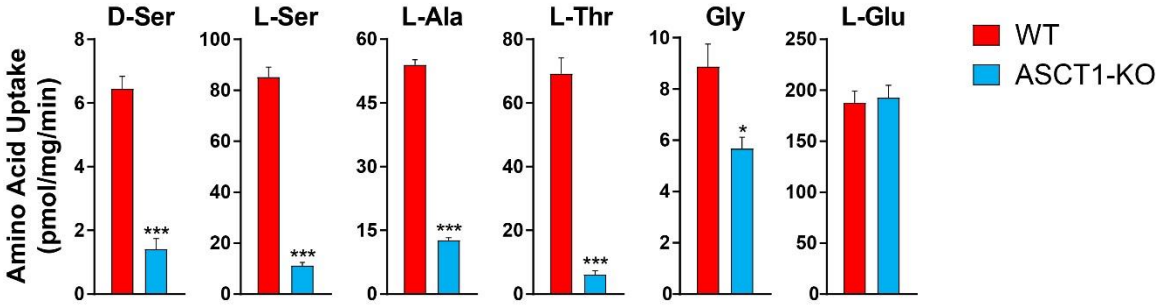

Figure 3-8: Amino acid transport by astroglia of WT and ASCT1-KO mice. Uptake decreased significantly in KO mice for all amino acids except L-glutamate. The results represent the average ± SEM of four to seven experiments with different astroglia preparations. Different from control at ****P < 0.001*, ***0.01*, and **0.05* (paired two-tailed Student's t test). Reprinted with permission from Kaplan, E. et al. PNAS. 2019, 115 (38), 9628-9633. Copyright 2019 National Academy of Sciences.

(OH-Pro), a selective ASCT1 substrate used to compete with other amino acids for uptake, inhibited uptake of D- and L-Ser only in WT synaptosomes.

The brain levels of ASCT1 substrates were measured in 4-day-old WT and ACST1-KO mice (**Figure 3-9**). ASCT1-KO mice showed a 20% decrease in L-Ser, 25% decrease in D-Ser, and 7% decrease in L-Glu at 4 days old. Conversely, Gly, L-Thr, and L-Ala were 40 – 60% higher in ACST1-KO mice. The ratio of NMDA receptor co-agonists Gly:D-Ser was increased nearly 2-fold in ASCT1-KO mice brains suggesting a large increase in brain Gly relative to D-Ser.

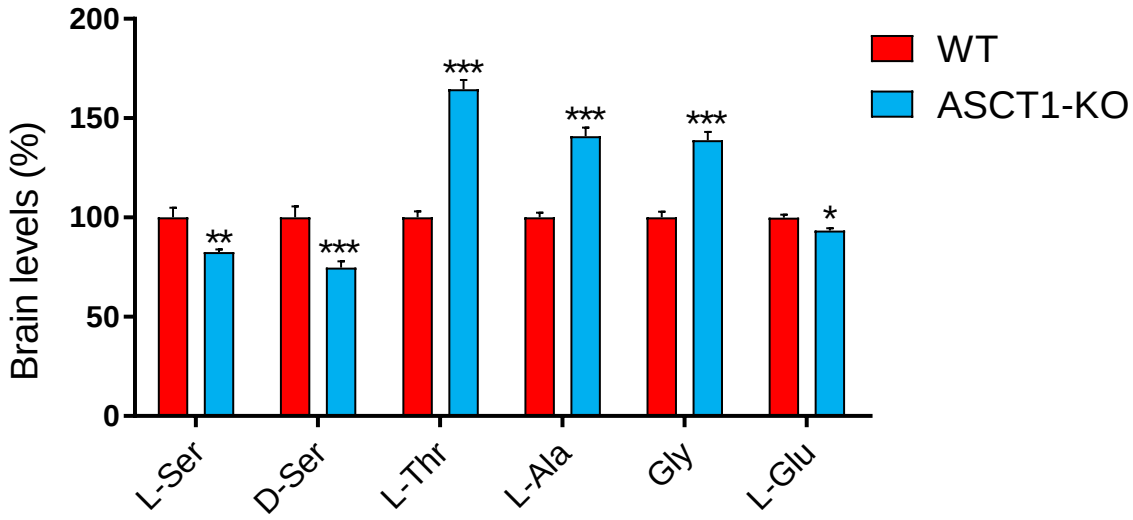

Figure 3-9: Amino acid levels in whole brains of 4-day-old WT (n=10) and ASCT1-KO (n=11) mice. Significant reductions in whole brain levels of L-serine, D-serine, and L-glutamate and increases in L-threonine, alanine, and glycine were observed. Different from control at ***$P < 0.001$, **0.01 and *0.05 (two-tailed Student's t test). Reprinted with permission from Kaplan, E. et al. PNAS. 2019, 115 (38), 9628-9633. Copyright 2019 National Academy of Sciences.

Mutations in ASCT1 have been shown to cause microcephaly in humans[108,109]. MRI was therefore used to investigate if a similar trend in brain volume was present in ASCT1-KO mice. Significant reduction was found in both the hippocampus ($p < 0.001$) and the striatum ($p < 0.01$). Motor functions were evaluated in 8-day-old mice and compared with WT mice, they displayed a longer latency in righting time when placed on their backs ($p <$

0.01) and weaker grip when placed on an inverted mesh ($p < 0.01$). When adult mice were placed in a water maze it took ASCT1-KO mice longer to learn the platform location than WT. Moreover, ASCT1-KO mice were significantly impaired when the location of the platform was changed, which may suggest impairments in learning flexibility.

Amino Acid Exchange by ASCT1 in WT and ASCT-KO Mice

The ability of ASCT1 to release endogenous amino acids was investigated with the use of OH-Pro in acute cortical brain slices. Because OH-Pro is a selective ASCT1 substrate we expect that it will freely exchange with intracellular ASCT1 substrates. The extracellular concentrations of such substrates should thus be increased by the addition of OH-Pro only in WT slices. OH-Pro increased release of L-Ser, Ala, and Thr in WT but not KO slices (**Figure 3-10B-D**). D-Ser and Gly showed no response to OH-Pro in WT or KO slices (**Figure 3-10A, E**). As D-Ser (but not Gly) is known to be an ASCT1 substrate, these results suggest that D-Ser experiences exclusively uptake through the transporter while L-Ser, Ala, Thr are released.

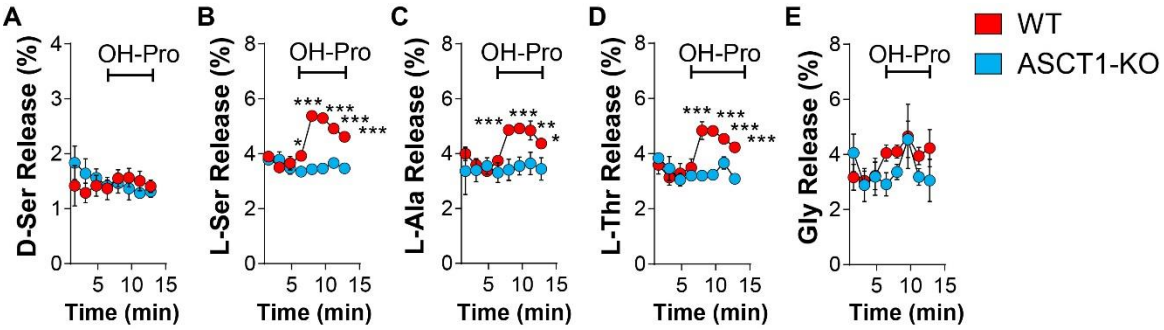

Figure 3-10: ASCT1-mediated release of amino acid substrates in cortical brain slices. Release of endogenous D-serine (A), L-serine (B), L-alanine (C), D-threonine (D), and glycine (E) was elicited by perfusion of slices with 1 mM OH-pro at the indicated times. Different from ASCT1-KO mice at *P < 0.05 and ***0.001 (two-way repeated measures ANOVA and Bonferroni's post hoc test). The data are average ± SEM (n=7). Reprinted with permission from Kaplan, E. et al. PNAS. 2019, 115 (38), 9628-9633. Copyright 2019 National Academy of Sciences.

To further validate our cortical slice results, *in vivo* microdialysis with SIL recovery correction was performed. The previously reported UHPLC-MS/MS method (**Figure 3-2**) was used for recovery-corrected measurements of Ser, Gly, Thr, Ala, Glu, and GABA while Boc-L-Cys-OPA derivatization was used for differentiation of D- and L-Ser enantiomers[105]. No significant differences were found between WT and ASCT1-KO extracellular levels of L-Ser, Ala, Thr, Gly, Glu, GABA (**Figure 3-11A, D-H**). There was, however, a 25% decrease in extracellular levels of D-Serine ($p < 0.01$, **11B**). The resulting ratio of D-Ser/Total Ser was also significantly different ($p < 0.01$, **11C**). These results are in agreement with the lower levels of total brain D-serine in young and adult ASCT1-KO mice (not shown).

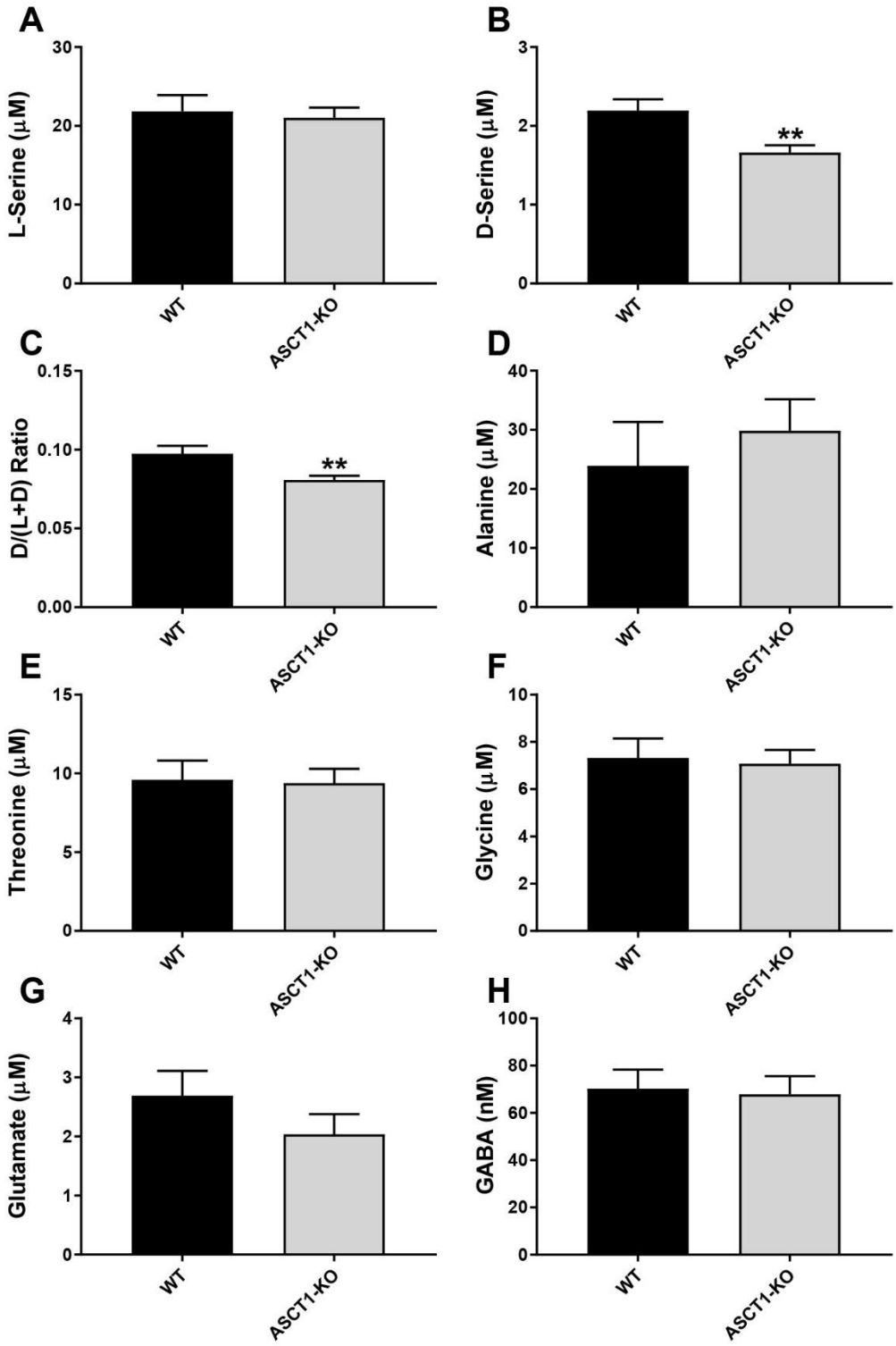

Figure 3-11: Extracellular amino acid concentrations in the striatum of 6- to 7-month-old mice by *in vivo* microdialysis. (n = 48, 12 mice per group, 2 probes/mouse). The data represent the mean ± SEM of the extracellular amino acid concentrations corrected by in vivo SIL calibration. Statistical analysis done with unpaired two-tailed Student's t test. Significance of $p < 0.01$ represented with **.

Despite unaltered brain L-Ser levels, observations that ASCT1-KO mice are deficient in L-Ser transport imply that ASCT1 is required to provide enough L-Ser from astrocytes to fuel D-Ser synthesis in neurons. The *in vivo* data does not exclude the possibility of other L-Ser transporters compensating for the lack of transport in ASCT1-KO mice. **Figure 3-12** shows our model of ASCT1 function within the Serine shuttle. We propose that all ASCT1 substrates undergo bidirectional transport (L-Ser, Ala, Thr) with the exception of undirectional transport (uptake) of D-Ser.

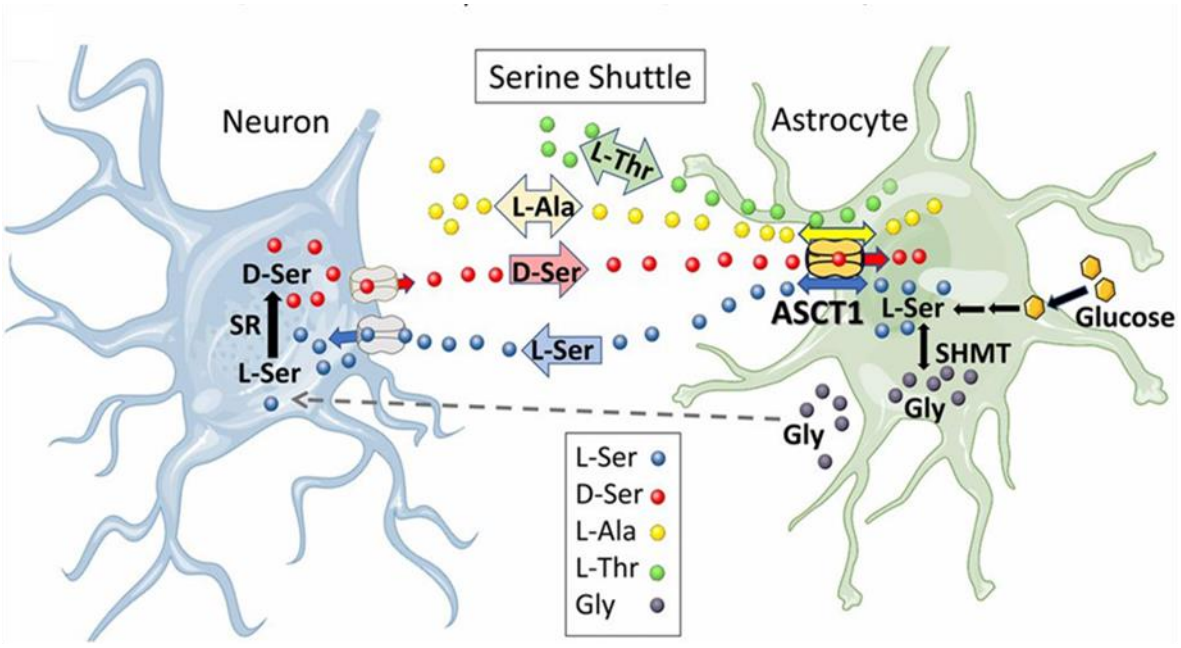

Figure 3-12: Proposed model of ASCT1 function in the serine shuttle. Astrocytic ASCT1 releases L-Ser, which is subsequently taken up by neurons to fuel the synthesis of D-Ser by serine racemase (SR). D-Ser may be released by neurons via the Asc-1 transporter and subsequently taken up by ASCT1 in astrocytes. L-Ala, L-Thr, and D-Ser may serve as extracellular substrates that stimulate L-Ser export via ASCT1 by hetero-exchange. Impairment in L-Ser transport in ASCT1-KO mice may lead to increased conversion of L-Ser into Gly by the serine hydroxymethyl transferase (SHMT) enzyme. When the Ser shuttle is impaired, Gly taken up by neurons (dashed arrow) may provide a compensatory pathway for supplying L-Ser to neurons via neuronal SHMT. Adapted with permission from Servier Medical Art, https://smart.servier.com. Reprinted with permission from Kaplan, E. et al. PNAS. 2019, 115 (38), 9628-9633. Copyright 2019 National Academy of Sciences.

Decrease in total and extracellular D-Ser suggests a partial impairment of brain D-Ser production. While extracellular L-serine remains unchanged *in vivo* likely due to

compensatory transport mechanisms, it is possible that the equilibrative nature of the ASCT1 transporter is required for supplying enough L-Ser for D-Ser production at local neuron-astrocyte contacts.

Conclusions

In this work we demonstrate the first in-depth study of the function of the ASCT1 transporter using a variety of different techniques including immunohistochemical imaging, electrophysiology, cell and tissue culture analysis, MRI, behavioral testing, and *in vivo* microdialysis. A UHPLC-MS/MS method was developed for absolute basal amino acid measurements from *in vivo* microdialysis with SIL recovery correction. The relationships between SIL calibrant concentration as well as dialysis flow rate and calibration accuracy were explored. Our findings were two-fold: 1) calibrant concentration was shown to inflate calibrated results as a reflection of calibrant purity and 2) we propose that there is an inverse relationship between dialysis flow rate and calibration accuracy. While more work is necessary to elucidate the underlying cause of this trend, it is clear that future use of SIL microdialysis calibration must be first validated through *in vitro* testing and, if possible, no-net flux measurements. After validation, SIL calibration was used to make absolute basal concentration measurements of serine, glycine, alanine, threonine, glutamate and GABA in WT and ASCT1-KO mice. Such measurements have enabled the development of a refined model of ASCT1 transporter function and its role in the serine shuttle.

Chapter 4: On-Chip Benzoyl Chloride Derivatization of Small Molecule Neurotransmitters

Introduction

Pre-column benzoyl chloride (BzCl) derivatization was first utilized in conjunction with high performance liquid chromatography (HPLC) in the 1970s for the analysis of polyamines[110,111] and sugars[112–114] using UV detection. Since then it has become widely adopted for the separation of biogenic compounds containing primary and secondary amines, phenols, thiols and alcohols. Benzoylation significantly improves reversed-phase retention of small, polar analytes allowing separation from complex biological matrices. When combined with tandem mass spectrometry (MS/MS) detection, the benzoyl group improves both electrospray ionization and fragmentation efficiency, improving sensitivity and helping to make BzCl derivatization a valuable tool for a variety of applications including neurochemical analysis[37,42,115–120].

Microdialysis can be used to make dynamic measurements of a wide variety of neurochemicals *in vivo*. In microdialysis, a semi-permeable membrane implanted into the brain is perfused with artificial cerebrospinal fluid (aCSF). Molecules in the extracellular space freely diffuse across the membrane according to their concentration gradients. The dialysis membrane molecular weight cutoff determines whether a given neurochemical can diffuse into the sampling stream. The perfusate can then be collected at the outlet of the probe and analyzed. Benzoylation was first performed for the analysis of 17 neurochemicals in microdialysis fractions using HPLC-MS/MS with an 8 min gradient[37].

More recently, improvements have been made including methods for 70 (20 min)[42] and 24 (2 min)[69] neurochemicals. Currently, the utility of BzCl derivatization for large sample sets and rapid sample collection is limited by the manual three-step reaction scheme: samples are buffered using 100 mM sodium carbonate, reacted with BzCl, and internal standards are added for quantitation.

Reaction automation presents an attractive alternative to manual sample generation for reducing sample handling and improving reaction throughput. In this work we report the use of an all-glass microfluidic chip for BzCl derivatization coupled to microdialysis and offline analysis using UHPLC-MS/MS. Microdialysis fractions were collected at 3 min intervals and 25 widely studied neurotransmitters, neuromodulators, and metabolites including acetylcholine (ACh), dopamine (DA), serotonin (5-HT), norepinephrine (NE), epinephrine (Epi), aspartate (Asp), glutamate (Glu), γ-aminobutyric acid (GABA), histamine (Hist), glycine (Gly), taurine (Tau), glutamine (Gln), phenylalanine (Phe), serine (Ser), tyrosine (Tyr), choline (Ch), 3-methoxytyramine (3-MT), homovanillic acid (HVA), 3,4-dihydroxyphenylacetic acid (DOPAC), 3,4-dihydroxyphenylalanine (L-DOPA), 5-hydroxyindoleacetic acid (5-HIAA), 5-hydroxytryptophan (5-HTP), normetanephrine (NM), adenosine (Ado), and glucose (Glc) were measured using a 2 min gradient separation.

Challenges faced when developing a platform for on-chip derivatization include compatibility with acetonitrile and aqueous reagents ranging in pH from 2 – 10. Furthermore, precipitation of reaction components on channel walls must be prevented to decrease chip clogging and analyte adsorption. Poly(dimethylsiloxane) (PDMS), though generally a popular microfluidic substrate due to its ease of device fabrication and low

manufacturing costs[121] suffers from moderate acetonitrile permeability[122] as well as surface fouling from hydrophobic components of biological fluids[123]. These difficulties were circumvented through the use of an all-glass device derivatized with 1H,1H,2H,2H-perfluorooctyl-trichlorosilane and through several modifications to current benzoylation protocol. This device provides possibilities for adapting BzCl derivatization to fully online workflows and for combining with current microfluidic systems for cell based secretion assays.

Methods

Chemicals and Reagents

All chemicals were purchased from Sigma Aldrich (Saint Louis, MO) unless otherwise noted. Acetonitrile was purchased from Honeywell Research Chemicals through VWR (Radnor, PA). NaCl, KCl, $MgSO_4$, $CaCl_2$, and sulfuric acid were purchased from Fisher Scientific (Fairlawn, NJ). DOPAC, 3-MT, sodium phosphate dibasic and sodium tripolyphosphate were purchased from Acros Organics (Geel, Belgium). 5-HT was purchased from Alfa Aesar (Ward Hill, MA). D4-ACh/Ch were purchased from CDN Isotopes (Pointe-Claire, Quebec). Stock solutions of 2 mM Tyr; 5 mM Ado; 10 mM 5-HT, NE, DA, NM, 3-MT, Epi, L-DOPA, 5-HIAA; 20 mM Hist, GABA, 5-HTP, Asp, HVA, Gly, Glu, DOPAC, Phe, Ser; 25 mM ACh; 40 mM Tau; 100 mM GSH, Gln, Glc; and 1 M Ch were prepared in HPLC grade water. A calibration standard mixture was prepared by diluting stocks into aCSF consisting of 145 mM NaCl, 2.68 mM KCl, 1.4 mM $CaCl_2$, 1.0 mM $MgSO_4$, 1.55 mM Na_2HPO_4, and 0.45 mM NaH_2PO_4 adjusted to pH of 7.4 with 0.1 M NaOH. Calibration curves were prepared in aCSF with 250 μM ascorbic acid for the following concentration ranges: 0.1 – 50 nM for 5-HT, NE, DA, NM, 3-MT, Epi and L-

DOPA; 0.25 – 125 nM for ACh; 0.5 – 250 nM for Hist; 1-500 nM for GABA, 5-HIAA, 5-HTP, GSH, and Ado; 0.002 – 1 μM for Asp; 0.0025 – 1.25 μM for HVA and Tyr; 0.01 – 5 μM for Glu, Gly, Phe, Ch, and DOPAC; 0.02 – 10 μM for Tau; 0.025 – 12.5 for Ser, 0.05 – 25 μM for Gln, 0.25 – 125 μM for Glc.

All-Glass Chip Fabrication

Microfluidic devices were fabricated from D263 glass slides (Telic Company, Valencia, CA). Photolithography and hydrofluoric acid etching were modified from previous protocols [124–128]. Briefly, slides were baked at 70 °C for 10 min, then coated with AZ1505 photoresist (Integrated Micro Materials, Argyle, TX). After exposure and development, slides were etched with 49% hydrofluoric acid: hydrochloric acid: water, 1:1:2 to a depth of 85 um. Following the wet etch, access holes were drilled with 1 mm drill bits. Slides were then washed for 20 mins in piranha solution and 40 mins in heated RCA solution. Post-wash, slides were aligned under a stream of water and bonded at 560 °C for 8 h. Captite Bonded-port connectors (LabSmith, Livermore, CA) were secured over each drill hole with Loctite Marine Epoxy (Loctite, Düsseldorf, Germany). Prior to device operation, channels were derivatized with 2% Trichloro(1H,1H,2H,2H-perfluorooctyl)silane dissolved in perfluorodecalin (PFD). The devices were left to dry at 70 °C overnight then flushed with PFD to remove excess silanes. PFD was flushed from chips with nitrogen and allowed to dry overnight at 70˚C.

On-Chip Mixing Analysis

For on-chip mixing visualization at different mixing strategies, cresol red pH indicator was mixed with sodium carbonate (both at 1 μL/min). Mixing was observed as a

color change from yellow (neutral pH) to magenta (basic pH). Color analysis was performed using ImageJ (version 1.52, NIH). The gray scale intensity profile of radial line scans were used to compare each geometry to complete mixing. A variety of geometries as well as ultrasonic mixing was explored using a speaker, a sonicator bath operated at 37 kHz or 80 kHz (P60H, Elma Ultrasonic) or direct coupling to piezoelectric actuators (Digikey, Thief River Falls, MN). Ceramic piezoelectric actuators with a range of resonant frequencies (2.5, 4.1, 4.6, 6, 7, 9 kHz) were glued to chips to generate vortices at mixing junctions.

UHPLC-MS/MS Assay for Bz-Labeled Neurochemicals

All analysis was done using a Thermo Fisher Vanquish UHPLC interfaced with a Thermo Fisher TSQ Quantum Ultra triple-quadrupole mass spectrometer. Briefly, samples were injected onto a Phenomenex Kinetex C18 column (2.1 mm x 100 mm, 1.7 μm). Mobile phase A consisted of 10 mM ammonium formate and 0.15% formic acid. Mobile phase B was pure acetonitrile. The method flow rate was 600 μL/min and the gradient was as follows: initial, 5% B; 0.01 min, 19 % B; 0.68 min, 26% B; 1.055 min, 75% B; 1.805 – 2.18 min, 100% B; 2.28-3 min, 5% B. The pressure range across each gradient was 350 – 800 bar. The autosampler was at 25˚C while the column was held at 30˚C in still air mode. ESI was used in positive mode with a spray voltage of 2.5 kV. Vaporizer and transfer capillary temperatures were 400˚C. Sheath gas was set to 10 and auxiliary gas was set to

5. The skimmer offset was -1 V and tube lens values were tuned for each individual analyte. The TSQ Quantum Ultra was operated in MRM mode. Total analysis time was 4 min.

On-Chip Calibration Curve Preparation

All reagents were prepared the day of the experiment. Reagent 1 (C/TP): 100 mM sodium carbonate/100 mM sodium tripolyphosphate in H_2O. Reagent 2 (BzCl): 0.5% BzCl in ACN (v/v). Reagent 3 (IS): $^{13}C_6$-Bz derivatized internal standards in 1:1 ACN:H2O with 1% H_2SO_4 (v/v). Each reagent as well as all standards were loaded into 1 mL glass syringes (Hamilton Company, Reno, NV) and driven by two separate fusion 400 syringe pumps (Chemyx, Strafford, TX). Standards were flowed at 1 μL/min while reagents were flowed at 0.5 μL/min to give a ratio of addition of 2:1:1:1 (standard:C/TP:BzCl:IS). Fractions were collected at 3 min intervals (7.5 μL total volume) in vials for offline UHPLC-MS/MS analysis. Each concentration was perfused through the system for 15 mins before collecting 5 fractions to generate both blanks and a 6-point calibration curve. All fluidic switching was done using a 6-port HPLC valve (VICI, Houston, TX) for uninterrupted flow.

Microdialysis Probe Construction

Briefly, custom concentric microdialysis probes were constructed for bilateral implantation into the rat striatum. An inlet (40/110, ID/OD) and outlet (75/150) fused silica capillary were glued into a 13.5 mm (25 G) piece of stainless steel hypodermic sheath tubing (Small Parts Inc., Logansport, In) with the inlet capillary protruding from the end of the tubing and the outlet capillary several mm within. The inlet capillary was cut to a length of 4 mm extending beyond the sheath and a regenerated cellulose dialysis membrane (Spectrum Life Sciences, LLC. Rando Dominquez, CA) was placed over the inlet and

inserted into the sheath. A 100 μm epoxy plug (Loctite, West Lake, OH) was placed at the tip of the membrane and epoxy was also used to seal the membrane to the sheath. Inlet (150/360) and outlet (180/360) fused silica adapting capillaries were glued onto the inlet and outlet capillaries, respectively. A small piece of pipette tip was then glued over the proximal end of the adapting capillaries to strengthen the probe. Before use the probe was rinsed with 70% ethanol, then flushed extensively with sterile aCSF.

In Vitro Concentration Step-Changes

Chip temporal response to concentration changes was explored through *in vitro* microdialysis step-change experiments. Briefly, a microdialysis probe perfused with aCSF at 1 μL/min was placed in a stirred vial of aCSF and connected to the inlet of the derivatization chip. For initial dead time calculation, cresol red was flowed through the probe at 1 μL/min while reagent 1 was sodium carbonate and reagents 2 and 3 were water (all at 0.5 μL/min). The color change was then visualized at the inlet and outlet of the chip to calculate time-on-chip as well as total system dead time. For step change experiments, all reagents were flowed at 0.5 μL/min. Once stable flow was established the chip was equilibrated for 30 min before fraction collection. A standard mixture was spiked into the stirred vial, gradually increasing in concentration. Five 3-min fractions were collected at each concentration and after the high-point the probe was quickly moved to a fresh vial of aCSF to collect another five blank samples.

in Vivo Temporal Response

In vivo temporal response was investigated in an anesthetized animal using 75 mM K^+ aCSF retrodialysis. Rats were anesthetized using 1-5% isoflurane and mounted to a

stereotaxic instrument (David Kopf Instruments, Tujunga, CA). A 4 mm microdialysis probe was implanted into the striatum using the following coordinates with reference to bregma: + 1 mm anterior, ± 3 mm lateral, and – 6.75 mm ventral to the surface of the brain[71]. The probe was connected to the chip and flowed at 1 μL/min for 15 min before fraction collection. A total of 10 baseline samples were collected (30 min) followed by two 3-min 75 mM K^+ stimulations separated by 30 min to allow for return to baseline.

Bicuculline Retrodialysis in Awake Animals

Male Sprague-Dawley rats weighing 300 – 350 g were anesthetized using 1-5% isoflurane and mounted to a stereotaxic instrument. A burr hole were drilled at above coordinates and probes were slowly lowered into place while being continuously perfused with aCSF at a flow rate of 4 μL/min to prevent deformation of the membrane. Three stainless steel skull screws (Plastics Once Inc, Roanoke, VA) were used to mount the probe to the brain. Dental cement (A-M Systems, Sequim, WA) was used to encase the probe and skull screw to secure the probe. Rats were tethered to a Raturn (Bioanalytical Systems, Inc., West Lafeyette, IN) and perfused continuously with aCSF at 0.5 μL/min during the 24-hr recovery period. Two hours prior to fraction collection a fresh syringe of aCSF (250 μM ascorbic acid) was perfused at 1 μL/min and 30 min prior to collection the reagents and dialysate were flowed through the chip. **Figure 4-1** shows the experimental setup for on-chip derivatization in awake rats.

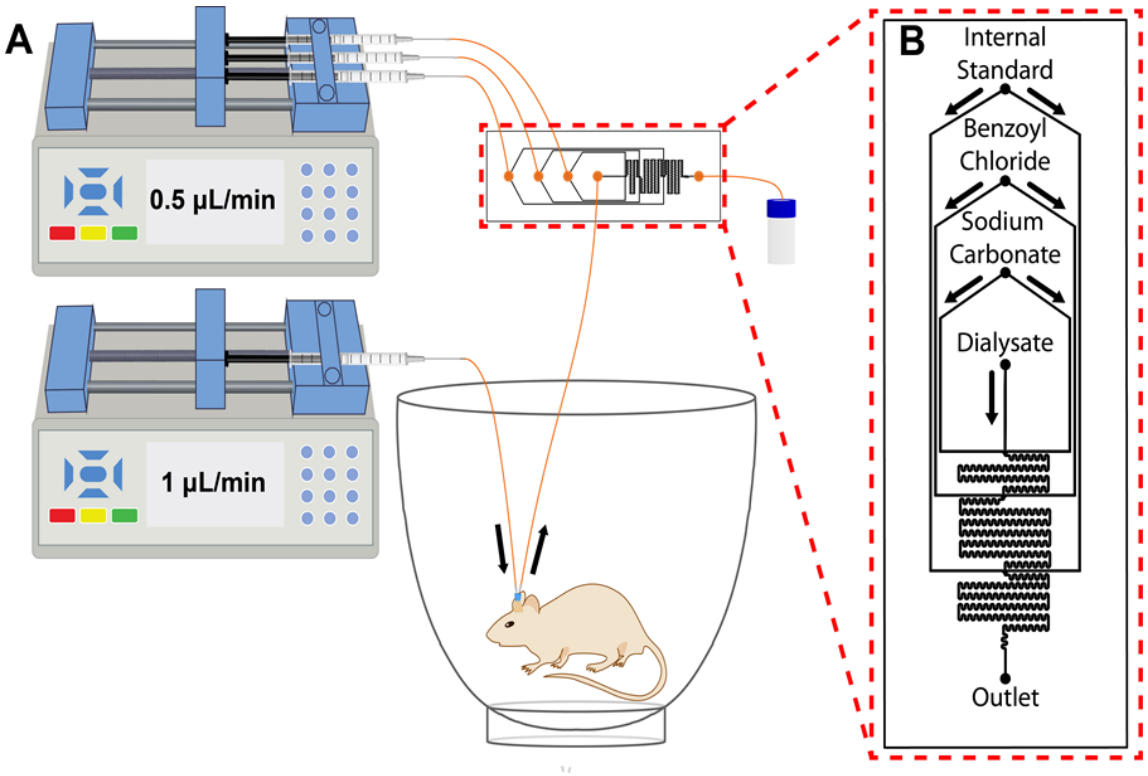

Figure 4-1: Illustration of experimental setup for coupling microdialysis sampling in awake animals with on-chip BzCl derivatization. (A) Microdialysis probes were perfused with aCSF at 1 µL/min. Perfusate was derivatized in a continuous stream by sequentially adding 100 mM sodium carbonate/sodium triphosphate, BzCl (0.5% (v/v) in acetonitrile, and internal standard mixture each at 0.5 µL/min. Samples were then collected offline and analyzed by UHPLC-MS/MS. (B) Diagram of all-glass microchip for derivatization. All Channels are 75 µm wide x 85 µm deep. Each reagent is split into two paths for improved mixing at the junction with the sample stream.

As in calibration curve preparation, a 6-port valve was used to switch between aCSF and 50 µM bicuculline. A 30 µL fused silica loop was filled with bicuculline and the HPLC valve was actuated to place the loop into the flow path for 30-min. The loop was then taken offline for 30 min to allow return to baseline. After post-bicuculline collection a 3-min 75 mM K^+ stimulation was used to verify tissue health.

Results and Discussion

Choosing a Microfluidic Chip Substrate

All initial work was performed on PDMS devices due to ease of fabrication. While a variety of designs could be rapidly fabricated and tested, PDMS suffers from ACN permeability as well as surface fouling as previously mentioned. **Figure 4-2** shows rapid formation of precipitate during addition of carbonate in the first reagent addition stage. Precipitation at this junction could be prevented with the removal of Mg^{2+} and Ca^{2+} from the aCSF. The likely source was insoluble carbonate salts ($CaCO_3$ and $MgCO_3$). Precipitation at the BzCl reagent junction could only be prevented by removing BzCl.

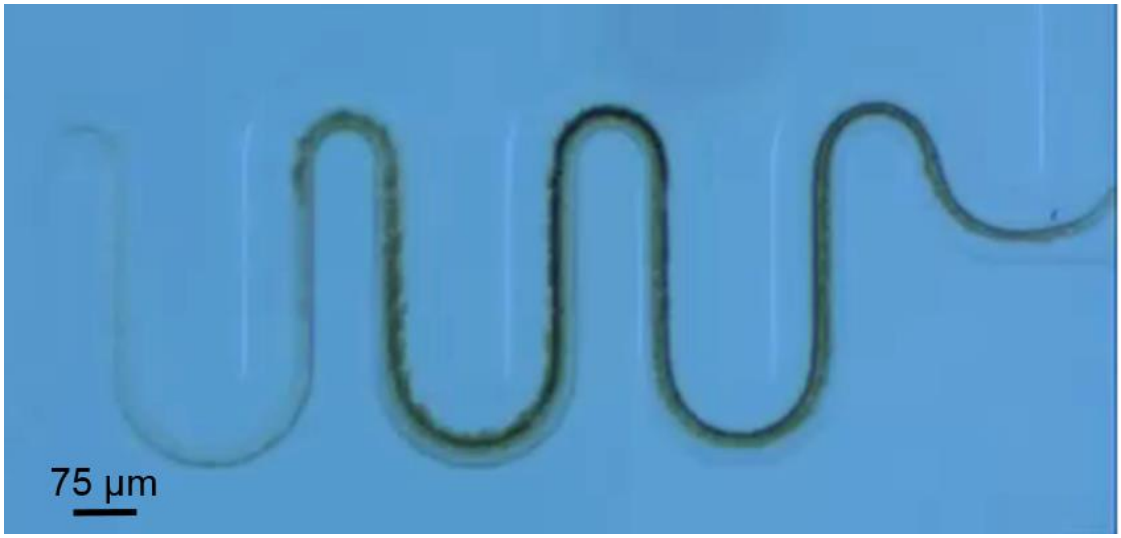

Figure 4-2: Precipitation at carbonate reagent addition junction in PDMS chip after 10 min of operation. Significant precipiation occurred at each of the three reagent addition junctions. Channel dimensions are 75 µm wide x 50 µm deep.

After a broad range of conditions were tested including basic buffers (carbonate/borate), chelating agents (EDTA), reagent solvents (methanol, DMSO), and a phase-transfer catalyst (tertbutylammonium chloride) it was determined that PDMS was an inappropriate substrate for the reaction. Precipitation of BzCl and Bz-neurochemicals likely results from moderate PDMS permeability to ACN as well as nonspecific adsorption to surface methyl groups. While similar results were obtained for carbonate precipitation in all-glass devices, there was a significant reduction in precipitation during BzCl reagent addition (**Figure 4-3**).

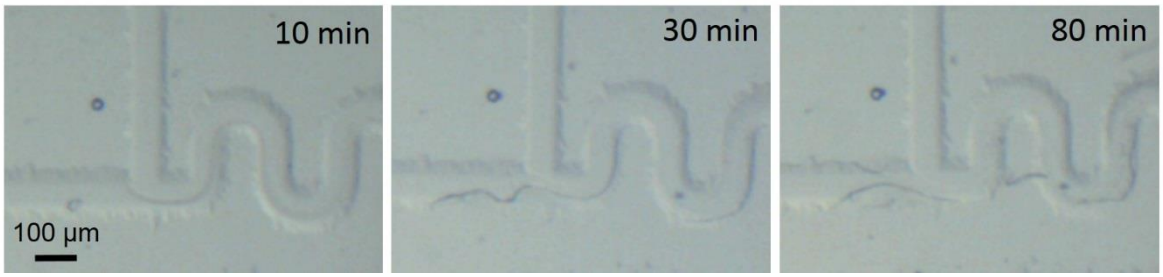

Figure 4-3: Images of the BzCl reagent addition junction on all-glass device taken after 10, 30, and 80 min of continuous flow. BzCl was flowed at 0.5 µL/min (from left) while premixed aCSF/sodium carbonate was flowed 1.5 at µL/min (from top). Channel dimensions are 75 µm wide x 85 µm deep. While a distinct phase boundary can be seen, no precipitation occurred.

Active On-Chip Mixing

Although BzCl did not precipitate when mixed with aCSF and sodium carbonate, addition of neurochemical standards led to a slow but significant buildup at the junction (**Figure 4-4**). Not only is this a concern for device clogging, but also loss of analyte via adsorption to the device walls can impact sensitivity as well as temporal response.

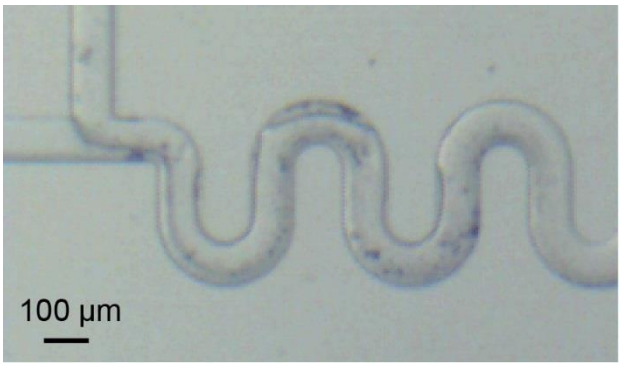

Figure 4-4: Precipitate formation at laminar interface of BzCl junction after on-chip derivatization of high concentration 25 compound standard mixture. Reagents were continuously flowed for the 2 hr duration of the experiment.

When laminar flow persists between acetonitrile and water phases following benzoyl chloride reagent addition, analytes may undergo the benzoylation at the solvent interface and precipitate due to poor solubility in 100% H_2O. At the range of Reynolds numbers found in microfluidic devices (generally < 100) laminar flow dominates and mixing requires input of energy, specialized geometries, or some combination of both[129]. Precipitation due to heterogeneity found at laminar solvent interfaces can be prevented by ensuring rapid and effective mixing of aqueous and organic phases. Active mixing within microfluidic devices has been reported through the transfer of intense vibrational energy into chip mixing channels from external sources. A wide range of mixing frequencies (200 Hz – 1.54 GHz) have been employed to investigate on-chip mixing for various applications[129–131].

For low frequency mixing, an audio exciter (Dayton Audio, Springboro, OH) was secured to the device with epoxy and a range of high frequency tones (0.1 – 20 kHz) was generated. Even at high volumes there was no effect on mixing (visualized with cresol red) within the device. It was hypothesized that ineffective coupling of the speaker to the device as well as poor frequency responses of audio speakers above ~5,000 Hz may have been

contributing factors to poor mixing performance. To examine the effect of ultrasonic frequencies (> 20 kHz) on mixing, devices were operated while submerged in a sonicator bath capable of resonating at both 37 and 80 kHz at high power. The bath was kept at room temperature by a circulating chiller and the addition of ice. By sonicating the device during the reaction, clogging was prevented for long enough to collect derivatized samples. **Figure 4-5** shows peak areas of analytes derivatized while the device was submerged in the sonicator bath compared with those derivatized manually.

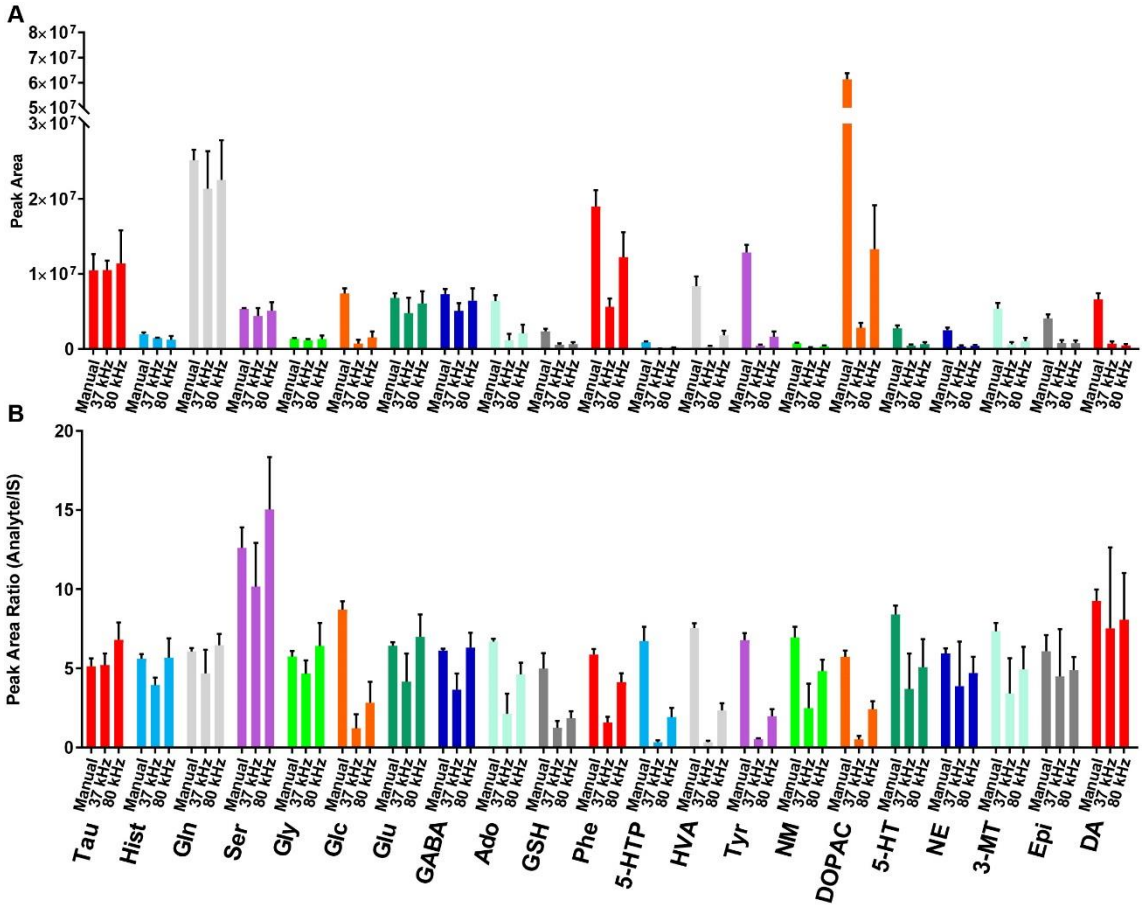

Figure 4-5: On-chip benzoylation reaction during chip sonication (37 and 80 kHz) compared with manual preparation. (A) 17 of 21 analyte peak areas (n = 5) are lower when prepared on-chip than manually. 80 kHz sonication improved peak areas for the majority of analytes. (B) Peak area ratio (Analyte/IS) show better agreement with manual preparation than peak area for most analytes. Values are mean ± SD.

Interestingly, a trend emerged in which analyte peak areas showed a larger loss (with respect to manual derivatization) with increasing retention time (left-to-right). Since retention time increases with the number of Bz groups, this suggests that multiply benzoylated analytes lost more signal than singly. Two potential sources are: (1) incomplete derivatization prior to IS addition (i.e. inadequate serpentine mixing channels between reagents) (2) increasing surface adsorption with decreasing Bz-analyte polarity. Both analyte and IS signal loss were compared with respect to manual derivatization for 80 kHz sonication (**Figure 4-6**). Despite being pre-derivatized, ISs also show a strong trend towards polarity-based loss in signal suggesting adsorption rather than incomplete benzoylation a source.

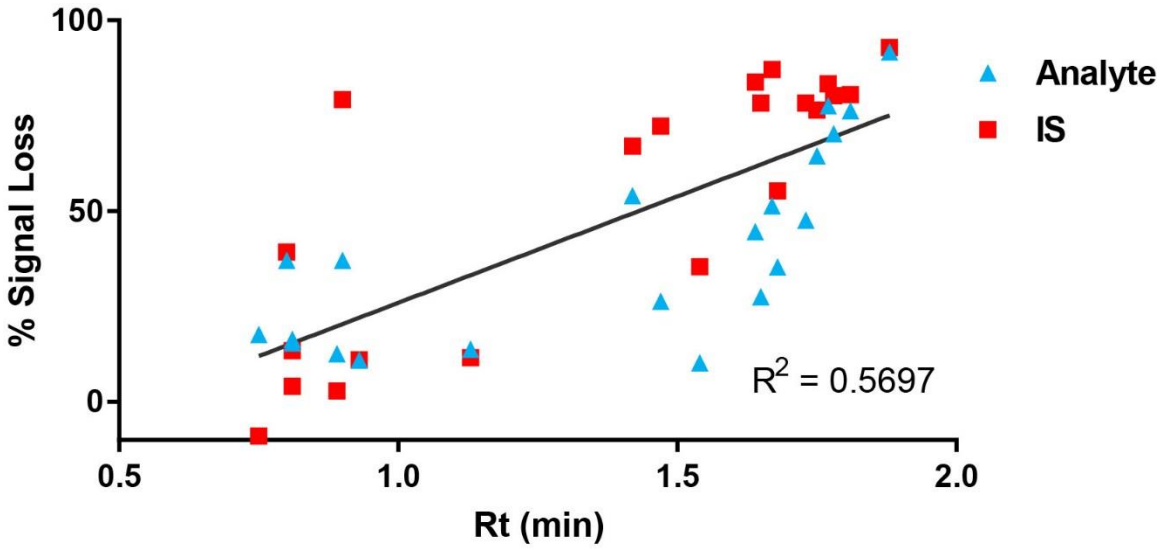

Figure 4-6: Analyte and IS signal loss (percent of manually derivatized) versus retention time (Rt) for 80 kHz sonication. More highly retained compounds (less polar/more benzoylated) showed a trend toward (R^2 = 0.5697) larger loss in signal for both analyte and IS, suggesting surface adsorption as the major contributor to signal loss.

Although mixing via sonication yielded promising results, lack of control over frequency range as well as vibrational dampening through the water bath itself are impediments in realizing the utility of ultrasonic mixing. Furthermore, precipitation still

occurred at the carbonate and BzCl reagent addition junctions. Sonicators use the piezoelectric effect as a driving force. Applying an alternating current to piezoelectric materials, or actuators, results in vibrations corresponding to the applied frequency. Available miniaturized piezo actuators are well matched to dimensions found in microfluidic devices and enable high powered vibrational energy to be transferred to very specific locations. We explored coupling small piezoelectric ceramic actuators to our benzoylation chip. The resonant frequency of an actuator is dictated by its size. Using available instrumentation we tested frequencies of 2.5, 4.1, 4.6, 6, 7, and 9 kHz, all of which yielded no effect on mixing. A specialized geometry based on rapid mixing through acoustic streaming generation with "sharp edge" geometries within this frequency range was also tested[131]. **Figure 4-7** is a representative image of laminar flow during chip coupling to the previously mentioned frequencies. It was concluded that this phenomenon does not occur due to the rigidity of glass and is only seen on devices in which the edges are fabricated from PDMS. Although there have been successful reports of high frequency acoustofluidic mixing in straight channels without specialized geometries[130,132], generating such frequencies (MHz – GHz) requires specialized equipment not readily available.

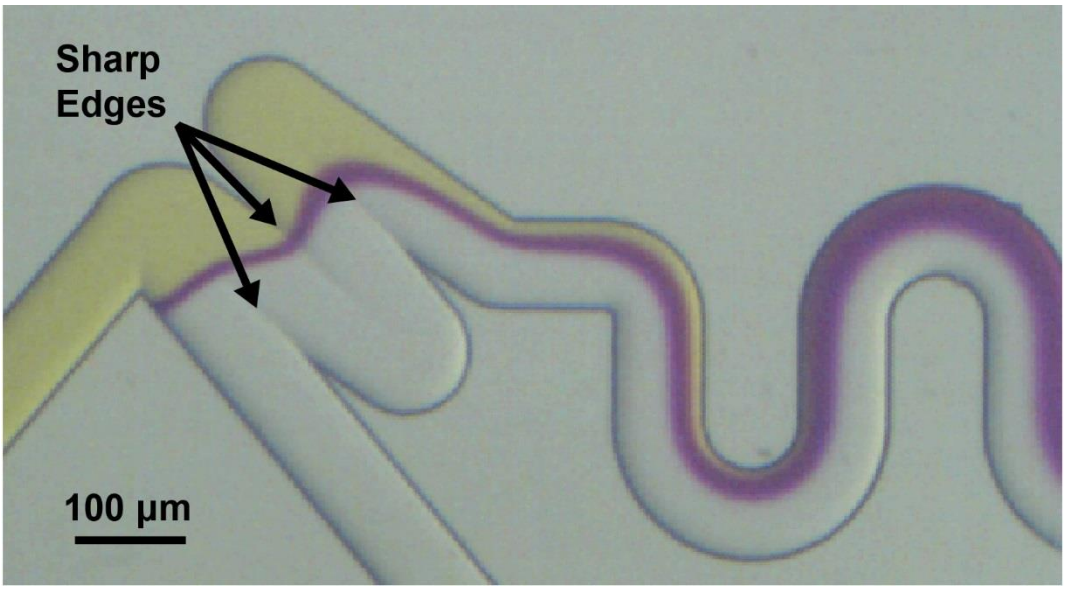

Figure 4-7: Laminar flow at reagent addition junction geometry based on sharp edge acoustic streaming. Cresol red (yellow) and carbonate (clear) were flowed at 1 µL/min. No effect was observed at the following frequencies: 2.5, 4.1, 4.6, 6, 7, and 9 kHz.

Passive On-Chip Mixing

Several reagent addition geometries were explored to maximize mixing. The two best-performing geometries included a sharp turn into serpentine mixers at the junction (**4-8A**) and dual-addition junction with each reagent split into parallel channels (**4-8B**).

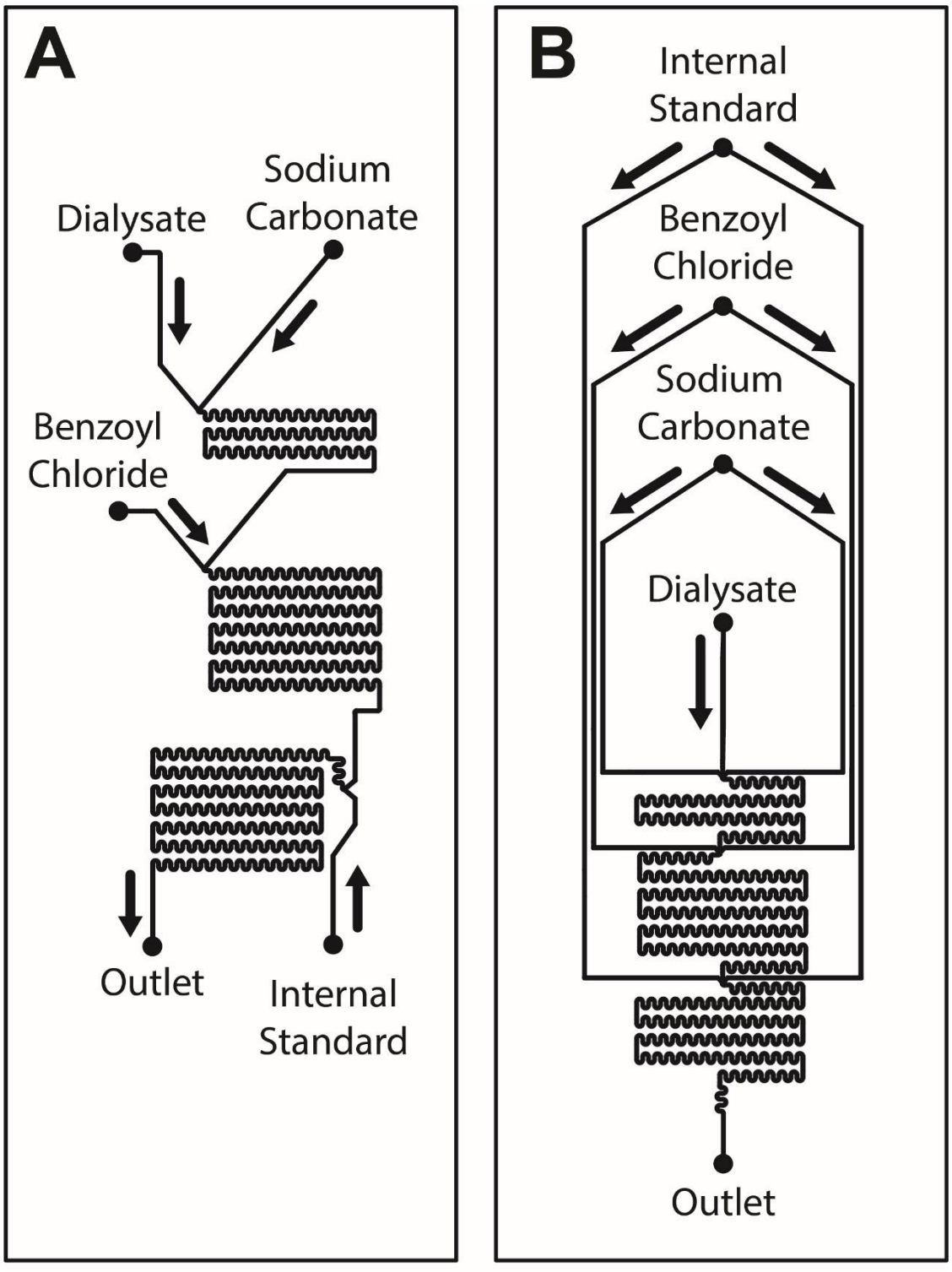

Figure 4-8: Best-performing reagent addition devices with respect to mixing. Design A utilizes a sharp turn into serpentine mixers at the junction. Desgin B has a duel-addition junction with each reagent split into parallel channels. Channel dimensions were 75 μm x 80 μm (width x depth). Split channels in design B narrow to 37.5 μm x 80 μm as they converge on dialysate stream.

As cresol red pH indicator mixed with the carbonate reagent, a color shift from yellow to magenta was observed (**Figure 4-9A-B**). Mixing rate was analyzed by comparing the intensity profile of a radial line scan of the channel after 10 mixing serpentines in design A and B to a line scan after 40 serpentines to visualize complete mixing. Complete mixing was seen as a relatively flat line scan at a gray value of ~125 across the diameter of the channel. A line scan of carbonate pre-mixing is also shown for visualization (**Figure 4-9C**). Design B was indistinguishable from complete mixing after 10 serpentines while design A showed large heterogeneity across the channel. Design A had two distinct regions across the channel: well mixed (0 – 30 μm) and completely unmixed (55 – 70 μm) suggesting laminar flow persisting much farther past the junction. Our results indicate that design B enabled the fastest mixing although Design A may still represent a viable alternative. Future experiments were performed using Design B (**Figure 4-9**).

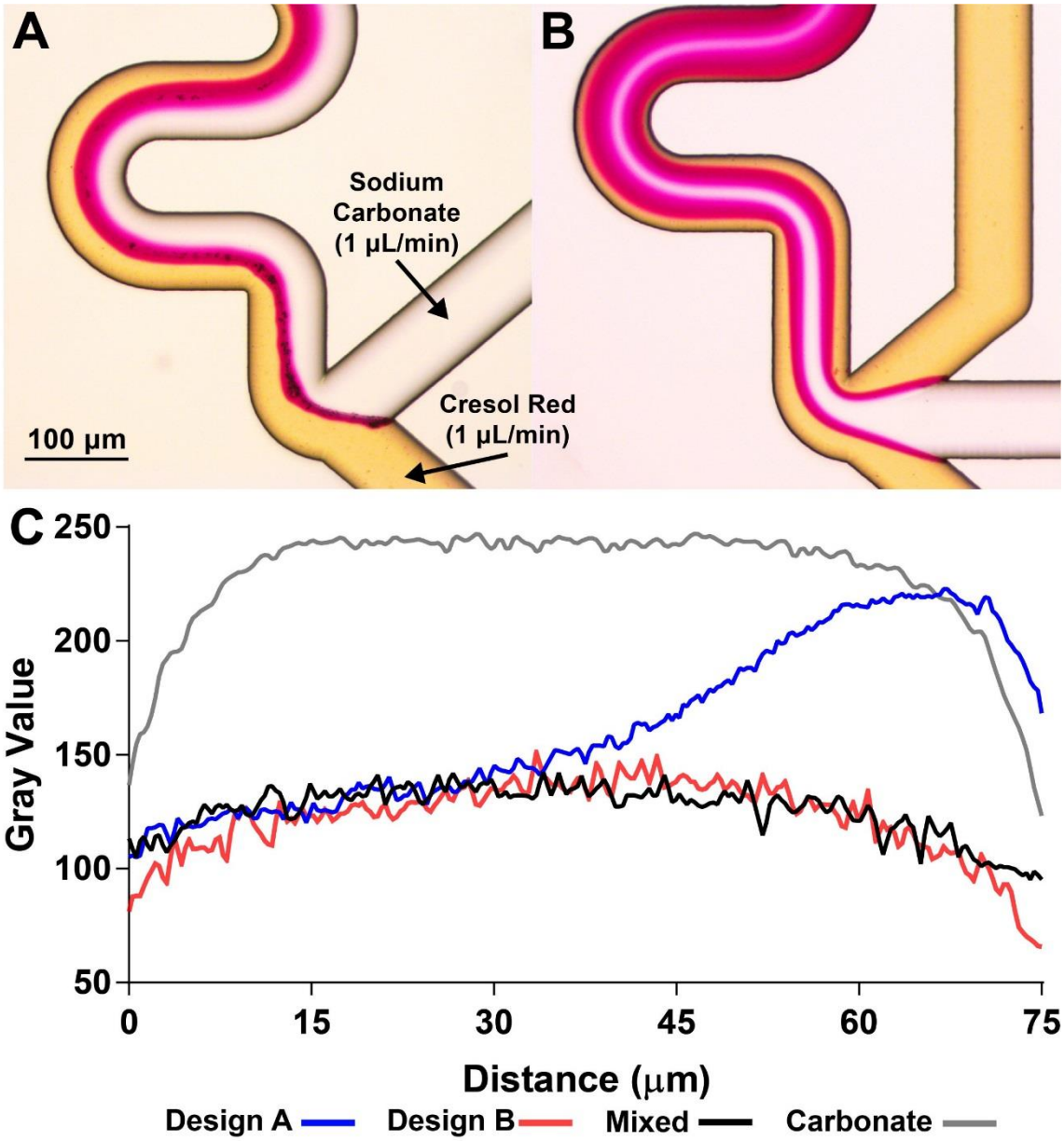

Figure 4-9: Mixing comparison between two different reagent addition geometries. 100 mM sodium carbonate was added to cresol red pH indicator at a 1:1 ratio (1 µL/min) to illustrate effect of geometry on mixing rate. (A) Design A: Tee junction proceeding into serpentine mixing channels. (B) Design B: Reagent flow added simultaneously from two parallel channels. (C) Intensity profile of a radial line scan after 10 mixing serpentines compared between designs A (blue) and B (red). To illustrate no mixing, a line scan of the sodium carbonate channel was taken (gray). For complete mixing (black), a line scan was taken after 40 serpentines.

Surface Modification

Fluoroalkyl silane surface modifications have been used to prevent surface fouling in microfluidic devices for a variety of applications[133–136]. 1H,1H,2H,2H-perfluorooctyl-trichlorosilane was chosen to reduce Bz-analyte adsorption to the channel walls. A large improvement in analyte peak areas and reduction in signal drift over time was seen in devices with surface modification (**Figure 4-10**).

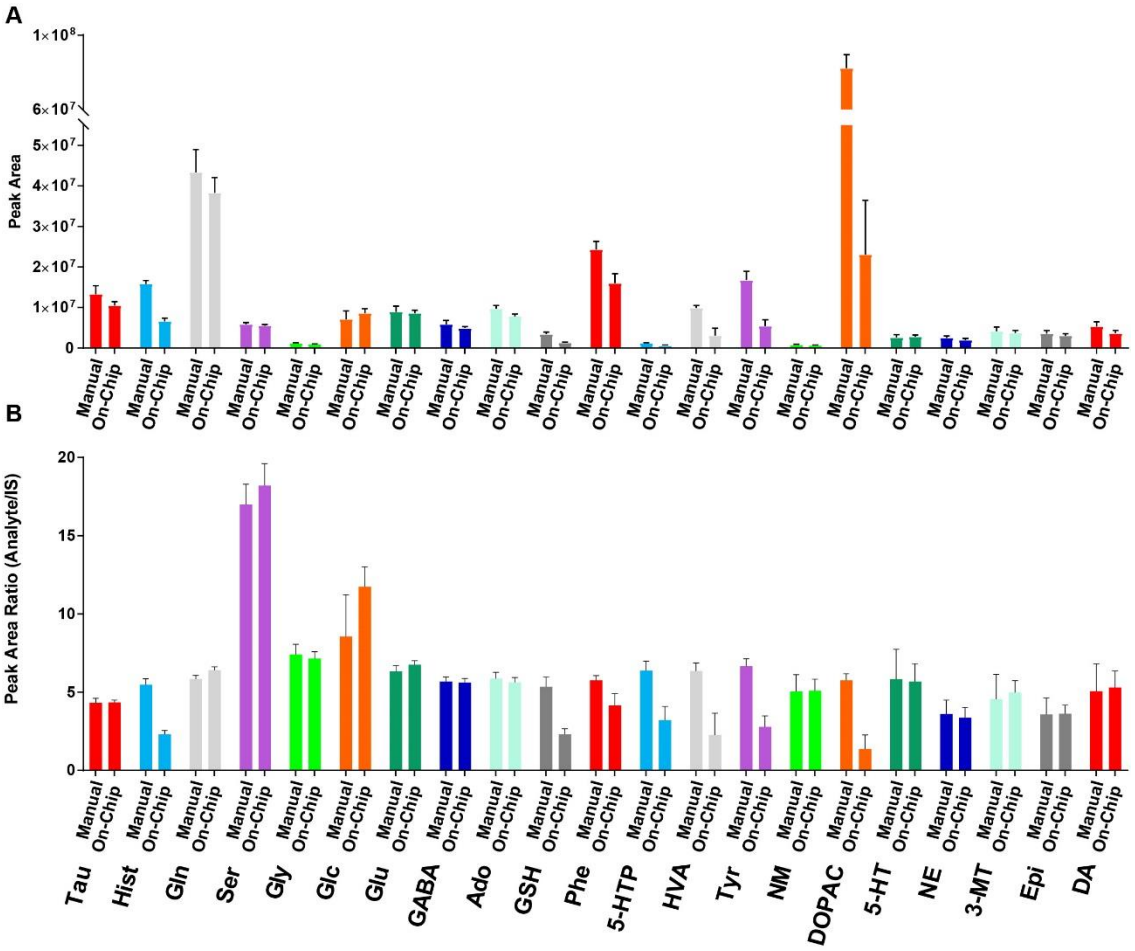

Figure 4-10: On-chip benzoylation of neurochemical standards (n=9) in device modified with 1H,1H,2H,2H-perfluorooctyl-trichlorosilane. Significant increase was seen in peak areas particularly for multiply benzylated analytes (A). Areas equivalent to manually derivatized samples except for the following analytes: Hist, GSH, Phe, 5-HTP, HVA, Tyr, and DOPAC. Peak area ratio improved on-chip samples in relation to manual preparation.

Precipitate Prevention using Sodium Triphosphate

Sodium triphosphate is a commonly used chelating agent in detergents and food preservative in meats[137]. It was chosen for our application because it binds tightly to divalent cations ($Ca^{2+/}Mg^{2+}$), is soluble in a wide pH range, and can tolerate moderate amounts of acetonitrile. Sodium triphosphate was dissolved in the carbonate reagent in large molar excess (100 mM) to the $CaCl_2$ (1.4 mM) and $MgSO_4$ (1 mM) in aCSF to prevent large-scale precipitation of carbonate salts. In **Figure 4-11** aCSF was mixed with 100 mM sodium carbonate (**11B**) or 100 mM sodium carbonate/100 mM sodium triphosphate (**11C**) at a 1:1 ratio. While precipitation was slowed by perfluorosilane surface modification there was still significantly more salt buildup in the absence of triphosphate (**Figure 4-11B-C**). It is clear that triphosphate addition will enable prolonged device operation. Precipitation was also reduced in the BzCl reagent addition portion by lowering the BzCl concentration from 2% to 0.5 %. This lead to no loss in peak area for analytes (data not shown).

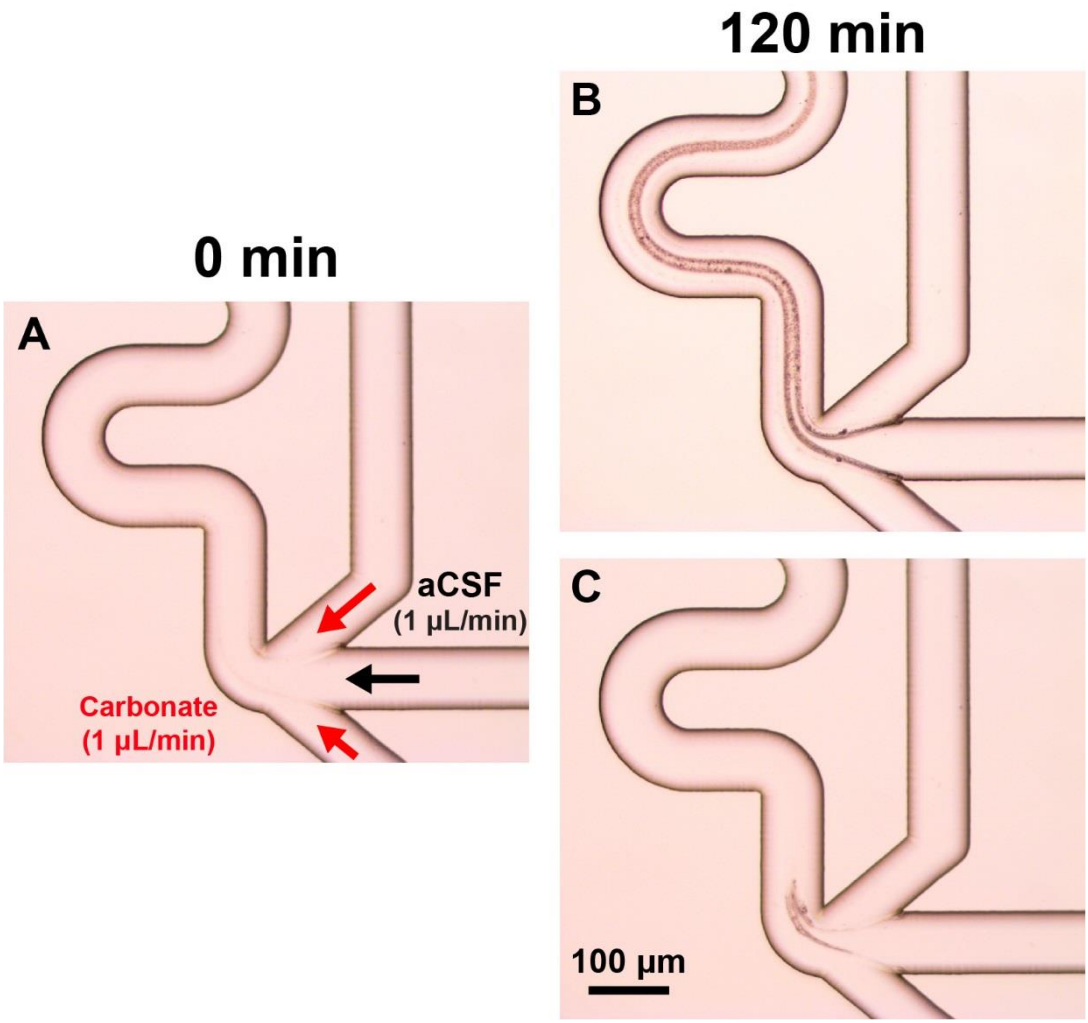

Figure 4-11: Effect of triphosphate chelation on rate of $CaCO_3$ and $MgCO_3$ precipitation. (A) Initial image of device at the start of flow. After 120 min the carbonate buffer precipitated more at the junction (B) than carbonate with 100 mM triphosphate (C).

On-Chip Calibration

Calibration curves were generated for all 25 analytes on-chip using syringe-driven flow and a 6-port valve for switching between concentrations using the online derivatization method (**Figure 4-12**).

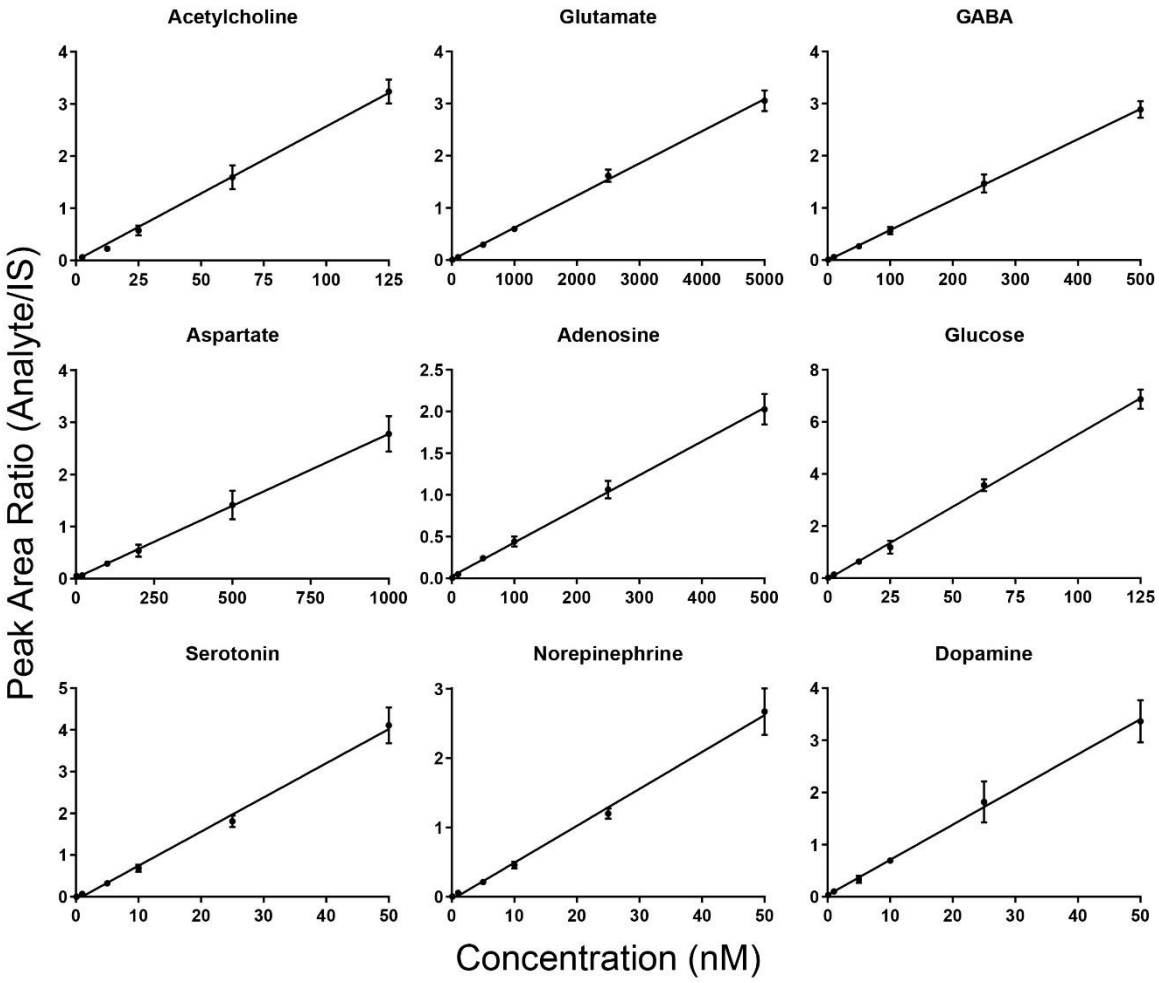

Figure 4-12: Calibration curves representing the range of chemical classes targeted in our method. ACh – unlabeled; Glu, GABA, Asp, Ado, Glucose - singly benzoylated; 5-HT – doubly benzoylated; NE, DA – triply benzoylated.

Limits of detection, linearity, and percent relative standard deviation (peak area ratio) were comparable to previous reports for manual benzoylation[37,42]. A method summary can be found in **Table 4-1**. Basal concentration was determined from the average of measured baseline concentrations *in vivo* in the striatum of awake rats. Analytes falling below the LoD are 5-HTP, NM, Tyr, and Epi.

Analyte	RSD (%)	Fit (R^2)	LoD (nM)	Basal Concentration (nM)
Choline	6	0.9999	50	160 ± 30
Acetylcholine	6	0.9979	2	4 ± 1
Bz-Taurine	10	0.9998	80	250 ± 100
Bz-Histamine	4	0.9989	0.7	3 ± 1
Bz-Serine	5	0.9998	160	8,800 ± 1,200
Bz-Glutamine	7	0.9997	20	34,000 ± 4,000
Bz-Aspartate	7	0.9996	20	40 ± 15
Bz-Glycine	11	0.9997	130	9,600 ± 2,500
Bz-Glucose	5	0.9986	500	530,000 ± 60
Bz-Glutamate	6	0.9990	10	250 ± 70
Bz-GABA	6	0.9998	1	60 ± 15
Bz-Adenosine	8	0.9993	0.9	7 ± 3
Bz-Phenylalanine	10	0.9993	6	660 ± 130
Bz-5-HIAA	18	0.9868	50	330 ± 130
Bz-HVA	4	0.9997	2	1,100 ± 470
Bz-5-HTP	46	0.9970	13	*
Bz-Normetanephrine	16	0.9996	0.6	*
Bz-Tyrosine	7	0.9968	105	*
Bz-DOPA	15	0.9957	3	3 ± 1
Bz-DOPAC	11	0.9983	6	1,200 ± 190
Bz-5-HT	14	0.9963	0.1	1 ± 0.05
Bz-Norepinephrine	11	0.9970	0.1	1 ± 0.06
Bz-3-MT	9	0.9996	0.1	3 ± 0.6
Bz-Epinephrine	5	0.9999	0.3	*
Bz-Dopamine	6	0.9985	0.4	6 ± 2

Table 4-1: Figures of merit for 25 analytes analyzed in 5 μL samples. Relative standard deviation, linearity (R^2), and limits of detection were calculated from 5 replicate on-chip calibration curve preparations. Basal concentrations were determined by averaging 10 baseline samples from awake experiments in the striatum. Below limit of detection in the striatum denoted by *. Basal values are Mean ± SD.

Device Temporal Resolution

We investigated temporal resolution of our system through *in vitro* step-change experiments as well as *in vivo* 75 mM K^+ retrodialysis. In order to isolate the temporal resolution of our device, the contribution of tubing was minimized by using 75 μm I.D. fused silica capillary to connect the dialysis probe to the chip. At a flow rate of 1 μL/min we expect a contribution of 12 s to the width of a 3 min wide K^+ stimulation[138]. Fractions

were collected at 3 min intervals and therefore the maximum temporal resolution achievable is 3 min. Defining resolution as the rise time from 10 – 90% our data shows that the device has an *in vitro* temporal resolution of 3 min (**Figure 4-13A**). In other words, despite the presence of inlet and outlet port dead volumes and on-chip mixing channels, derivatizing online does not significantly reduce temporal resolution. While rise time is rapid, it is important to note the presence of ~20% carryover in the first fraction after the returning to a blank aCSF solution. Aside from smoothing of concentration steps within the tubing and mixing channels, two potential sources for the carryover are: 1) analyte adsorption within the device 2) mechanical carryover from switching between solutions. Carryover for ACh and Ch (unlabeled, data not shown) resemble that of GABA which implies mechanical carryover.

An *in vivo* experiment was performed on an anesthetized rat to further validate our platform for measuring concentration dynamics. We collected 10 baseline samples followed by a pair of 3 min 75 mM K^+ stimulations administered via retrodialysis through the sampling probe separated by 30 min to allow for return to baseline. DA, 5-HT, GABA, and Glu all show a rapid rise in concentration in response to the 75 mM K^+ but a delayed return to baseline similar to the step-change experiment (**Figure 4-13B-E**). DA takes much longer to return to baseline than Glu or GABA suggesting the possibility of carryover scaling with hydrophobicity. An in-depth exploration of carryover is required in order to further improve our system's temporal response.

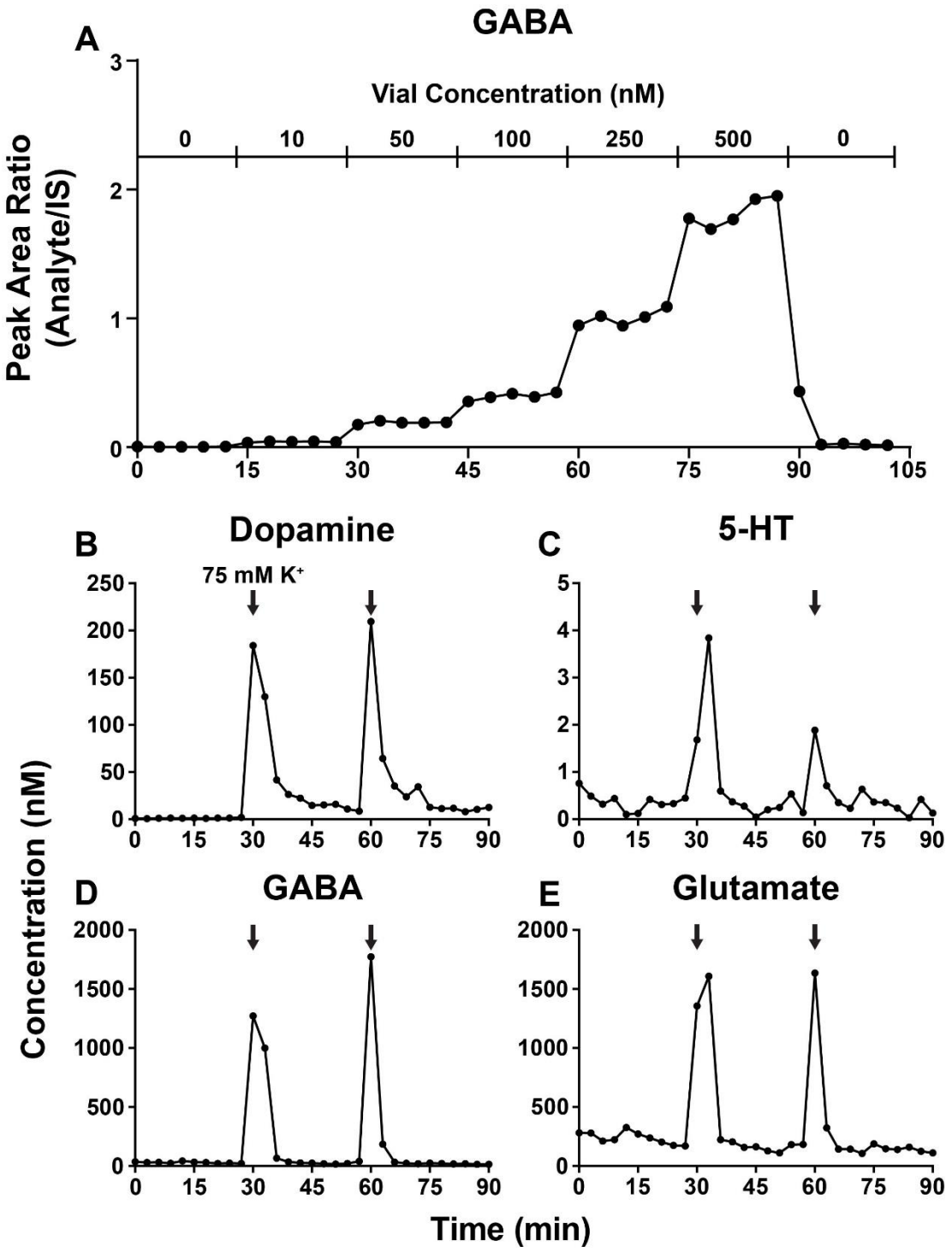

Figure 4-13: Temporal response of on-chip derivatization was investigated by *in vitro* microdialysis sampling of step changes and *in vivo* 75 mM K^+ stimulations. (A) shows a step change experiment in which a standard mixture was spiked into a stirred vial to prepare a range of 5 analyte concentrations while a microdialysis probe was sampling 3-min fractions. (B-D) In vivo microdialysis sampling from the striatum of an anesthetized rat. aCSF with 75 mM K^+ was perfused for a pair of 3 min fractions (black arrows) to demonstrate rapid increase in extracellular concentrations and return to baseline.

In Vivo Bicuculline Retrodialysis in Awake Rats

On-chip benzoylation for *in vivo* microdialysis in awake, freely moving rats was explored by analyzing the effects of local administration of 50 μM bicuculline, a competitive $GABA_A$ receptor antagonist, on our panel of neurochemicals. A pilot study (n = 3) was performed in which rats were housed in a ratturn and the probe outlet was connected to the benzoylation device. After collection of 30 min of baseline samples (10 fractions) bicuculline was administered via retrodialysis for 30 min followed by a 30 min washout period. Only two analytes, ACh and Ch (both unlabeled), showed a concentration change from baseline during the bicuculline period (**Figure 4-14**). A two-way ANOVA showed that there was a significant effect of collection period (baseline, bicuculline, post-bicuculline) on [ACh] ($F[2,84] = 12.35$, $p < 0.0001$). Post hoc Tukey testing reveal a significant increase in [ACh] during 50 μM over both baseline and post-bicuculline periods ($p < 0.0005$). This implies that GABA inhibits ACh release in the striatum which agrees with previous reports of significant GABAergic medium spiny neuron innervation of cholinergic interneurons within the striatum[139]. ACh is rapidly hydrolyzed to Ch in the extracellular space by acetylcholinesterase[140,141] and, therefore, changes in [Ch] often track with those of [ACh]. These results validate our platform for use *in vivo* in freely moving rodents which enables simultaneous collection of behavior data.

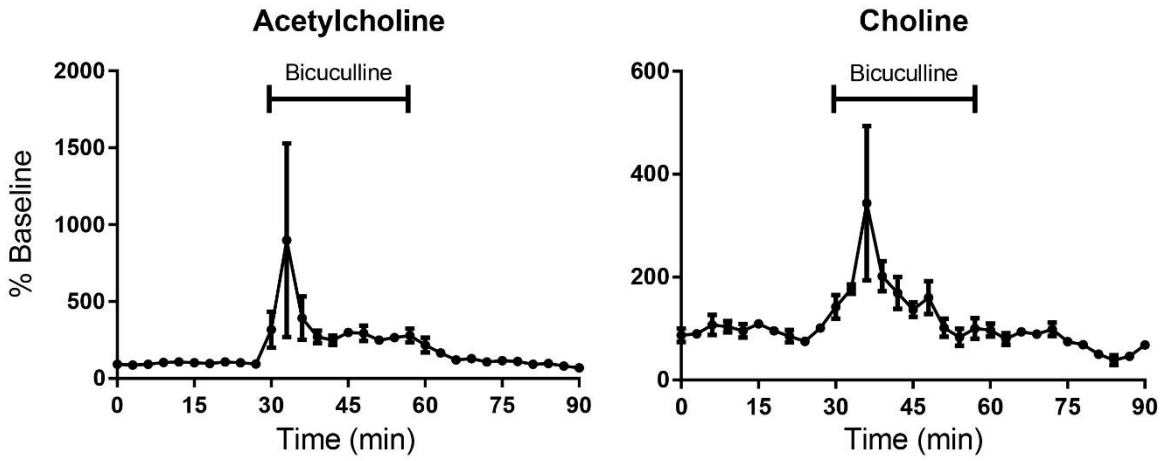

Figure 4-14: Timecourse of dialysate concentrations (as % baseline) of ACh and Ch during 50 μM bicuculline retrodialysis. Three min fractions were collected from the outlet of the derivatization device (10 baseline, 10 bicuculline, 10 post-bicuculline). Both ACh and Ch show rapid increase and elevated levels during retrodialysis. Data was analyzed using a two-way ANOVA with a post hoc Tukey test. All values are Mean ± SEM (n = 3).

Conclusions

In this work we demonstrate the use of a novel all-glass microfluidic device for the benzoylation of neurochemicals directly coupled to *in vivo* microdialysis. Calibration curves were generated and figures of merit showed strong linearity, LoDs, and repeatability for 25 widely studied neurochemicals. Active forms of mixing including acoustic streaming and passive mixing through various reagent addition geometries were investigated for improved analyte/reagent on-chip solubility. Best results were seen when using a parallel reagent addition geometry with 1H,1H,2H,2H-perfluorooctyl-trichlorosilane surface modification. Temporal response was investigated *in vitro* with step change experiments and *in vivo* by anesthetized 75 mM K^+ retrodialysis. Devices exhibited rapid rise times in response to concentration increases with moderate carryover seen when returning to blank/baseline concentrations. Our platform was applied to the monitoring of basal and bicuculline-stimulated levels of all 25 neurochemicals in freely moving rats. ACh and Ch increased significantly during bicuculline retrodialysis which agrees with previous

reports of GABAergic modulation of ACh release in the striatum[142]. Future work will be done to investigate surface coverage of various perfluoroalkyl silanes.

Chapter 5: Measuring Proopiomelanocortin Peptides Using Capillary Liquid Chromatography-Mass Spectrometry

Introduction

The central melanocortin system is comprised of a group of neurons projecting outward from the arcuate nucleus of the hypothalamus (Arc) which possess a critical role in energy homeostasis[143,144]. This group of cells, termed proopiomelanocortin (POMC) neurons, have potent anorexigenic activity which is initiated through production of the POMC peptide precursor and its products[145]. **Figure 5-1** shows the neuropeptide processing pathway that leads to a variety of peptide products with α-melanocyte-stimulating hormone (α-MSH), [des-acetyl] α-MSH, β-MSH, and β-endorphin all having a role in energy regulation[146].

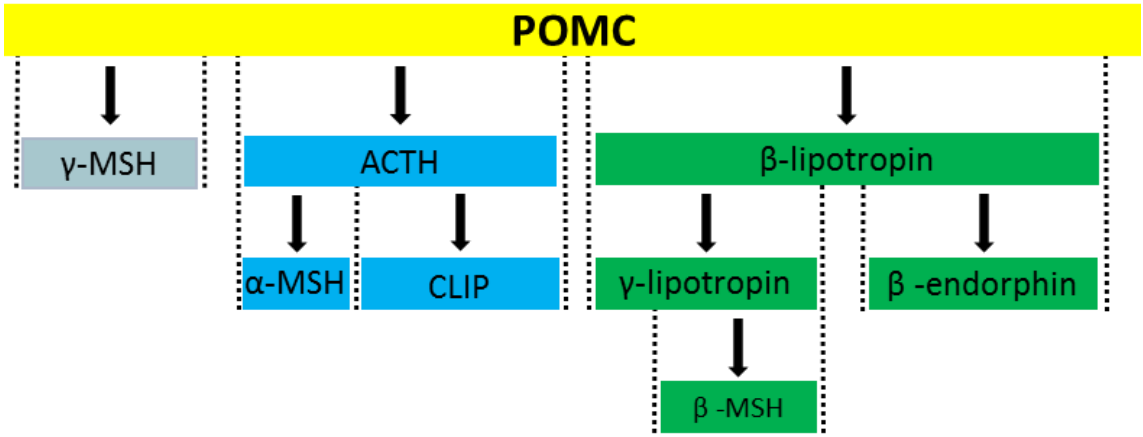

Figure 5-1: Processing of POMC pro-peptide into peptide products. Peptide products include: γ-MSH, adrenocorticotropic hormone (ACTH), α-MSH, corticotropic-like intermediary peptide (CLIP), β-lipotropin, γ-lipotropin, β-MSH, and β-endorphin. [Des-acetyl] α-MSH is acetylated by an N-acetyltransferase to produre mature α-MSH, both of which are anorexigenic peptides.

A null mutation of the *Pomc* gene causes obesity in both mouse models as well as human patients[147–149]. Individuals with a homozygous loss of POMC expression are obese

while those with a heterozygous loss show an intermediate phenotype[150]. More specifically, the functional loss of α-MSH, the an endogenous agonist of the melanocortin-3 and -4 receptors (MCR3 and MCR4), induces obesity in mice which can be reversed through the peripheral administration of an MCR4 agonist[151]. Furthermore, fasting in WT mice results in a reduction of POMC gene expression[152]. While we have accumulated significant knowledge regarding the importance of POMC neurons in maintaining normal body weight and energy expenditure, little is known regarding the process by which this relatively small group of neurons exhibits such control. α-MSH has been measured in rat tissue homogenate[153,154], culture media from human hypothalamic cells[155], and in cerebrospinal fluid from the rat cisterna magna[156] but there has yet to be any dynamic measurements made in awake mice. Here we aim to undertake the first *in vivo* study of POMC release of melanocortin peptides in awake mice to aid in our understanding of the roles the active form of α-MSH (α-MSH (1-13)) and [des-acetyl] α-MSH as well as the degradation product α-MSH (1-12) in regulating food intake and energy expenditure.

Understanding neuropeptide concentration dynamics *in vivo* requires the use of high-sensitivity assays capable of measuring sub-pM concentrations in low volume samples (< 20 μL, low amol of peptide)[157]. Moreover, high specificity is also required in order to differentiate peptide isoforms which may only differ by a single modification. Microdialysis can be used for sample collection due to its flexibility to couple to a variety of analytical techniques. While radioimmunoassays have traditionally been used due to their high sensitivity[49,158–160] they suffer from high sample volume requirements and lack sequence specificity necessary to differentiate the three target isoforms, α-MSH, α-MSH (1-12), and [des-acetyl] α-MSH. Capillary liquid chromatography-mass spectrometry

(cLC-MS) offers the high sensitivity and low volume requirements of capillary-based separations as well as the improved sequence specificity of tandem mass spectrometry[51,161–163]. In this work we aim to improve upon previous methods[52,164,165] for *in vivo* neuropeptide measurement and optimize microdialysis for the three α-MSH isoforms. One of the main challenges when measuring trace concentrations of peptides is adsorptive loss to nonspecific interactions with surfaces during sample collection, preparation, and analysis. A variety of conditions were explored to maximize microdialysis recovery and minimize analyte loss during sample injection.

Methods

Chemicals and Reagents

All chemicals were purchased from Sigma Aldrich (Saint Louis, MO) unless otherwise noted. Acetonitrile was purchased from Honeywell Research Chemicals through VWR (Radnor, PA). NaCl, KCl, $MgSO_4$, $CaCl_2$, and sulfuric acid were purchased from Fisher Scientific (Fairlawn, NJ). Waters MassPrep Enolase digestion standard was used for blocking nonspecific adsorption. Stock solutions of 1 mM α-MSH, α-MSH (1-12), and [des-acetyl] α-MSH (Pheonix Pharmaceuticals, Inc, Burlingame, CA) were prepared in 1:1 H_2O:ACN (0.2 % formic acid). A 100 μM calibration standard mixture was prepared by diluting stocks into 1:1 H_2O:ACN (0.5 % formic acid). On the day of the experiment the standard mixture was diluted to 5 nM in 1:1 H_2O:ACN (0.5% formic acid). A non-serial dilution was performed to generate a calibration curve from 10 pM – 2.5 nM. The curve was then diluted 100-fold in 85:15 aCSF:ACN (0.5% FA) to give a final curve from 0.1 pM – 25 pM. aCSF consisted of 145 mM NaCl, 2.68 mM KCl, 1.4 mM $CaCl_2$, 1.0 mM $MgSO_4$, 1.55 Mm Na_2HPO_4, and 0.45 mM NaH_2PO_4 adjusted to pH of 7.4 with 0.1 M NaOH. A stock of $^{13}C_9$,^{15}N-α-MSH (Biosynthesis, Lewisville, TX) was prepared at in the

same fashion as the standards. On the experiment day a solution of 250 pM $^{13}C_9$,^{15}N-α-MSH was prepared in 75:25 ACN:H2O (2.5% formic acid) and spiked into the calibration curve and samples (5-fold dilution) to serve as an internal standard (IS).

Capillary Column Preparation

Alltima C18 5 μm reversed-phase fully porous particles were acquired from Grace Davidson (Deerfield, IL). Capillary columns were prepared in house using 75/360 μm (ID/OD) fused silica 10 μm PicoTip emitter tips (New Objective, Woburn, MA). In brief, particles were suspended at 15 mg/mL in 75:25 acetone:H_2O and stirred constantly during packing. Particles were slurry packed directly into emitter tips at a constant 1,500 psi until a length of 5 cm was reached. After a gradual pressure release, tips were flushed at the same pressure with H_2O. Columns were then cut to a length of 4 cm and a frit was made by pressing the column head onto a glass microfiber sheet spotted with a 1:1 ratio of Kasil 2130 (PQ Corporation, Valley Forge, PA):formamide[166]. Columns were then left at room temperature for 48 hr before use.

Capillary Liquid Chromatography Mass Spectrometry

A method similar to previous reports was used for rapid loading and elution on a single capillary column[165]. In brief, 10 μL were automatically injected onto the column using a Waters nanoACQUITY autosampler and a high pressure syringe pump (Teledyne ISCO, Lincoln, NE) at 95:5 H2O:MeOH (0.1% FA) at 4,000 psi for 9 min to load and desalt samples. A 6-port valve (Valco, Houston TX) was used to switch between the syringe pump and nanoACQUITY UHPLC. During syringe pump loading the tee connecting the column was blocked to prevent sample loss. After loading the UHPLC was placed online at a flow rate of 95 μL/min split down to ~130 nL/min. MPA was H_2O (0.1 % formic acid) and MPB was

MeOH (0.1% formic acid). The gradient was as follows: initial, 5 % B; 2.5 min, 100 % B; 15.5 min, 100 % B; 16 min, 5 % B; 20.5 min, 5% B.

The capillary column was interfaced directly with a linear ion trap mass spectrometer (LTQ XL, Thermo Scientific, Waltham, MA) operated in positive ion mode with a PV-550 nanospray ESI source (New Objective, Woburn, MA). The spray voltage was set to 2 kV, the heated capillary was 150˚C, capillary voltage was 39 V, and the tube lens was set to 155 V. **Table 5-1** shows the method summary for the a-MSH isoforms.

Analyte	Precursor (m/z)	Product (m/z)	CE (V)	R_t (min)
$^{13}C_9$,^{15}N-α-MSH	559 $[M+3H]^{3+}$	690 $(y11)^{2+}$	44	4.25
α-MSH	556 $[M+3H]^{3+}$	687 $(y11)^{2+}$	44	4.25
α-MSH (1-12)	523 $[M+3H]^{3+}$	726 $(b11)^{2+}$	23	4.35
[des-acetyl]α-MSH	407 $[M+4H]^{4+}$	458.5 $(y11)^{3+}$	30	4

Table 5-1: Table of transitions for neuropeptide method. Transitions were identified and collision energies were tuned at 1 μL/min. All source conditions were tuned using α-MSH. Analytes were normalized to $^{13}C_9$,^{15}N-α-MSH for quantitation.

Microdialysis Probe Construction and Implantation

Custom 1mm side-by-side microdialysis probes were made using AN69 dialysis membrane (Hospal, Bologna, Italy). Probes were implanted into several brain regions including the bed nucleus of the stria terminalis (BNST), the paraventricular nucleus of the hypothalamus (PVH), the paraventricular thalamic nucleus (PVT), and the dorsomedial hypothalamic nucleus/arcuate nucleus (DMH/Arc, **Table 5-2**). Male C57 BL/6 mice between 20 – 30 g were anesthetized using 1-5 % isoflurane and mounted to a stereotaxic instrument (David Kopf Instruments, Tujunga, CA, USA). Probes were slowly lowered into place while being continuously perfused with aCSF at a flow rate of 2 μL/min to prevent deformation of the membrane. Dental cement (A-M Systems, Sequim, WA) was used to encase the probe and skull screws to secure the probe. In order to prevent any

bubbles from being trapped in the probe membrane, mice were perfused continuously with aCSF at 0.5 μL/min during the 24-hr recovery period. Two Sprague-Dawley rats were used for anesthetized experiments in the DMH/Arc with a 2 mm probe at the following coordinates: -3.25 mm posterior, + 0.4 mm lateral to bregma, and 10.25 mm ventral to the surface of the brain. For awake experiments, on the day of the experiment the probe was switched to a syringe of fresh aCSF and allowed to circulate for 2 hours at 0.5 μL/min. Fractions were collected every 24 min (12 μL + 3 μL of IS) for a total of 4 baseline, 4 100 mM K^+ stim, and 3 post-stim samples. Blue dye was infused through the dialysis probes post-experiment for probe localization.

Brain Region	AP (mm)	ML (mm)	DV (mm)	N
DMH/Arc	-1.67	0.35	-5.5	7
BNST	0.26	0.75	-4.15	6
PVH	-0.8	0.15	-4.87	5
PVT	-0.47	0.15	-3.4	1

Table 5-2: Summary of mouse brain regions in which probes were implanted, their coordinates, and the number of microdialysis experiments performed. AP and ML are measured with respect to bregma and DV is measured with respect to the surface of the brain. Not shown are two additional anesthetized experiments performed on rats (DMH/Arc) to utilize a large probe area to improve recovery.

Polyethylenimine Probe Modification

A subset of microdialysis probes were modified with polyethylenimine (PEI) to reduce nonspecific adsorption to the membrane. Briefly, a 5 % PEI solution was prepared in aCSF using HCl to aid in solubility and bring the pH to 7. Probes were perfused at 2 μL/min with PEI for 10 min, then at 0.5 μL/min for 12 hours while submerged in a vial of 5 % PEI. Standard aCSF was flushed through the probe at 2 μL/min for 10 min and the probe was switched to a vial of clean aCSF. The aCSF was replaced after 10 min (3x) and then left to perfuse at 5 μL/min overnight.

Results and Discussion

cLC-MS/MS Method for Quantitation of MSH Peptides

When developing an LC-MS method for measuring trace concentrations (< nM) of neuropeptides, it is critical to optimize injection conditions. Specifically, large volume samples are often injected onto capillary columns to preconcentrate the peptides. For example, 5 – 10 μL can be injected onto capillary columns which have total internal volumes of < 150 nL yielding a substantial preconcentration if peptides are retained or "stacked" at the head of the column. However, if the proper sample solvent is not used it can significantly affect peak shape and result in reduced sensitivity. Organic modifiers are often spiked into samples to reduce nonspecific adsorption to vials and within UHPLC fluidic components[53,54]. The effect is most prominent at low concentrations in which all analyte may be lost to surfaces throughout the fluidic pathway. **Figure 5-2** shows calibration curves comparing samples injected with 15% of two organic modifiers, ACN and methanol. The calibration curves for methanol are more shallow and, in the case of [des-acetyl] α-MSH, show no response below 20 pM. ACN was chosen because it improved sensitivity and linearity for each of the three peptide isoforms.

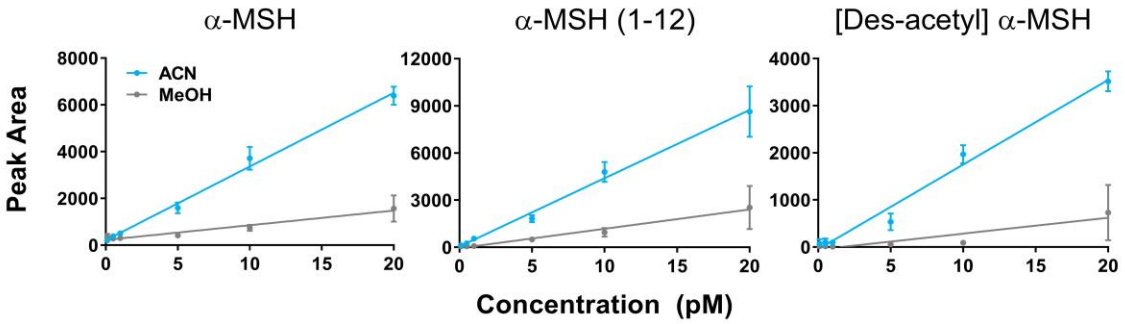

Figure 5-2: Calibration curves comparing 15% ACN and MeOH injection solvents. Slopes for ACN for α-MSH, α-MSH (1-12), and [Des-acetyl] α-MSH were 315, 434, and 180 while those for MeOH were 63, 123, and 34, respectively. Lineariy also improved using ACN with R^2 of 0.98, 0.96, and 0.98 while MeOH yielded 0.81, 0.77, and 0.54, respectively. Sample injections of 5 µL (0.5% FA) were made in triplicate.

To further investigate the effect of organic content on analyte calibration, the amount of ACN in the sample was varied from 0 – 20%. If the sample solvent is too strong of an eluent, analyte bands will not effectively preconcentration on the head of the column, reducing sensitivity. Calibration curves below 10% showed a large drop in peak areas and were, therefore, excluded. **Figure 5-3** shows a comparison of three different ACN sample diluents, 10%, 15%, and 20%. Across all three analytes 20% had the highest linearity while when considering both linearity and sensitivity 15% was the best performer. Ultimately 15% was chosen because it had the highest sensitivity.

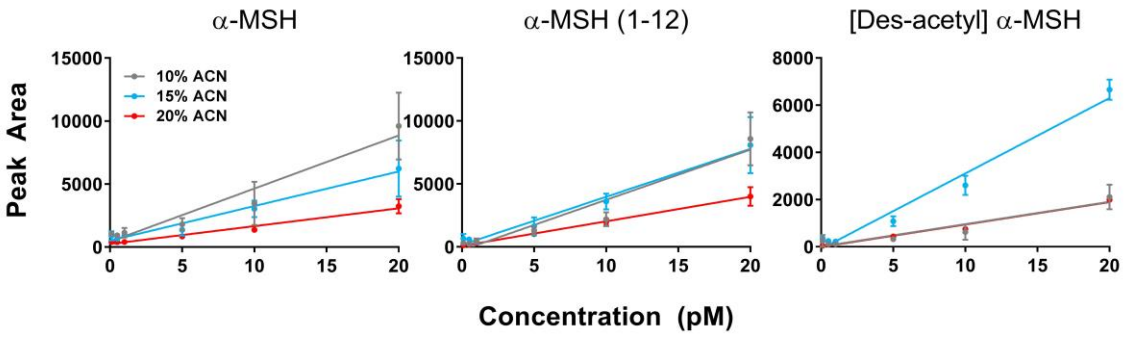

Figure 5-3: Calibration curves comparing 10%, 15%, and 20% ACN in sample diluent for each of the α-MSH isoforms. 20% ACN showed the strongest linearity for α-MSH, α-MSH (1-12), and [Des-acetyl] α-MSH at R^2 of 0.936, 0.964, and 0.974, respectively. Conversely, 15% ACN yielded an average of 2.5-fold higher sensitivity than 20%. For all future experiments 15% was chosen. All concentrations were injected 3 times.

For our method, peak area RSDs were at times in excess of 50%, significantly limiting quantitation of low concentration samples. In order to address this, a custom-made isotopically labeled internal standard (IS) was purchased. All analyte signals were normalized to $^{13}C_9$,^{15}N-α-MSH (+10 Da). Inclusion of the IS increased linearity ($R^2 > 0.99$) for all isoforms but did not drastically improve linearity. Previous reports have shown large improvements in method repeatability for peptides and proteins when spiking a carrier protein into samples to effectively block nonspecific adsorption[54,167,168]. An enolase digest standard was evaluated as a carrier peptide mixture for the α-MSH isoforms. The digest had no significant interferences at each mass transition and the effect of five concentrations of enolase on peak area %RSD were compared (**Figure 5-4**). An enolase concentration of 100 pM was chosen because it had the largest decrease in %RSD for 2 of the 3 isoforms. Compared with those in the absence of enolase the %RSDs decreased by the following amounts for α-MSH, α-MSH (1-12), and [Des-acetyl] α-MSH, respectively: 65%, 66%, and 34%.

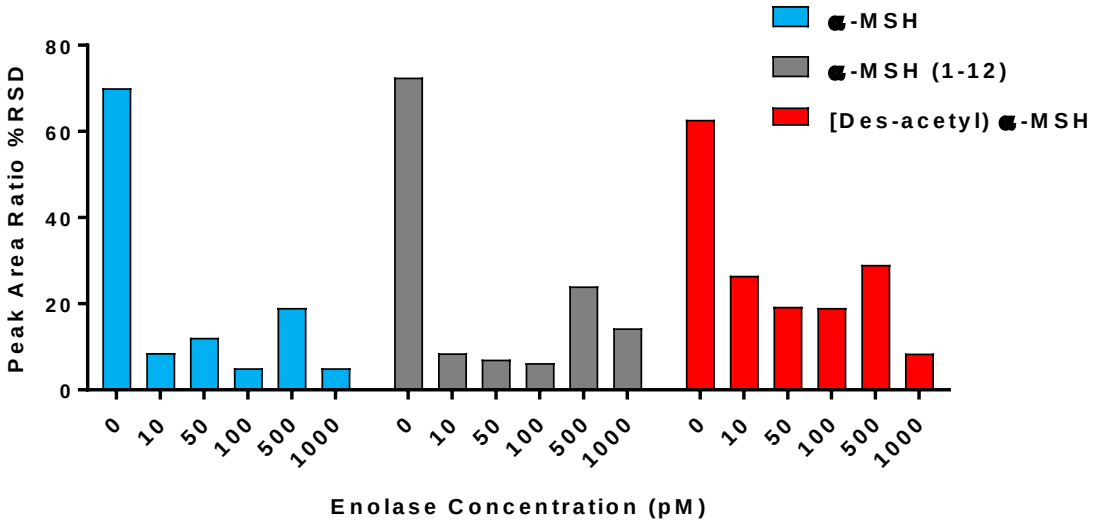

Figure 5-4: Effect of enolase digest concentration on peak area ratio (analyte/IS) %RSD. Enolase concentration refers to the concentration of enolase present prior to protein digestion. No clear trend was seen for varying concenctrations so 100 pM was chosen because it yielded excellent RSDs for both α-MSH and α-MSH (1-12) and because it was the lowest concentration that significantly helped repeatability. % RSDs were decreased by an average of 55% (n = 3 replicate injections).

At elution flow rates within the range for our method (120 – 150 nL/min) post-column dead volume can have a significant deleterious effect on peak shape. Traditionally, the nanoelectrospray ionization emitter tip is connected to the column outlet through a union. The amount of post-column volume can differ from connection to connection and, when large, limit sensitivity by diluting analyte bands. In order to mitigate this effect, packing reversed-phase particles directly into an emitter tip was explored. When the emitter tip orifice is 2-5x larger than the particle diameter a keystone effect is observed in which particles smaller than the orifice are retained even under high pressures[169]. As a result we were able to pack 5 μm particles into both 10 μm and 15 μm emitter tips with a high success rate. The post-column dead volume was effectively completely removed and the peak width contribution of the separate emitter tip could be evaluated (**Figure 5-5**). The resulting peak widths were halved and peak areas increased by 2.5-fold when using the packed tip.

Peak shape also improved with much less tailing resulting from negligible post-column volume in the packed emitter tip. This ultimately improved both method sensitivity and LoDs for all three isoforms (**Figure 5-6**).

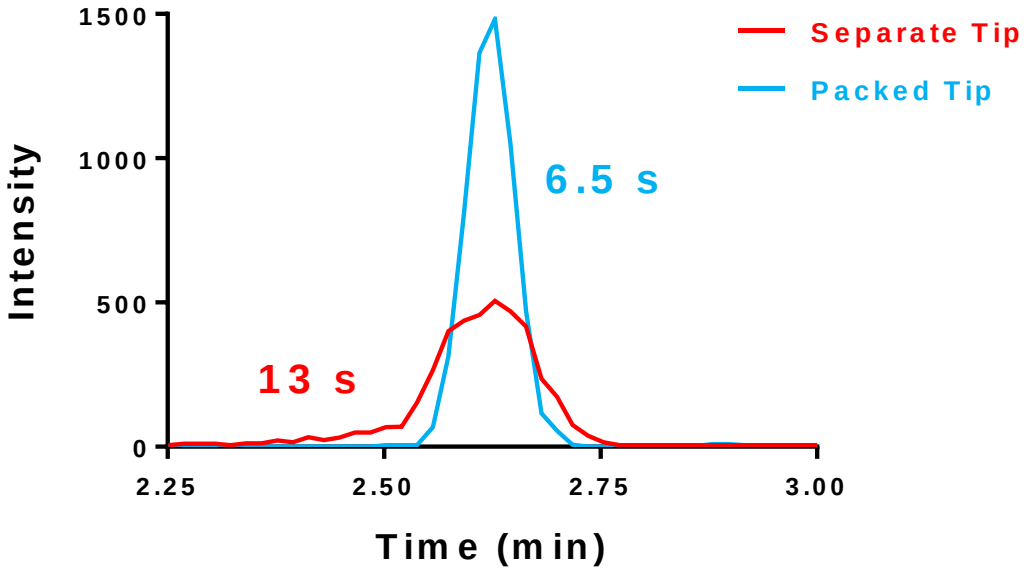

Figure 5-5: RIC of [Des-acetyl] α-MSH for a packed emmitter tip and separate column-emitter tip. Peak width (4σ) decreased by 50% when particles were packed directly into a 15 μm tip. Peak area also increased by a factor of 2.4x.

A method was developed using packed emitter tips, enolase carrier peptides, and IS for the sensitive measurement of α-MSH isoforms in dialysate. Strong linearity and peak area % RSDs across the range from 0.1 – 10 pM was achieved which allowed sub-pM LoDs for each isoform (**Figure 5-6**).

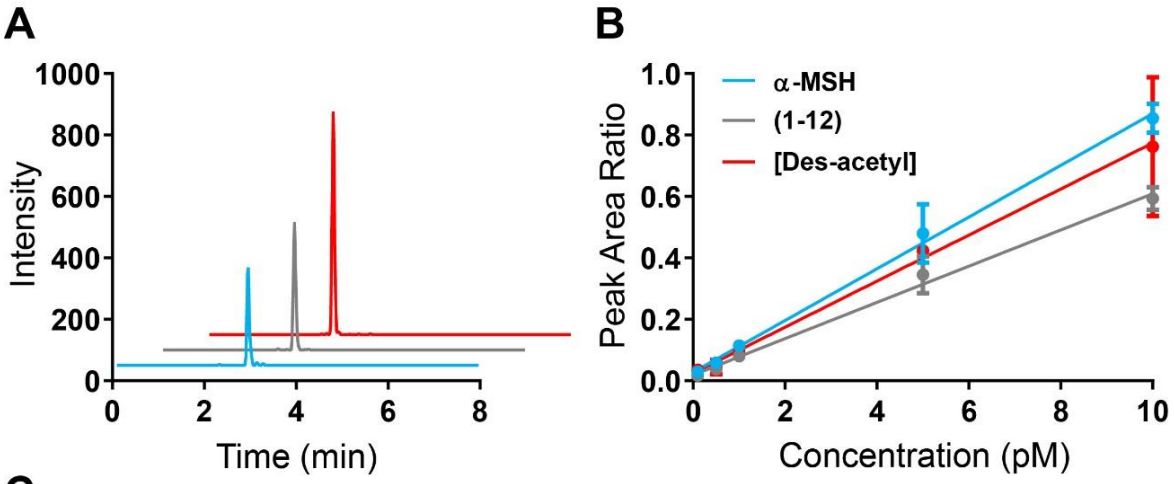

C

Analyte	LoD (pM)	RSD	R^2
α-MSH	0.2 - 1.5	5	0.9973
α-MSH (1-12)	0.2 - 1.5	6	0.9945
[des-acetyl]α-MSH	0.3 - 0.8	19	0.9974

Figure 5-6: cLC-MS method for measuring α-MSH isoforms in dialysate. It utilizes optimized injection solvent and carrier peptides for reduced nonspecific adsorption to system components as well as a packed tip column for improved peak shape. (A) Reconstructed ion chromatograms for 10 µL injection of 1 pM MSH standards (10 amol). (B) Calibration curves from 0.1 – 10 pM standards. (C) Figures of merit for α-MSH isoforms including LoD ranges, peak area %RSDs, and linearity (R^2).

In Vitro Microdialysis of MSH Peptides

Both custom-made 1 mm AN69 and regenerated cellulose membranes were tested for *in vitro* recovery. In agreement with other reports[53,161,165] AN69 (**Figure 5-7**) outperformed regenerated cellulose (data not shown) although the recovery was still too low to be of practical use. **Figure 5-7** shows *in vitro* extraction fractions for three dialysis flow rates (1 µL/min, 0.75 µL/min, and 0.5 µL/min) sampling out a stirred vial of 5 nM peptide. To reduce nonspecific adsorption, 100 pM enolase was included in the perfusate and the sampling vial. Even at the 0.5 µL/min extraction fractions were < 0.03 (3% recovery), too low to be useful *in vivo*.

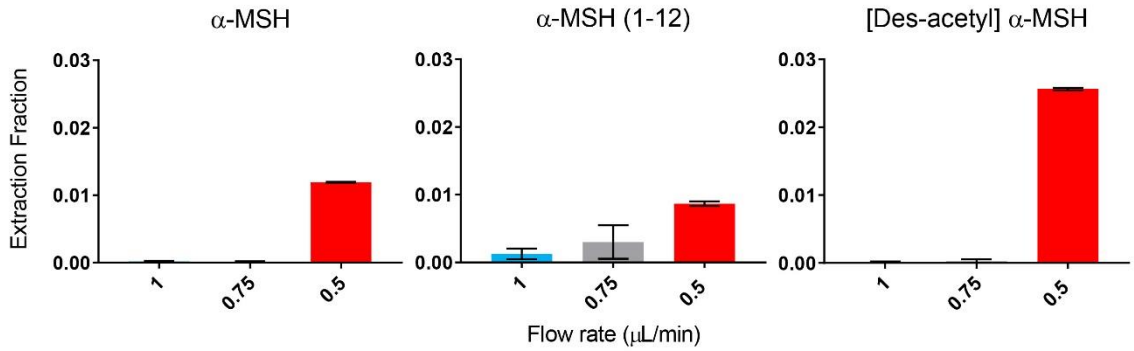

Figure 5-7: Calculated extraction fractions for three different dialysis flow rates in an *in vitro* stirred vial experiment. Probes were submerged in a stirred vial containing 5 nM peptide and 100 pM enolase (also present in perfusate). After equilibrating for 5x the system volume 3 x 8 μL fractions were collected from the probe outlet. As expected, recovery varied with flow rate, although even 0.5 μL/min yields too low of a recovery to be useful in vivo.

To confirm that the membrane was still functional, an experiment was performed with small molecule neurotransmitters at 1 μL/min which resulted in a calculated recovery of ~17%, suggesting that the membrane pores were intact. As nonspecific adsorption had been such a prominent issue during method development it was hypothesized that the sampling matrix was still too "clean" to effectively block all available sites within the probe membrane. Previously collected mouse dialysate was used for the sample matrix instead of aCSF. It was first confirmed that the dialysate had no detectable α-MSH isoforms present. On the day of the experiment fresh dialysate was thawed and the MSH peptides were spike into it for a final concentration of 100 pM. The flow rate experiment was repeated and it was found that recovery increased dramatically for each flow rate and a linear trend of increasing recovery with decreasing flow rate was seen (**Figure 5-8**). These results support that *in vivo* microdialysis sampling should have a similar improvement in recovery over clean standards because of the presence of a large number of compounds capable of blocking nonspecific adsorption of the α-MSH isoforms. 0.5 μL/min was chosen

for in vivo experimentation because it has the best recovery and is still within the target range for the desired temporal resolution (~20 min).

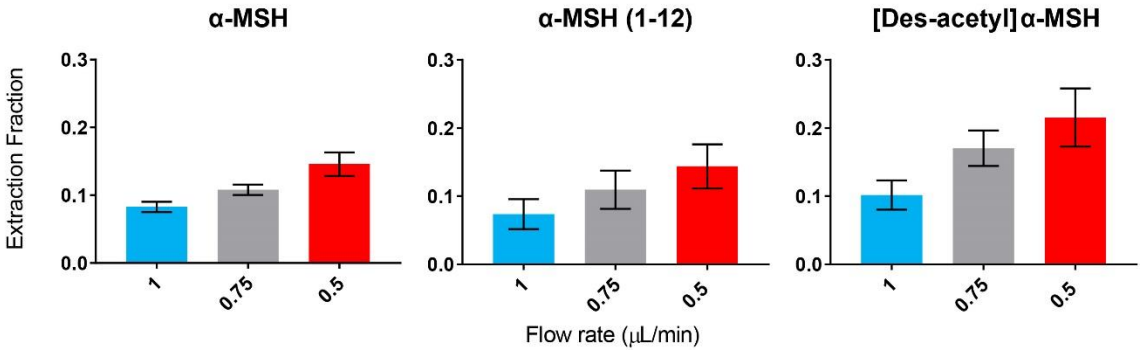

Figure 5-8: Calculated extraction fractions for three different dialysis flow rates in an *in vitro* stirred vial experiment using dialysate sample matrix. Probes were submerged in a stirred vial containing 100 pM peptide. After equilibrating for 5x the system volume, 3 x 8 μL fractions were collected from the probe outlet for each flow rate. Recovery was more than 10-fold higher when using a "dirtier" matrix. A linear trend of increasing recovery with decreasing flow rate was observed.

In Vivo Microdialysis of MSH Peptides

Probes were implanted into several brain regions believed to be innervated by POMC neurons including the BNST, PVH, PVT, and DMH/Arc[143]. A summary can be found in **Table 5-2**. In a pilot targeting the BNST (n = 4) and PVH (n = 2) we were unable to measure any basal or 100 mM potassium-stimulated levels of the α-MSH isoforms. A previous report demonstrated that basal and potassium-stimulated extracellular concentrations of dynorphin B and several small molecule neurotransmitters could be enhanced in the presence of higher levels of Ca^{2+} in the perfusion buffer[170]. Standard and 100 mM K^+ aCSF with elevated Ca^{2+} (2.5 mM rather than 1.4 mM) were prepared and used for another set of animals targeting the BNST (n = 2), PVH (n = 2), DMH/Arc (n = 2), and PVT (n = 1). As before, there were no measurable quantities of the MSH peptides. In order to utilize large probes for better recovery, 2 rats were used for anesthetized sampling from

the DMH/Arc using a 2 mm probe. No MSH peptides were measurable even though that region had previously been shown to contain α-MSH immunoreactivity[159]. PEI modification of polyacrylonitrile membranes (AN69) has been shown to improve recovery of neuropeptides[53] and was explored for a pilot of four mice: 3 DMH/Arc and 1 PVH. A single animal had measurable quantities of α-MSH (**Figure 5-9**). It was concluded that because α-MSH was measurable in a single animal it was likely that endogenous concentrations are lower than anticipated and not routinely measurable using microdialysis. While previous reports have found higher levels in tissue homogenate[146,153,154,156] and cell culture media[146], it may be that *in vivo* concentrations of α-MSH, α-MSH (1-12), and [des-acetyl] α-MSH fall below the pM range.

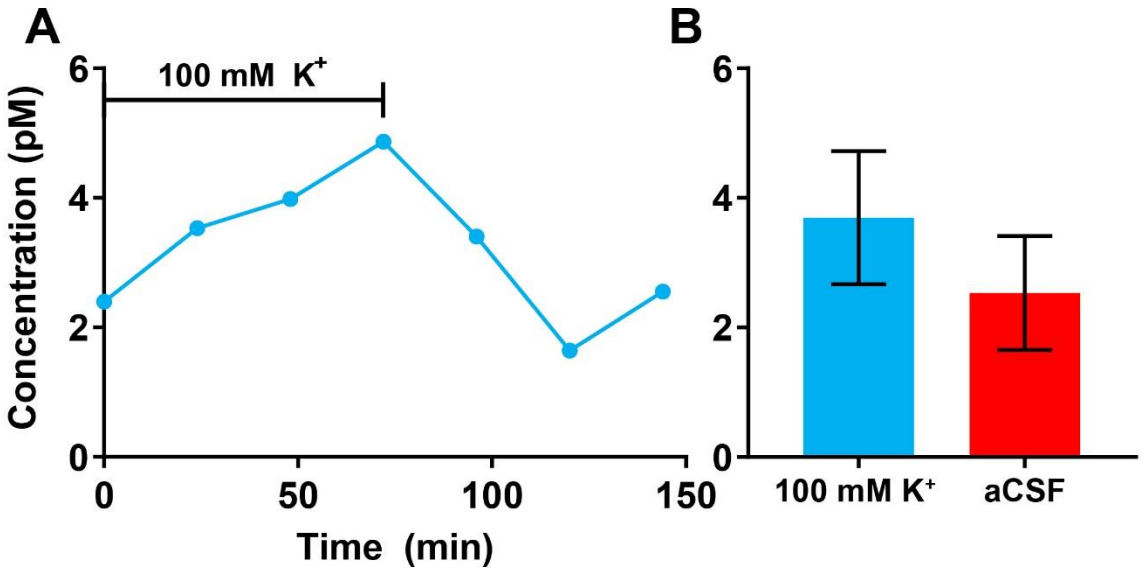

Figure 5-9: *In vivo* microdialysis data of α-MSH collected from animal implanted in the DHM/Arc. (A) Time course of data collected. Baseline samples were lost due to instrument malfunction, but K^+ and post-stim samples were successfully analyzed. (B) Bar graph of K^+ stim and post-stim periods showed insignificant difference (unpaired two-tailed students t test, $p > 0.1$).

Conclusions

In this work we demonstrate the development of a sensitive method for the measurement of α-MSH, α-MSH (1-12), and [des-acetyl] α-MSH in biological samples. Optimal injection solvent conditions were explored and 15 % ACN (0.5% formic acid) was chosen because it yielded the highest sensitivity. Addition of an isotopically labeled internal standard improved calibration curve linearity to > 0.99 for all isoforms. An enolase digest was used as a source of carrier peptides, reducing peak area ratio % RSDs by an average of 50%. A packed column emitter tip was developed to remove significant post-column system volume which resulted in a 2-fold reduction in peak widths and 2.4-fold increase in peak areas. When combining these modifications, limits of detection as low as 0.2, 0.2, and 0.3 pM were achieved for α-MSH, α-MSH (1-12), and [des-acetyl] α-MSH, respectively. *In vitro* microdialysis testing showed that 0.5 μL/min yielded > 15% recovery for the three isoforms only when a sufficiently complex analyte matrix was used for sampling. *In vivo* microdialysis was performed on awake C57 BL/6 mice and anesthetized Sprague Dawley rats during standard and high potassium (100 mM K^+) retrodialysis. Of 19 mice implanted in 4 different brain regions only 1 had measurable levels of α-MSH. No measurable α-MSH isoforms were found in rats using a larger probe membrane. We hypothesize that measurable concentrations of the MSH peptides were not found for one (or a combination of) the following reasons: extracellular concentrations are below our LoDs, rapid degradation occurs in the extracellular space, or sampling from such a small group of neurons without damaging them may require a less invasive technique. Moreover, because there are so few POMC neurons innervating a number of different nuclei, dilution into the sampling stream may further decrease concentration for analysis. Positron emission tomography, a noninvasive technique for *in vivo* imaging, has previously been

used to study neuropeptides[171,172] and represent a viable alternative to microdialysis sampling.

Chapter 6: Future Directions

Improving Accuracy of In Vivo Microdialysis SIL Calibration

Retrodialysis of SIL forms of endogenous analytes enables dynamic concentration calibration microdialysis probes. Interestingly, we demonstrated the first report of amino acid recovery calibration accuracy having an inverse relationship with perfusion flow rate. **Figure 6-1** shows the % RMSD of recovery corrected concentration values compared to the known concentration as a function of dialysis flow rate. All amino acids except Thr showed a positive correlation with % RMSD increases from 6 – 160 % between 0.1 and 1

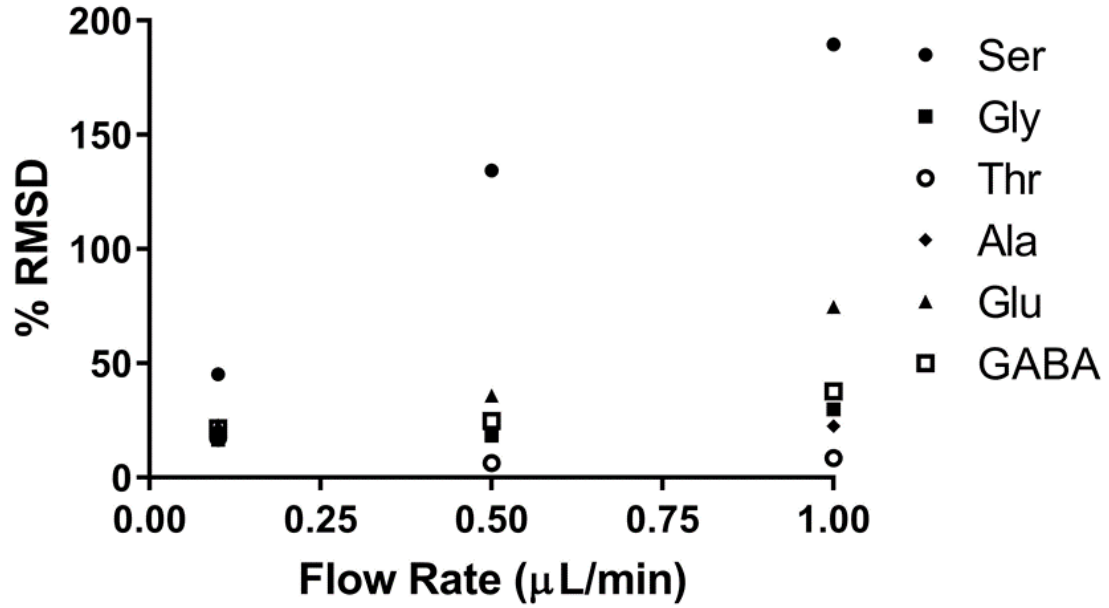

Figure 6-1: *In vitro* comparison of % RMSDs of SIL recovery corrected values. Each point represents % RMSD of three replicates. Thr was the only amino acid without a positive correlation between % RMSD and flow rate. For the remaining five amino acids individual analyte slopes ranged from 6 – 160 with R^2 values ranging from 0.893 – 0.998. Corrected values were were all similarly elevated due to unlabeled contamination of SIL stocks, using a lower SIL concentration resulted in more accurate values (**Figure 3-7**).

μL/min. More in-depth experimentation is required to determine the exact cause of this phenomenon. Flow rates from 0.1 – 1.5 μL/min should be tested with the lower SIL concentrations to determine if the trend is still significant. Furthermore, other neurochemicals such as the catecholamines, indolamines, and acetylcholine might be investigated to determine whether this observation is seen across different classes of compounds.

Improving LoDs Poorly-Retained Compounds

Chapter 2 included a comparison of a rapid, 2 min gradient separation with previous 10 and 20 min gradients published by our group[37,42]. As we move toward faster gradient separations of Bz-labeled compounds, sensitivity of early eluting analytes such as ACh, Ch, and Bz-amino acids is disproportionately affected because of decreased separation efficiency. Traditionally our fast methods utilize superficially porous 2.1 x 100 mm C18 (d_p = 1.7) columns which show more favorable retention of catecholamines and indolamines. There are now available, however, columns capable of withstanding greater than 1,000 bar with polar endcapping that are 100% aqueous stable. Such columns may enhance retention for early eluting compounds enough to yield better sensitivity and lower limits of detection.

Reducing Carryover in Benzoylation Device

While rapid rise times were seen in response to concentration step changes for all analytes during on-chip benzoylation (**Figure 4-12**) significant carryover was observed when returning to blank/baseline. The number of samples with significant carryover appears to scale with the degree of benzoylation (**4-12B-E**) suggesting that analyte adsorption increases with hydrophobicity. We hypothesize that this may be related either

to limited surface coverage or analyte retention on perfluoroalkyl chains. Carryover can be addressed through three strategies: 1) increasing analyte solubility by increasing the amount of ACN present during and after derivatization; 2) improving surface coverage of perfluoroalkyl modification; 3) reducing surface roughness.

By increasing the BzCl reagent channel flow rate and reducing % BzCl, the ACN concentration can be increased without increasing the mass of BzCl delivered. Increasing the ACN content will aid in solubilizing highly hydrophobic Bz-analytes, thus reducing adsorption and resulting in lower carryover. It has been previously reported that reducing the concentration of 1H,1H,2H,2H-perfluorodecyltrichlorosilane (PFDS) to as low as 0.02% (v/v) can improve surface coverage on glass microfluidic devices[173]. It was also demonstrated that using a combination of short and long chain perfluoralkyl silanes such as PFDS and trifluoropropyltrichlorosilane improved surface stability in strong acidic and basic conditions. Such routes may prove beneficial in reducing BzCl and Bz-analyte surface adsorption. Surface roughness affects adsorption and rougher surfaces tend to exhibit higher rates of surface fouling[174]. Within our batch-to-batch variability higher rates of chip clogging have been witnessed on chips with rougher surfaces. Therefore, a careful examination of the various steps in our etching procedure and their effect on surface smoothness may be beneficial.

Online UHPLC-MS/MS Analysis of Benzoylated Neurochemicals in Dialysate

The ultimate goal of on-chip benzoylation is to develop an online system for near-real time monitoring of neurochemicals. As shown in **Figure 6-2**, the benzoylation device will be directly connected to an 8-port valve and, using a dual-sample loop configuration the dialysate will fill one loop while the other loop is loaded onto a column. In this valve

configuration no sample is wasted because there is always a sample loop in line with the probe.

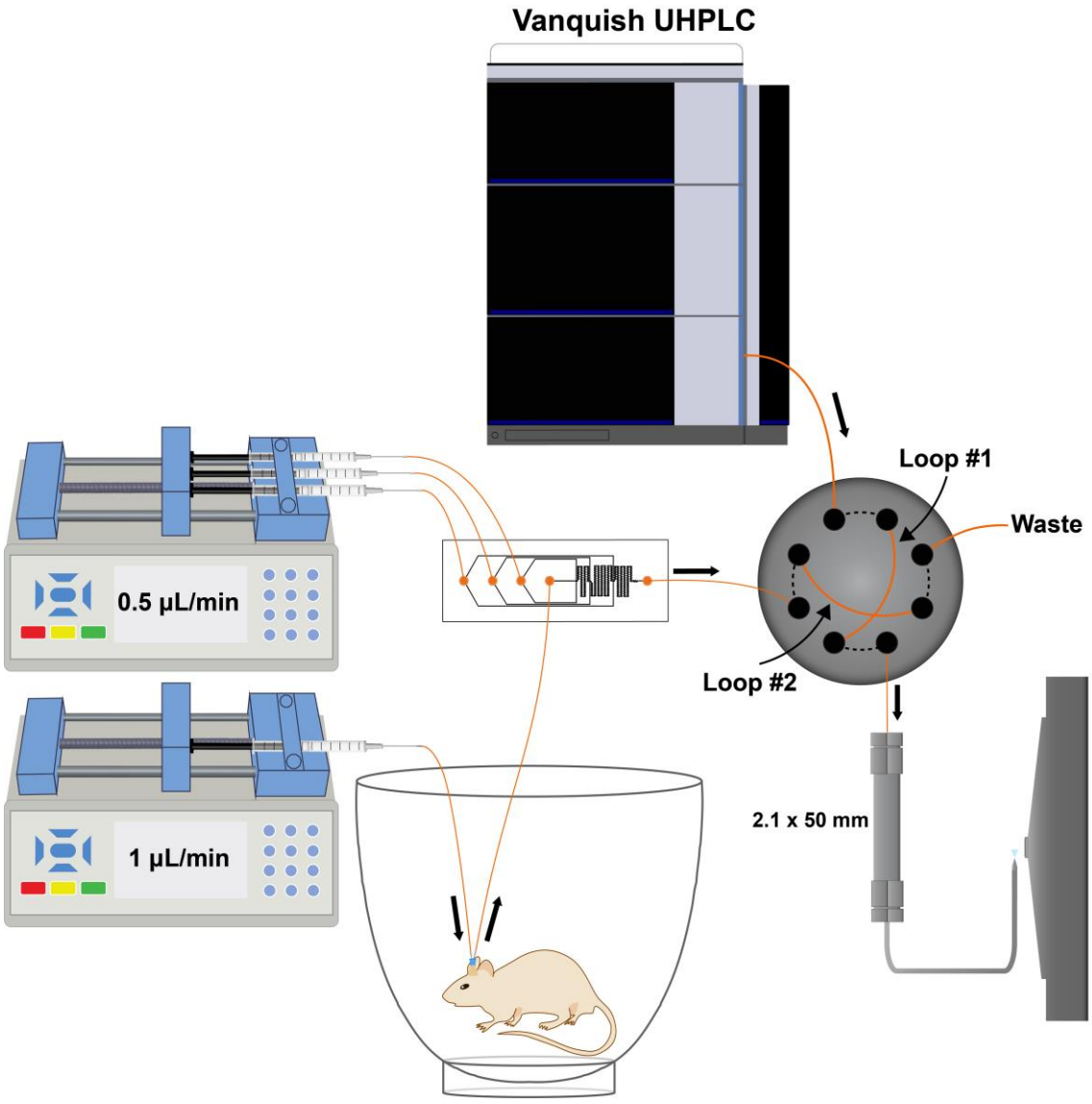

Figure 6-2: Schematic of system for near-real time online monitoring of Bz-labeled neurochemicals *in vivo*. The sample stream from the benzoylation device flows into one of two sampe loops in an 8-port valve. While the contents of Loop #1 are analyzed Loop #2 is being filled. A 2.1 x 50 mm C18 column will be used to reduce backpressure and allow reduced system equilibration times.

Matching analysis time with collection time requires rapid analysis times with flow rates higher than 600 µL/min and shorter columns. We aim to achieve temporal resolution at or below 1 min which will necessitate total gradient times under 30s. While resolution

suffers when moving from 100 to 50 mm column length, gradients can be tailored to monitor only a subset of analytes (ideally with similar retention factors) at a time. Elevated temperatures will also be explored for decreasing solvent viscosity and the effect of mass transfer at high flow rates. For further improvements in throughput, isocratic separations can be performed on well-retained analytes. Under isocratic conditions there is no column equilibration and injections can be made as rapidly as method sensitivity allows.

Although there have been previous reports of systems for online chromatographic analysis of neurochemicals with high temporal resolution in capillary columns, all have focused on a single analyte[175–179]. By utilizing the analyte specificity of MS/MS we can avoid interferences from matrix components that limit sensitivity of such methods requiring electrochemical detection. Moreover, benzoylation improves analyte retention on RPLC columns enabling higher efficiency separations of small, polar neurochemicals. In using this system we plan to produce the first report of high temporal resolution *in vivo* measurements of amino acids, catecholamines, and indolamines in a single run.

Conclusions

This thesis has described the novel application of *in vivo* microdialysis SIL calibration of dopamine for the study of rat models of cocaine addiction and of glutamate, GABA, alanine, serine, threonine and glycine for the study of the ASCT1 transporter in mice. Improvements were made to previous methods for measuring Bz-labeled neurochemicals enabling the measurement of 26 widely studied neurochemicals in a single 2 min gradient. The method was validated against longer gradients and compared favorably in LoDs, repeatability, and linearity. A trend was discovered in which SIL calibration accuracy may have a dialysis flow rate dependence. There is potential for further

improvements to SIL microdialysis calibration by gaining an in-depth understanding of its limitations with regards to flow rate.

In order to move towards near-real time analysis of *in vivo* concentrations of neurochemicals in dialysis, a platform was developed for on-chip benzoylation. Calibration curves were prepared and figures of merit were comparable to offline preparation. The platform was applied to *in vivo* neurochemical monitoring in both anesthetized and awake, freely moving rats, and basal and potassium/bicuculline-stimulated levels of 21 out of 25 analytes were above our LoDs. Adapting our reagent addition device to online analysis will require a reduction in carryover which may be possible through the use of combinations of perfluoroalkyl silanes for surface modification. We intend to use this system to broaden the scope of analytes measurable with high temporal resolution *in vivo*.

In **Chapter 5,** a method was developed for the quantitation of POMC peptides *in vivo*. Microdialysis sampling was optimized to improve recovery and a packed-tip column configuration was utilized. Limits of detection below 1 pM are reported for all three α-MSH isoforms: α-MSH (1-13), α-MSH (1-12), [des-acetyl] α-MSH. Strong linearity was observed in calibration curves from 0.1 – 20 pM. A study of 19 awake mice and 2 anesthetized rats was performed to determine if extracellular concentrations of any of the isoforms were measurable. Out of a total of 17 successful experiments (16 mice, 1 rat) α-MSH was measured in a single mouse. Although *in vivo* levels were below our LoDs, this system can be adapted for the quantitation of other neuropeptides such as Leucine and Methionine-enkephalin.

References

(1) McQueen, J. K. In *Basic and Clinical Aspects of Neuroscience Vol 2*; Springer, Berlin, Heidelberg, 1987; pp 7–16.

(2) Fuxe, K.; Borroto-Escuela, D. O.; Romero-Fernandez, W.; Zhang, W. B.; Agnati, L. F. *Chin. J. Integr. Med.* **2013**, *19* (5), 323.

(3) van den Pol, A. N. *Neuron* **2012**, *76* (1), 98.

(4) Dauer, W.; Przedborski, S. *Neuron*. Cell Press September 11, 2003, pp 889–909.

(5) Francis, P. T. *CNS Spectr*. **2005**, *10* (S18), 6.

(6) Volkow, N. D.; Wise, R. A.; Baler, R. *Nature Reviews Neuroscience*. Nature Publishing Group December 1, 2017, pp 741–752.

(7) Ungerstedt, U.; Pyock, C. *Bull. Schweiz. Akad. Med. Wiss.* **1974**, *30* (1–3), 44.

(8) Ahmari, S. E.; Smith, S. J. *Neuron*. Cell Press April 25, 2002, pp 333–336.

(9) Imperato, A.; Di Chiara, G. *J. Neurosci.* **1984**, *4* (4), 966.

(10) Kalén, P.; Strecker, R. E.; Rosengren, E.; Björklund, A. *J. Neurochem.* **1988**, *51* (5), 1422.

(11) Di Chiara, G. *Trends Pharmacol. Sci.* **1990**, *11* (3), 116.

(12) Chefer, V. I.; Thompson, A. C.; Zapata, A.; Shippenberg, T. S. *Current Protocols in Neuroscience*. John Wiley & Sons, Ltd April 1, 2009, pp 7.1.1-7.1.28.

(13) Benveniste, H.; Drejer, J.; Schousboe, A.; Diemer, N. H. *J. Neurochem.* **1987**, *49* (3), 729.

(14) Borland, L. M.; Shi, G.; Yang, H.; Michael, A. C. *J. Neurosci. Methods* **2005**, *146* (2), 149.

(15) Mitala, C. M.; Wang, Y.; Borland, L. M.; Jung, M.; Shand, S.; Watkins, S.; Weber, S. G.; Michael, A. C. *J. Neurosci. Methods* **2008**, *174* (2), 177.

(16) Jaquins-Gerstl, A.; Michael, A. C. *J. Neurosci. Methods* **2009**, *183* (2), 127.

(17) Jaquins-Gerstl, A.; Shu, Z.; Zhang, J.; Liu, Y.; Weber, S. G.; Michael, A. C. *Anal. Chem.* **2011**, *83* (20), 7662.

(18) Nesbitt, K. M.; Jaquins-Gerstl, A.; Skoda, E. M.; Wipf, P.; Michael, A. C. *Anal. Chem.* **2013**, *85* (17), 8173.

(19) Varner, E. L.; Jaquins-Gerstl, A.; Michael, A. C. *ACS Chem. Neurosci.* **2016**, *7* (6), 728.

(20) Robbins, E. M.; Jaquins-Gerstl, A.; Fine, D. F.; Leong, C. L.; Dixon, C. E.; Wagner, A. K.; Boutelle, M. G.; Michael, A. C. *ACS Chem. Neurosci.* **2019**, *10* (8), 3521.

(21) Lee, W. H.; Slaney, T. R.; Hower, R. W.; Kennedy, R. T. *Anal. Chem.* **2013**, *85* (8), 3828.

(22) Ngernsutivorakul, T.; Steyer, D. J.; Valenta, A. C.; Kennedy, R. T. *Anal. Chem.* **2018**, *90* (18), 10943.

(23) Lee, W. H.; Ngernsutivorakul, T.; Mabrouk, O. S.; Wong, J.-M. T.; Dugan, C. E.; Pappas, S. S.; Yoon, H. J.; Kennedy, R. T. *Anal. Chem.* **2016**, *88*, 1230.

(24) Klinker, C. C.; Bowser, M. T. *Anal. Chem.* **2007**, *79* (22), 8747.

(25) Hapuarachchi, S.; Aspinwall, C. A. *Electrophoresis* **2007**, *28* (7), 1100.

(26) Lada, M. W.; Vickroy, T. W.; Kennedy, R. T. *Anal. Chem.* **1997**, *69* (22), 4560.

(27) Klampfl, C. W. *Electrophoresis*. John Wiley & Sons, Ltd June 1, 2009, pp S83–S91.

(28) Gritti, F.; Höltzel, A.; Tallarek, U.; Guiochon, G. *J. Chromatogr. A* **2015**, *1376*, 112.

(29) Kartsova, L. A.; Bessonova, E. A.; Somova, V. D. *Journal of Analytical Chemistry*. Pleiades Publishing May 29, 2019, pp 415–424.

(30) Tufi, S.; Lamoree, M.; de Boer, J.; Leonards, P. *J. Chromatogr. A* **2015**, *1395*, 79.

(31) Defaix, C.; Solgadi, A.; Pham, T. H.; Gardier, A. M.; Chaminade, P.; Tritschler, L. *J. Pharm. Biomed. Anal.* **2018**, *152*, 31.

(32) Yang, J. C.; Liu, T. Y.; Chang, Y. F.; Chi, C. W.; Liu, H. C.; Shih, Y. H.; Lee, L. S. *J. Liq. Chromatogr.* **1991**, *14* (19), 3559.

(33) Gustavsson, S. Å.; Samskog, J.; Markides, K. E.; Långström, B. *J. Chromatogr. A* **2001**, *937* (1–2), 41.

(34) Shi, S.; Zhao, B.; Yagnik, G.; Zhou, F. *Anal. Chem.* **2013**, *85* (14), 6598.

(35) Zhang, T.-Y.; Li, S.; Zhu, Q.-F.; Wang, Q.; Hussain, D.; Feng, Y.-Q. *TrAC Trends Anal. Chem.* **2019**, *119*, 115608.

(36) Zecca, L.; Ferrario, P. *J. Chromatogr. B Biomed. Sci. Appl.* **1985**, *337* (C), 391.

(37) Song, P.; Mabrouk, O. S.; Hershey, N. D.; Kennedy, R. T. *Anal. Chem.* **2012**, *84* (1), 412.

(38) Cai, H. L.; Zhu, R. H.; Li, H. De. *Anal. Biochem.* **2010**, *396* (1), 103.

(39) Schotten, C. *Berichte der Dtsch. Chem. Gesellschaft* **1883**, *16* (1), 643.

(40) Baumann, E. *Berichte der Dtsch. Chem. Gesellschaft* **1886**, *19* (2), 3218.

(41) Wilson, G. S.; Michael, A. C.; Kehr, J.; Yoshitake, T. In *Compendium of In Vivo Monitoring in Real-Time Molecular Neuroscience*; WORLD SCIENTIFIC, 2017; pp 193–216.

(42) Wong, J.-M. T.; Malec, P. A.; Mabrouk, O. S.; Ro, J.; Dus, M.; Kennedy, R. T. *J. Chromatogr. A* **2016**, *1446*, 78.

(43) Bungay, P. M.; Morrison, P. F.; Dedrick, R. L. *Life Sci.* **1990**, *46* (2), 105.

(44) Lönnroth, P.; Jansson, P. A.; Smith, U. *Am. J. Physiol.* **1987**, *253* (2 Pt 1), E228.

(45) Bengtsson, J.; Boström, E.; Hammarlund-Udenaes, M. *J. Pharm. Sci.* **2008**, *97* (8), 3433.

(46) Sun, L.; Stenken, J. A.; Brunner, J. E.; Michel, K. B.; Adelsberger, J. K.; Yang, A. Y.; Zhao, J. J.; Musson, D. G. *Anal. Biochem.* **2008**, *381* (2), 214.

(47) Hershey, N. D.; Kennedy, R. T. *ACS Chem. Neurosci.* **2013**, *4* (5), 729.

(48) Hokfelt, T. *Nature* **1980**, *284* (5756), 515.

(49) Maidment, N. T.; Evans, C. J. In *Handbook of Behavioral Neuroscience*; Elsevier, 1991; Vol. 7, pp 275–303.

(50) Sauerstein, K.; Klede, M.; Hilliges, M.; Schmelz, M. *J. Physiol.* **2000**, *529* (3), 803.

(51) Li, Q.; Jon-Kar Zubieta; Kennedy, R. T. *Anal. Chem.* **2009**, *81* (6), 2242.

(52) Haskins, W. E.; Wang, Z.; Watson, C. J.; Rostand, R. R.; Witowski, S. R.; Powell, D. H.; Kennedy, R. T. *Anal. Chem.* **2001**, *73* (21), 5005.

(53) Zhou, Y.; Wong, J.-M. T.; Mabrouk, O. S.; Kennedy, R. T. *Anal. Chem.* **2015**, *87* (19), 9802.

(54) Maes, K.; Smolders, I.; Michotte, Y.; Van Eeckhaut, A. *J. Chromatogr. A* **2014**, *1358*, 1.

(55) Van Wanseele, Y.; Maes, K.; Lanckmans, K.; Van Schoors, J.; Smolders, I.; Van Eeckhaut, A. *Chromatographia* **2017**, 1.

(56) Maes, K.; Van Liefferinge, J.; Viaene, J.; Van Schoors, J.; Van Wanseele, Y.; Béchade, G.; Chambers, E. E.; Morren, H.; Michotte, Y.; Vander Heyden, Y.; Claereboudt, J.; Smolders, I.; Van Eeckhaut, A. *J. Chromatogr. A* **2014**, *1360*, 217.

(57) Weeks, J. R. *Science (80-.).* **1962**, *138* (3537), 143.

(58) Hyman, S. E.; Malenka, R. C. *Nat. Rev. Neurosci.* **2001**, *2* (10), 695.

(59) Ahmed, S. H.; Koob, G. F. *Science (80-.).* **1998**, *282* (5387), 298.

(60) Edwards, S.; Koob, G. F. *Behavioural Pharmacology*. September 2013, pp 356–362.

(61) Calipari, E. S.; Ferris, M. J.; Zimmer, B. A.; Roberts, D. C. S.; Jones, S. R. *Neuropsychopharmacology* **2013**, *38* (12), 2385.

(62) Calipari, E. S.; Ferris, M. J.; Jones, S. R. *J. Neurochem.* **2014**, *128* (2), 224.

(63) Zimmer, B. A.; Oleson, E. B.; Roberts, D. C. *Neuropsychopharmacology* **2012**, *37* (8), 1901.

(64) Kawa, A. B.; Bentzley, B. S.; Robinson, T. E. *Psychopharmacology (Berl).* **2016**, 1.

(65) Allain, F.; Roberts, D. C. S.; Lévesque, D.; Samaha, A. N. *Neuropharmacology* **2017**, *117*, 227.

(66) James, M. H.; Stopper, C. M.; Zimmer, B. A.; Koll, N. E.; Bowrey, H. E.; Aston-Jones, G. *Biol. Psychiatry* **2019**, *85* (11), 925.

(67) Kawa, A. B.; Robinson, T. E. *Psychopharmacology (Berl).* **2019**, *236* (2), 625.

(68) Vanderschuren, L. J. M. J.; Everitt, B. J. *Science (80-.).* **2004**, *305* (5686), 1017.

(69) Grinias, J. P.; Wong, J.-M. T.; Kennedy, R. T. *J. Chromatogr. A* **2016**, *1461*, 42.

(70) Hursh, S. R. *Drug Alcohol Depend.* **1993**, *33* (2), 165.

(71) Paxinos, G.; Watson, C. *The Rat Brain Atlas in Stereotaxic Coordinates*, 6th ed.; Elsevier B.V., 2007.

(72) Bentzley, B. S.; Jhou, T. C.; Aston-Jones, G. *Proc. Natl. Acad. Sci. U. S. A.* **2014**, *111* (32), 11822.

(73) Neue, U. D. *J. Chromatogr. A* **2005**, *1079* (1-2 SPEC. ISS.), 153.

(74) Armbruster, D. A.; Pry, T. *Clin. Biochem. Rev.* **2008**, *29 Suppl 1*, S49.

(75) Ahmed, S. H. In *Routledge Handbook on Philosophy and Science of Addiction H.*; 2018; pp 192–203.

(76) Deroche-Gamonet, V.; Belin, D.; Piazza, P. V. *Science (80-.).* **2004**, *305* (5686), 1014.

(77) Ahmed, S. H. *Neuroscience*. June 1, 2012, pp 107–125.

(78) Allain, F.; Samaha, A. N. *Addict. Biol.* **2019**, *24* (4), 641.

(79) Meissner, W.; Harnack, D.; Paul, G.; Reum, T.; Sohr, R.; Morgenstern, R.; Kupsch, A. *Neurosci. Lett.* **2002**, *328* (2), 105.

(80) Singer, B. F.; Fadanelli, M.; Kawa, A. B.; Robinson, T. E. *J. Neurosci.* **2018**, *38* (1), 60.

(81) Ferris, M. J.; Mateo, Y.; Roberts, D. C. S.; Jones, S. R. *Biol. Psychiatry* **2011**, *69* (3), 201.

(82) Mateo, Y.; Lack, C. M.; Morgan, D.; Roberts, D. C. S.; Jones, S. R. *Neuropsychopharmacology* **2005**, *30* (8), 1455.

(83) Ahmed, S. H.; Lin, D.; Koob, G. F.; Parsons, L. H. *J. Neurochem.* **2003**, *86* (1), 102.

(84) Calipari, E. S.; Ferris, M. J.; Zimmer, B. A.; Roberts, D. C.; Jones, S. R. *Neuropsychopharmacology* **2013**, *38* (12), 2385.

(85) Calipari, E. S.; Siciliano, C. A.; Zimmer, B. A.; Jones, S. R. *Neuropsychopharmacology* **2015**, *40* (3), 728.

(86) Robinson, T. E.; Berridge, K. C. *Brain Research Reviews*. 1993, pp 247–291.

(87) Zito, K.; Scheuss, V. In *Encyclopedia of Neuroscience*; Elsevier Ltd, 2009; pp 1157–1164.

(88) Laube, B.; Hirai, H.; Sturgess, M.; Betz, H.; Kuhse, J. *Neuron* **1997**, *18* (3), 493.

(89) Traynelis, S. F.; Wollmuth, L. P.; McBain, C. J.; Menniti, F. S.; Vance, K. M.; Ogden, K. K.; Hansen, K. B.; Yuan, H.; Myers, S. J.; Dingledine, R. *Pharmacological Reviews*. September 2010, pp 405–496.

(90) Kemp, J. A.; Foster, A. C.; Leeson, P. D.; Priestley, T.; Tridgett, R.; Iversen, L. L.; Woodruff, G. N. *Proc. Natl. Acad. Sci. U. S. A.* **1988**, *85* (17), 6547.

(91) Fletcher, E. J.; Millar, J. D.; Zeman, S.; Lodge, D. *Eur. J. Neurosci.* **1989**, *1* (3), 196.

(92) Matsui, T. -a; Sekiguchi, M.; Hashimoto, A.; Tomita, U.; Nishikawa, T.; Wada, K. *J. Neurochem.* **1995**, *65* (1), 454.

(93) Hashimoto, A.; Nishikawa, T.; Hayashi, T.; Fujii, N.; Harada, K.; Oka, T.; Takahashi, K. *FEBS Lett.* **1992**, *296* (1), 33.

(94) Hashimoto, A.; Nishikawa, T.; Oka, T.; Takahashi, K. *J. Neurochem.* **1993**, *60* (2), 783.

(95) Yamamori, H.; Hashimoto, R.; Fujita, Y.; Numata, S.; Yasuda, Y.; Fujimoto, M.; Ohi, K.; Umeda-Yano, S.; Ito, A.; Ohmori, T.; Hashimoto, K.; Takeda, M. *Neurosci. Lett.* **2014**, *582*, 93.

(96) Potier, B.; Turpin, F. R.; Sinet, P. M.; Rouaud, E.; Mothet, J. P.; Videau, C.; Epelbaum, J.; Dutar, P.; Billard, J. M. *Frontiers in Aging Neuroscience*. Frontiers Media SA 2010,.

(97) Panizzutti, R.; Scoriels, L.; Avellar, M. *Curr. Pharm. Des.* **2014**, *20* (32), 5160.

(98) Wolosker, H.; Blackshaw, S.; Snyder, S. H. *Proc. Natl. Acad. Sci. U. S. A.* **1999**, *96* (23), 13409.

(99) Basu, A. C.; Tsai, G. E.; Ma, C. L.; Ehmsen, J. T.; Mustafa, A. K.; Han, L.; Jiang, Z. I.; Benneyworth, M. A.; Froimowitz, M. P.; Lange, N.; Snyder, S. H.; Bergeron, R.; Coyle, J. T. *Mol. Psychiatry* **2009**, *14* (7), 719.

(100) Li, Y.; Sacchi, S.; Pollegioni, L.; Basu, A. C.; Coyle, J. T.; Bolshakov, V. Y. *Nat. Commun.* **2013**, *4*.

(101) Perez, E. J.; Tapanes, S. A.; Loris, Z. B.; Balu, D. T.; Sick, T. J.; Coyle, J. T.; Liebl, D. J. *J. Clin. Invest.* **2017**, *127* (8), 3114.

(102) Balu, D. T.; Takagi, S.; Puhl, M. D.; Benneyworth, M. A.; Coyle, J. T. *Cell. Mol. Neurobiol.* **2014**, *34* (3), 419.

(103) Ehmsen, J. T.; Ma, T. M.; Sason, H.; Rosenberg, D.; Ogo, T.; Furuya, S.; Snyder, S. H.; Wolosker, H. *J. Neurosci.* **2013**, *33* (30), 12464.

(104) Wolosker, H.; Radzishevsky, I. In *Biochemical Society Transactions*; 2013; Vol. 41, pp 1546–1550.

(105) Hashimoto, A.; Nishikawa, T.; Oka, T.; Takahashi, K.; Hayashi, T. *J. Chromatogr. B Biomed. Sci. Appl.* **1992**, *582* (1–2), 41.

(106) Mabrouk, O. S.; Han, J. L.; Wong, J. M. T.; Akil, H.; Kennedy, R. T.; Flagel, S. B. *ACS Chem. Neurosci.* **2018**, *9* (4), 715.

(107) Kawa, A. B.; Valenta, A. C.; Kennedy, R. T.; Robinson, T. E. *Eur. J. Neurosci.* **2019**, *50* (4), 2663.

(108) Damseh, N.; Simonin, A.; Jalas, C.; Picoraro, J. A.; Shaag, A.; Cho, M. T.; Yaacov, B.; Neidich, J.; Al-Ashhab, M.; Juusola, J.; Bale, S.; Telegrafi, A.; Retterer, K.; Pappas, J. G.; Moran, E.; Cappell, J.; Yeboa, K. A.; Abu-Libdeh, B.; Hediger, M. A.; Chung, W. K.; Elpeleg, O.; Edvardson, S. *J. Med. Genet.* **2015**, *52* (8), 541.

(109) Heimer, G.; Marek-Yagel, D.; Eyal, E.; Barel, O.; Oz Levi, D.; Hoffmann, C.; Ruzzo, E. K.; Ganelin-Cohen, E.; Lancet, D.; Pras, E.; Rechavi, G.; Nissenkorn, A.; Anikster, Y.; Goldstein, D. B.; Ben Zeev, B. *Clin. Genet.* **2015**, *88* (4), 327.

(110) Redmond, J. W.; Tseng, A. *J. Chromatogr. A* **1979**, *170* (2), 479.

(111) Seiler, N. *J. Chromatogr. B Biomed. Sci. Appl.* **1986**, *379*, 157.

(112) Lehrfeld, J. *J. Chromatogr. A* **1976**, *120* (1), 141.

(113) Ross, M. S. F. *J. Chromatogr. A* **1977**, *141* (1), 107.

(114) White, C. A.; Kennedy, J. F.; Golding, B. T. *Carbohydr. Res.* **1979**, *76* (1), 1.

(115) Malec, P. A.; Oteri, M.; Inferrera, V.; Cacciola, F.; Mondello, L.; Kennedy, R. T. *J. Chromatogr. A* **2017**, *1523*, 248.

(116) Le, J.; Lin, Z.; Song, L.; Wang, H.; Hong, Z. *J. Pharm. Biomed. Anal.* **2019**, *176*.

(117) Fleszar, M. G.; Wiśniewski, J.; Krzystek-Korpacka, M.; Misiak, B.; Frydecka, D.; Piechowicz, J.; Lorenc-Kukuła, K.; Gamian, A. *Chromatographia* **2018**, *81* (6), 911.

(118) Yuan, T. F.; Huang, H. Q.; Gao, L.; Wang, S. T.; Li, Y. *Free Radic. Biol. Med.* **2018**, *118*, 119.

(119) Dong, Y.; Ma, Y.; Yan, K.; Shen, L.; Wang, X.; Xu, Y.; He, G.; Wu, Y.; Lu, J.; Yang, Z.; Feng, F. *J. Chromatogr. B Anal. Technol. Biomed. Life Sci.* **2014**, *957*, 30.

(120) Cappiello, A.; Famiglini, G.; Palma, P.; Termopoli, V.; Trufelli, H.; Di Mento, R.; Mannozzi, M. *Talanta* **2009**, *80* (1), 257.

(121) Ng, J. M. K.; Gitlin, I.; Stroock, A. D.; Whitesides, G. M. *Electrophoresis*. John Wiley & Sons, Ltd October 1, 2002, pp 3461–3473.

(122) Lee, J. N.; Park, C.; Whitesides, G. M. *Anal. Chem.* **2003**, *75* (23), 6544.

(123) Zhang, H.; Chiao, M. *J. Med. Biol. Eng.* **2015**, *35* (2), 143.

(124) Harrison, D. J.; Fluri, K.; Seiler, K.; Fan, Z.; Effenhauser, C. S.; Manz, A. *Science (80-.).* **1993**, *261* (5123), 895.

(125) Roper, M. G.; Shackman, J. G.; Dahlgren, G. M.; Kennedy, R. T. *Anal. Chem.* **2003**, *75* (18), 4711.

(126) Simpson, P. C.; Woolley, A. T.; Mathies, R. A. *Biomed. Microdevices* **1998**, *1* (1), 7.

(127) OpenWetWare contributors. Mathies: Glass Etching in BNC https://openwetware.org/mediawiki/index.php?title=Mathies:Glass_Etching_in_BNC&oldid=330217 (accessed Nov 11, 2019).

(128) Lagally, E. T.; Simpson, P. C.; Mathies, R. A. *Sensors Actuators, B Chem.* **2000**, *63* (3), 138.

(129) Oberti, S.; Neild, A.; Wah Ng, T. *Lab Chip* **2009**, *9* (10), 1435.

(130) Yaralioglu, G. G.; Wygant, I. O.; Marentis, T. C.; Khuri-Yakub, B. T. *Anal. Chem.* **2004**, *76* (13), 3694.

(131) Huang, P. H.; Xie, Y.; Ahmed, D.; Rufo, J.; Nama, N.; Chen, Y.; Chan, C. Y.; Huang, T. J. *Lab Chip* **2013**, *13* (19), 3847.

(132) Cui, W.; Zhang, H.; Zhang, H.; Yang, Y.; He, M.; Qu, H.; Pang, W.; Zhang, D.; Duan, X. *Appl. Phys. Lett.* **2016**, *109* (25).

(133) Owen, M. J.; Williams, D. E. *J. Adhes. Sci. Technol.* **1991**, *5* (4), 307.

(134) Song, P.; Hershey, N. D.; Mabrouk, O. S.; Slaney, T. R.; Kennedy, R. T. *Anal. Chem.* **2012**, *84* (11), 4659.

(135) Steyer, D. J.; Kennedy, R. T. *Anal. Chem.* **2019**, acs. analchem.9b00571.

(136) Zhang, J.; Yang, S.; Chen, C.; Hartman, J. H.; Huang, P. H.; Wang, L.; Tian, Z.; Zhang, P.; Faulkenberry, D.; Meyer, J. N.; Huang, T. J. *Lab Chip* **2019**, *19* (6), 984.

(137) Klenk, Herbert; Gotz, Peter; Siegmeier, Rainer; Mayr, W. *Ullman's Encycl. Ind. Chem.* **2012**, 325.

(138) Gowers, S. A. N.; Hamaoui, K.; Cunnea, P.; Anastasova, S.; Curto, V. F.; Vadgama, P.; Yang, G. Z.; Papalois, V.; Drakakis, E. M.; Fotopoulou, C.; Weber, S. G.; Boutelle, M. G. *Analyst* **2018**, *143* (3), 715.

(139) Lim, S. A. O.; Kang, U. J.; McGehee, D. S. *Front. Synaptic Neurosci.* **2014**, *6* (SEP).

(140) Taylor, P.; Radić, Z. *Annual Review of Pharmacology and Toxicology*. 1994, pp 281–320.

(141) Uutela, P.; Reinilä, R.; Piepponen, P.; Ketola, R. A.; Kostiainen, R. *Rapid Commun. Mass Spectrom.* **2005**, *19* (20), 2950.

(142) DeBoer, P.; Westerink, B. H. C. *J. Neurochem.* **1994**, *62* (1), 70.

(143) Cone, R. D. *Nat. Neurosci.* **2005**, *8* (5), 571.

(144) Smart, J. L.; Tolle, V.; Low, M. J. *J. Clin. Invest.* **2006**, *116* (2), 495.

(145) Mountjoy, K. G. *Biochem. J.* **2010**, *428* (3), 305.

(146) Kirwan, P.; Kay, R. G.; Brouwers, B.; Herranz-Pérez, V.; Jura, M.; Larraufie, P.; Jerber, J.; Pembroke, J.; Bartels, T.; White, A.; Gribble, F. M.; Reimann, F.; Farooqi, I. S.; O'Rahilly, S.; Merkle, F. T. *Mol. Metab.* **2018**, *17*, 82.

(147) Yaswen, L.; Diehl, N.; Brennan, M. B.; Hochgeschwender, U. *Nat. Med.* **1999**, *5* (9), 1066.

(148) Cowley, M. A.; Smart, J. L.; Rubinstein, M.; Cerdán, M. G.; Diano, S.; Horvath, T. L.; Cone, R. D.; Low, M. J. *Nature* **2001**, *411* (6836), 480.

(149) Low, M. J. *J. Endocrinol. Invest.* **2004**, *27* (6 Suppl), 95.

(150) Huszar, D.; Lynch, C. A.; Fairchild-Huntress, V.; Dunmore, J. H.; Fang, Q.; Berkemeier, L. R.; Gu, W.; Kesterson, R. A.; Boston, B. A.; Cone, R. D.; Smith, F. J.; Campfield, L. A.; Burn, P.; Frank, L. *Cell* **1997**, *88* (1), 131.

(151) Yaswen, L.; Diehl, N.; Brennan, M. B.; Hochgeschwender, U. *Nat. Med.* **1999**, *5* (9), 1066.

(152) Schwartz, M. W.; Seeley, R. J.; Woods, S. C.; Weigle, D. S.; Campfield, L. A.; Burn, P.; Baskin, D. G. *Diabetes* **1997**, *46* (12), 2119.

(153) Perroud, B.; Alvarado, R. J.; Espinal, G. M.; Morado, A. R.; Phinney, B. S.; Warden, C. H. *Mol. Brain* **2009**, *2* (1), 14.

(154) Frese, C. K.; Boender, A. J.; Mohammed, S.; Heck, A. J. R.; Adan, R. A. H.; Altelaar, A. F. M. *Anal. Chem.* **2013**, *85* (9), 4594.

(155) Kirwan, P.; Kay, R. G.; Brouwers, B.; Herranz-Pérez, V.; Jura, M.; Larraufie, P.; Jerber, J.; Pembroke, J.; Bartels, T.; White, A.; Gribble, F. M.; Reimann, F.; Farooqi, I. S.; O'Rahilly, S.; Merkle, F. T. *Mol. Metab.* **2018**, *17*, 82.

(156) Pritchard, L. E.; Oliver, R. L.; McLoughlin, J. D.; Birtles, S.; Lawrence, C. B.; Turnbull, A. V.; White, A. *Endocrinology* **2003**, *144* (3), 760.

(157) Perry, M.; Li, Q.; Kennedy, R. T. *Analytica Chimica Acta*. Elsevier October 19, 2009, pp 1–22.

(158) Maidment, N. T.; Brumbaugh, D. R.; Rudolph, V. D.; Erdelyi, E.; Evans, C. J. *Neuroscience* **1989**, *33* (3), 549.

(159) O'Donohue, T. L.; Miller, R. L.; Jacobowitz, D. M. *Brain Res.* **1979**, *176* (1), 101.

(160) Zhang, G.; Zhang, Y.; Fast, D. M.; Lin, Z.; Steenwyk, R. *Anal. Biochem.* **2011**, *416* (1), 45.

(161) Mabrouk, O. S.; Kennedy, R. T. *J. Neurosci. Methods* **2012**, *209* (1), 127.

(162) Shackman, H. M.; Shou, M.; Cellar, N. a.; Watson, C. J.; Kennedy, R. T. *J. Neurosci. Methods* **2007**, *159* (1), 86.

(163) Maes, K.; Béchade, G.; Van Schoors, J.; Van Wanseele, Y.; Van Liefferinge, J.; Michotte, Y.; Harden, S. N.; Chambers, E. E.; Claereboudt, J.; Smolders, I.; Van Eeckhaut, A. *Bioanalysis* **2015**, *7* (5), 605.

(164) Li, Q.; Zubieta, J.-K.; Kennedy, R. T. *Anal. Chem.* **2009**, *81* (6), 2242.

(165) Zhou, Y.; Mabrouk, O. S.; Kennedy, R. T. *J. Am. Soc. Mass Spectrom.* **2013**, *24* (11), 1700.

(166) Maiolica, A.; Borsotti, D.; Rappsilber, J. *Proteomics* **2005**, *5* (15), 3847.

(167) van Midwoud, P. M.; Rieux, L.; Bischoff, R.; Verpoorte, E.; Niederländer, H. A. G. *J. Proteome Res.* **2007**, *6* (2), 781.

(168) Goebel-Stengel, M.; Stengel, A.; Taché, Y.; Reeve, J. R. *Anal. Biochem.* **2011**, *414* (1), 38.

(169) Ishihama, Y.; Rappsilber, J.; Andersen, J. S.; Mann, M. *J. Chromatogr. A* **2002**, *979* (1–2), 233.

(170) You, Z. B.; Nylander, I.; Herrera-Marschitz, M.; O'Connor, W. T.; Goiny, M.; Terenius, L. *Neuroscience* **1994**, *63* (2), 415.

(171) Flanigan, M.; Tollefson, S.; Himes, M. L.; Jordan, R.; Roach, K.; Stoughton, C.; Lopresti, B.; Mason, N. S.; Ciccocioppo, R.; Narendran, R. *Biol. Psychiatry* **2019**.

(172) Smith, A. L.; Freeman, S. M.; Barnhart, T. E.; Abbott, D. H.; Ahlers, E. O.; Kukis, D. L.; Bales, K. L.; Goodman, M. M.; Young, L. J. *Bioorganic Med. Chem. Lett.* **2016**, *26* (14), 3370.

(173) Breisch, S.; De Heij, B.; Löhr, M.; Stelzle, M. *J. Micromechanics Microengineering* **2004**, *14* (4), 497.

(174) Kota, A. K.; Kwon, G.; Tuteja, A. *NPG Asia Materials*. Nature Publishing Group 2014,.

(175) Ngo, K. T.; Varner, E. L.; Michael, A. C.; Weber, S. G. *ACS Chem. Neurosci.* **2017**, *8* (2), 329.

(176) Gu, H.; Varner, E. L.; Groskreutz, S. R.; Michael, A. C.; Weber, S. G. *Anal. Chem.* **2015**, *87* (12), 6088.

(177) Zhang, J.; Jaquins-Gerstl, A.; Nesbitt, K. M.; Rutan, S. C.; Michael, A. C.; Weber, S. G. *Anal. Chem.* **2013**, *85* (20), 9889.

(178) Yang, H.; Thompson, A. B.; McIntosh, B. J.; Altieri, S. C.; Andrews, A. M. *ACS Chem. Neurosci.* **2013**, *4* (5), 790.

(179) Yang, H.; Sampson, M. M.; Senturk, D.; Andrews, A. M. *ACS Chem. Neurosci.* **2015**, *6* (8), 1487.